In-situ impedances measurement and influence of 2 k - 150 kHz disturbances on measurement of electrical parameters

BY

Junzhe Tan

A thesis submitted in partial fulfillment of the

requirements for the degree of

MASTER OF SCIENCE IN

ELECTRICAL ENGINEERING

at the

DELFT UNIVERSITY OF TECHNOLOGY

2014

This thesis of Junzhe Tan is approved by the Thesis Examining Committee.

Prof. dr. J. A. Ferreira (Chairman, Supervisor)

Prof. ir. L. van der Sluis (Advisor)

Dr. A. Smets (Advisor)

Dr. D. Zhao (Supervisor)

DELFT UNIVERSITY OF TECHNOLOGY

2014

Table of Contents

List of figures iii

List of tables vii

Acknowledgements viii

ABSTRACT OF THE THESIS ix

1 Introduction 1

1.1 Background and problem statement 1

1.2 Theoretical background and objectives 4

1.3 Thesis layout 5

2 Methodological approach 6

2.1 Challenges 6

2.2 Measurement systems 6

3 Monitor probe and BCI probe analysis, modeling and characterization 9

3.1 Current probe and current shunt 9

3.2 Transfer impedance measurement of monitor probes and their modeling 13

3.3 Transfer impedance of BCI probe and its modeling 28

3.4 Summary 38

4 Discussion of source and load impedance measurement approach 39

4.1 The two-probe approach 39

4.1.1 Basic theory of the two-probe approach 39

4.1.2 Performances of the two-probe approach at 2 kHz – 150 kHz 41

4.2 The three-probe approach 44

4.2.1 Basic theory of the three-probe approach 44

4.2.2 Performances of the three-probe approach at 2 kHz – 150 kHz 46

4.3 Summary 48

5 Source impedance and load impedance measurements 49

5.1 Source impedance measurements 49

5.1.1 Source impedances in different wall sockets 50

5.1.2 Source impedance in smart power supply 52

5.2 Load impedance measurements 53

5.3 Comparison between L1 and L16 59

5.4 Summary 62

6 Disturbance influences on the measurement of electrical parameters and the smart meter 63
6.1 Measurement with the variable-inductance box 65
6.2 Measurements with variable-capacitance box 75
6.3 Summary and possible explanations 83
7 Conclusions and recommendations 85
7.1 Conclusions 85
7.2 Recommendations 86
Reference 87

List of figures

Fig 2-1 Main measurement system……6
Fig 2-2 Injecting noise source……7
Fig 2-3 Basic setup of the two current probes approach……7
Fig 2-4 Impedance measurement system……8
Fig 2-5 Current probe measurement system……8
Fig 3-1 Power supply……9
Fig 3-2 Current probe ETS 94430-5……10
Fig 3-3 Basic current probe testing structure……10
Fig 3-4 Typical transfer impedance variation with frequency for model 94430-5……10
Fig 3-5 Current shunt……11
Fig 3-6 NI digitizer……11
Fig 3-7 Current probe/shunt property test schematic……12
Fig 3-8 Current probe/shunt property test circuit……12
Fig 3-9 Results from using current probe and shunt……13
Fig 3-10 Simplified current transformer model……13
Fig 3-11 Thevenin equivalent circuit of secondary winding……14
Fig 3-12 HP 33120A function generator……15
Fig 3-13 R&S spectrum analyzer……15
Fig 3-14 VNA……16
Fig 3-15 Jig……16
Fig 3-16 F75 (left) and F75red (right)……17
Fig 3-17 Transfer impedance measurement circuit at low frequency……17
Fig 3-18 Source measurement circuit……17
Fig 3-19 Implementation of Z_t measurement circuit at low frequency……18
Fig 3-20 Zt measurement at high frequency……18
Fig 3-21 Z_t of F75 at low frequency……19
Fig 3-22 Z_t test structure via VNA……20
Fig 3-23 Z_t of F75 at high frequency……20
Fig 3-24 Z_t of F75red at low frequency……21
Fig 3-25 Z_t of F75red at high frequency……21
Fig 3-26 Z_t of 94430-5 at low frequency……22
Fig 3-27 Z_t of 94430-5 at high frequency……23
Fig 3-28 SPICE model of F75……23
Fig 3-29 F75 Z_t comparison at low frequency……24
Fig 3-30 F75 Z_t comparison at high frequency……24
Fig 3-31 SPICE model of F75red……25
Fig 3-32 F75red Z_t comparison at low frequency……25
Fig 3-33 F75red Z_t comparison at high frequency……25
Fig 3-34 SPICE model of ETS 94430-5……26
Fig 3-35 ETS 94430-5 Z_t comparison at low frequency……26
Fig 3-36 ETS 94430-5 Z_t comparison at high frequency……27

Fig 3-37 BCI probe CIP 9136A……28
Fig 3-38 QuadTech 7600 precision LCR meter……28
Fig 3-39 Agilent E4980A precision LCR meter……29
Fig 3-40 Implementation of Z_t measurement of BCI probe……29
Fig 3-41 Z_t of BCI at low frequency……30
Fig 3-42 Z_t of BCI at high frequency……30
Fig 3-43 Equivalent current probe operating circuit……31
Fig 3-44 T Equivalent current probe operating circuit……31
Fig 3-45 Implementation of Z_{in} measurement……32
Fig 3-46 Reflection coefficient……32
Fig 3-47 Input impedance……33
Fig 3-48 Z_t with correction at low frequency……33
Fig 3-49 Z_t with correction at high frequency……34
Fig 3-50 Z_{in} of F75red with a 50 Ω resistor……34
Fig 3-51 Z_t of F75red……35
Fig 3-52 Typical required forward power to inject 100 mA……35
Fig 3-53 Typical injected current with 100 W forward power……36
Fig 3-54 BCI probe modeling circuit……36
Fig 3-55 Modeling results of typical required forward power to inject 100 mA……37
Fig 3-56 Modeling results of typical injected current with 100 W forward power……38
Fig 4-1 Basic structure of two-probe measurement……39
Fig 4-2 Equivalent circuit of the injection probe……39
Fig 4-3 Equivalent circuit of the two-probe measurement setup……40
Fig 4-4 Source in frequency domain……42
Fig 4-5 Test circuit for the 2-probe approach……42
Fig 4-6 Measurement by the 2-probe approach……43
Fig 4-7 Measurement (zoom in above 40 kHz) by the 2-probe approach……43
Fig 4-8 Test circuit for the 3-probe approach……44
Fig 4-9 Test circuit (simplified) for the 3-probe approach……44
Fig 4-10 Thevenin equivalent circuit of the three-probe measurement setup……45
Fig 4-11 Measurement of a 1 Ω resistor using three-probe approach……46
Fig 4-12 Comparison between measurements with and without phase information……47
Fig 4-13 Measurement of a 10 Ω resistor using three-probe approach……47
Fig 4-14 Measurement of a 50 Ω resistor using three-probe approach……47
Fig 4-15 Measurement of a 47 μH inductor using three-probe approach……48
Fig 5-1 Source impedance measurement equivalent circuit……49
Fig 5-2 Implementation of source impedance measurement circuit……50
Fig 5-3 Load 1 – OSRAM 4.5 W LED lamp……50
Fig 5-4 Grid source impedance measurement……51
Fig 5-5 Grid source impedance measurement (real)……51
Fig 5-6 Grid source impedance measurement (imaginary)……51
Fig 5-7 Source impedance comparison between wall sockets' and power supply's……52
Fig 5-8 Source impedance (real) comparison between wall sockets' and power supply's……52
Fig 5-9 Source impedance (imag) comparison between wall sockets' and power supply's.....53

Fig 5-10 Load impedance measurement equivalent circuit……53
Fig 5-11 Lamps……54
Fig 5-12 Fans……54
Fig 5-13 Load impedance comparison (L1 to L6)……55
Fig 5-14 Load impedance comparison (real) (L1 to L6)……55
Fig 5-15 Load impedance comparison (imaginary) (L1 to L6)……55
Fig 5-16 Load impedance comparison (L11 to L16)……56
Fig 5-17 Load impedance comparison (real) (L11 to L16)……56
Fig 5-18 Load impedance comparison (imaginary) (L11 to L16)……56
Fig 5-19 10 times measurements of L1 impedance……57
Fig 5-20 Range of L1 impedance variation……57
Fig 5-21 Load impedance comparison (F1 and F2)……58
Fig 5-22 Load impedance comparison (real) (F1 and F2)……58
Fig 5-23 Load impedance comparison (imaginary) (F1 and F2)……58
Fig 5-24 Schematics of L1……59
Fig 5-25 Schematics of L16……59
Fig 5-26 Equivalent model of L1……60
Fig 5-27 Modeling results of L1……60
Fig 5-28 Equivalent circuit of L16……60
Fig 5-29 Modeling results of L16……61
Fig 5-30 Result of using three-probe method to measure a 4.7 mH inductor……61
Fig 6-1 Main test circuit……63
Fig 6-2 Smart meter setup……63
Fig 6-3 Load L1 (upper-left), L5 (upper-right), L13 (down-left) and L16 (down-right)……64
Fig 6-4 The variable-inductance box……65
Fig 6-5 Current comparison of L1 without injection using inductance box……65
Fig 6-6 Voltage comparison of L1 without injection using inductance box……66
Fig 6-7 Current comparison of L1 with injection using inductance box……66
Fig 6-8 Voltage comparison of L1 with injection using inductance box……66
Fig 6-9 Current comparison of L5 without injection using inductance box……66
Fig 6-10 Voltage comparison of L5 without injection using inductance box……67
Fig 6-11 Current comparison of L5 with injection using inductance box……67
Fig 6-12 Voltage comparison of L5 with injection using inductance box……67
Fig 6-13 Current comparison of L13 without injection using inductance box……67
Fig 6-14 Voltage comparison of L13 without injection using inductance box……68
Fig 6-15 Current comparison of L13 with injection using inductance box……68
Fig 6-16 Voltage comparison of L13 with injection using inductance box……68
Fig 6-17 Current comparison of L16 without injection using inductance box……68
Fig 6-18 Voltage comparison of L16 without injection using inductance box……69
Fig 6-19 Current comparison of L16 with injection using inductance box……69
Fig 6-20 Voltage comparison of L16 with injection using inductance box……69
Fig 6-21 Equivalent circuit of measurement with L1 using inductance box……69
Fig 6-22 Equivalent circuit of measurement with L16 (L5 or L13) using inductance box……70
Fig 6-23 Power of L1 using inductance box……71

Fig 6-24 Power of L16 using inductance box……72
Fig 6-25 Power of L5 using inductance box……72
Fig 6-26 Power of L13 using inductance box……72
Fig 6-27 RMS current of L1 using inductance box……73
Fig 6-28 RMS current of L16 using inductance box……74
Fig 6-29 RMS current of L5 using inductance box……74
Fig 6-30 RMS current of L13 using inductance box……74
Fig 6-31 The variable-capacitance box……75
Fig 6-32 Equivalent circuit of measurement with L1 using capacitance box……75
Fig 6-33 Equivalent circuit of measurement with L16 (L5 or L13) using capacitance box……75
Fig 6-34 Current comparison of L1 without injection using capacitance box……76
Fig 6-35 Voltage comparison of L1 without injection using capacitance box……76
Fig 6-36 Current comparison of L1 with injection using capacitance box……76
Fig 6-37 Voltage comparison of L1 with injection using capacitance box……77
Fig 6-38 Current comparison of L5 without injection using capacitance box……77
Fig 6-39 Voltage comparison of L5 without injection using capacitance box……77
Fig 6-40 Current comparison of L5 with injection using capacitance box……77
Fig 6-41 Voltage comparison of L5 with injection using capacitance box……78
Fig 6-42 Current comparison of L13 without injection using capacitance box……78
Fig 6-43 Voltage comparison of L13 without injection using capacitance box……78
Fig 6-44 Current comparison of L13 with injection using capacitance box……78
Fig 6-45 Voltage comparison of L13 with injection using capacitance box……79
Fig 6-46 Current comparison of L16 without injection using capacitance box……79
Fig 6-47 Voltage comparison of L16 without injection using capacitance box……79
Fig 6-48 Current comparison of L16 with injection using capacitance box……79
Fig 6-49 Voltage comparison of L16 with injection using capacitance box……80
Fig 6-50 Power of L1 using capacitance box……80
Fig 6-51 Power of L16 using capacitance box……81
Fig 6-52 Power of L5 using capacitance box……81
Fig 6-53 Power of L13 using capacitance box……81
Fig 6-54 RMS current of L1 using capacitance box……82
Fig 6-55 RMS current of L5 using capacitance box……82
Fig 6-56 RMS current of L13 using capacitance box……83
Fig 6-57 RMS current of L16 using capacitance box……83

List of tables

Table 1-1 Effects of EMI to equipment in the frequency range 2 - 150 kHz……3
Table 6-1 Smart meter readings of L1 and L16 using inductance box……..70
Table 6-2 Power of L1 and L16 via digitizer using inductance box……71
Table 6-3 RMS current of L1 and L16……73
Table 6-4 Smart meter readings of L1 and L16 using capacitance box……80

Acknowledgements

I would like to thank all those people who made this thesis possible and an unforgettable experience for me.

First of all, I would like to gratefully thank my daily supervisor Dr. Dongsheng Zhao at VSL Dutch Metrology Institute, who offered his continuous advice and encouragement throughout the course of this thesis. His patient guidance and great assistance in the past nine months were the keys to make me overcome every difficulty during the experiments. I thank him for the great effort he put into training me in the scientific field. His rigorous academic attitude during the research made me admire and also led me to be more patient and strict to deal with technical problems.

I would like to sincerely express my gratitude to supervisor Professor J. A. Ferriera from Delft University of Technology. He has been supportive since the days I began working on this project. His encouragement and academic assistance were important for me to whip myself on the improvements of this thesis.

I would like to thank Mr. George Teunisse for providing valuable feedback and correction on my thesis writing.

I am thankful to those professors at Delft University of Technology who lectured me during my master studies. Their passionate and vivid lectures motivated me to explore the principles and knowledge behind every interesting experiment or phenomenon in electrical engineering.

I also thank my friends and my classmates for providing support and friendship that I need throughout these years.

Finally, I especially thank my family for always providing their unconditional love and care for me. In the past years, they gave me absolute support, trust and freedom to choose what I like and tolerated my unreasonable tempers. I love them so much and I would not make it this far without them.

ABSTRACT OF THE THESIS

In-situ impedances measurement and influence of 2 k - 150 kHz disturbances on measurement of electrical parameters

by

Junzhe Tan
Master of Science in Electrical Engineering
Delft University of Technology, 2014
Professor J. A. Ferreira, Supervisor
Dr. DongSheng Zhao, Supervisor

With the growth of the number of electric appliances which suffer from electromagnetic inference (EMI) in the frequency range 2 k – 150 kHz, the setting up of researches in this field has become more and more popular. Measuring impedances accurately in this frequency range is of great assistance for better understanding of the circuit as well as for EMI filter designs. Thus, this thesis aims to develop a safe, flexible and accurate in-situ measurement approach to measure the source and load impedances at 2 kHz – 150 kHz and then apply it to investigate the influences of the variable impedances on measurements of electrical parameters when experiencing disturbances.

In this thesis, the current probe being one of the most important measurement devices is discussed first. To investigate the transfer impedance of the current probes used in the measurements a spectrum analyzer, a vector network analyzer (VNA) and a LCR meter are applied respectively. It is found that the input impedance on the wire side influences the bulk current injection (BCI) probe but not the normal current monitor probe in the transfer impedance measurements at discussed frequency range. The electric models are illustrated. Secondly, an in-situ measurement method – the three-probe method which is verified to be applicable at discussed frequency - is proposed. The measurement accuracy is guaranteed through a proper Fast Fourier Transform (FFT) process by collecting both amplitude and phase information of the measurement. In addition, the three-probe method was compared with its predecessor – the two-probe method which was proposed in 2004 to measure noise source impedance at 150 k – 30 MHz. Then the impedances measurement results of different sources and loads are illustrated by using this three-probe method. At last, by using a variable inductance/capacitance box to simulate different source conditions, it comes out that the loads which property will turn out to be capacitive at certain frequency (2 k – 150 kHz) are sensitive for source impedance variations. Their voltages and currents all are influenced significantly with the resonance between source and load impedances. Fortunately, with further investigation, this effect seems not to interfere with the reading of the smart meter under the test.

Index terms – Current probe, In-situ measurement, Frequency 2 k – 150 kHz, Source impedance, Load impedance

1 Introduction

1.1 Background and problem statement

Electricity has become one of the most important forms of energy in our lives because of its ease of transportation over large distances and easy conversion to other energy forms. The traditional ways of transferring the fossil fuels into electrical power are gradually reducing. The renewable energy is playing an increasingly important role in generating electricity. In order to make optimal use of those different types of energy and increase comfort in application of electrical energy, diverse power electronics equipment and their relevant control strategies are widely applied in power systems [1][2]. However, the electromagnetic inferences (EMI) as side-effect resulting from the harmonics caused by those power electronics equipments due to their frequent switching behavior certainly disturb some electric appliances and affect their normal operation, which should be avoided [1-3]. Certainly, power electronics equipment is not the only source of EMI, and in facts, this EMI effect could be initiated by any occurrence of unintentional emission coming from one or more non-communication or communication equipment or a combination of both. Thus, the source of EMI could be a phone, a PC, a TV, a lamp or even a DVD player etc [4]. In order to ensure that electronic devices in our lives work as best as possible, standards and rules to limit the level of EMI are produced and published.

International electromagnetic compatibility (EMC) standards have already covered the level of disturbance for the EM frequency range below 2 kHz and above 150 kHz, but for the frequency range between 2 kHz and 150 kHz there are no satisfactory EMC standards. A new basic standard for this range IEC61000-4-19 with the title “Testing and measurement techniques – Test for immunity to conducted, differential mode disturbances and signaling in the frequency range 2 kHz to 150 kHz at a.c. power ports” is just published in May 2014 [5][6-8] and it only concerns harmonics and some specific emissions. The reason why there is a gap for relevant standards at this frequency range is mostly due to the facts that, firstly in the past no significant emissions or disturbance sources existed and, secondly seldom appliances worked in this frequency range. Since these facts mentioned above exist, almost no widespread problems due to the high disturbance levels in the discussed range have been reported, which results in the lack of motivation to manage the distortion in this range [5][9][10].

However, things have changed in recent years and this frequency range has become more important. On one hand, of course, this is due to the increasing use of appliances generating current distortion in frequency range 2 kHz - 150 kHz. On the other hand, this frequency range is partly used for power-line communication (PLC) (in the range 9 kHz - 95 kHz) [3][9-11].

As far as what we know, the EMI in this frequency range comes from firstly, non-intentional emissions from network users’ equipments at or close to frequencies used for mains communicating systems (MCS) which interfere with intentional MCS signals, leading to disturbance of, or loss of MCS communication. Secondly, Harmonics of non-intentional emissions from this equipment will also cause interference with MCS communication resulting in failures. Thirdly, discontinuous currents or voltages from the users’ devices as well as signal voltages from MCS may cause distortion, which leads to disturbances in users’ equipment and results in poor performances. Moreover, the low-impedance path caused by equipment may

lead to MCS signal attenuation and disturb the communication. At last, overheat and accelerated aging effect as a result of higher current due to non-intentional emission from users' equipment or MCS signal voltages can also be regarded as a side effect of EMI in this frequency range [4][12-14].

With more profound research, some of the EMI sources in our lives at related frequency range have already been recognized. First, as what is mentioned at the beginning of this thesis, inverters (e.g. in PV installations) as a typical kind of power electronics equipment are surely in this list. Apart from that, variable speed drives (VSD) (e.g. in elevator drives, ski lift drives, heating system circulation pumps, ventilation systems, household equipment), switch-mode power supplies (e.g. in lighting equipment, PCs, consumer electronic/home entertainment equipment such as TV and DVD player, ICT equipment, uninterruptible power supplies (UPS), charging devices), lighting equipments (e.g. fluorescent lamps, compact lamps, LEDs), household equipments (e.g. induction cookers, washing machines, electric shavers), portable mains operated tools and automated meter reading PLC (AMR-PLC) can be also regarded as EMI sources [2-7][9][10][15-18].

At the same time, AMR-PLC is also considered to be an EMI victim. Besides, solid state meters, electronic control (e.g. touch-controlled equipment like Touch Dimmer lamps (TDL), alarm systems, traffic control systems, traffic lights, in heating systems, street lights, in urinals, for doors, in kitchen appliances such as steam irons, coffee machines, ceramic hobs etc.), communication systems (e.g. Ethernet-system, ISDN-, ADSL-modems, IP network branch exchange, routers, LAN), telephone systems including inductive train ratio systems, earth leakage circuit breakers (ELB), contactless magnetic card readers, credit card terminals, notebooks (cursor position), broadcast standard time-signal system such as DCF77, road vehicle smart keys, TV as well as radio receivers, mobile radio and amateur radio are all more or less affected by EMI in frequency range 2 kHz - 150 kHz [2-7][9][10][15-18].

The effects which have been found according to experiment results and investigations from customers' reports on the victim devices mentioned above are summarized in table 1-1 [2-7][9][10][15-18].

With this overview of potential EMI victims and sources as well as EMI effects on victims, we should notice that the devices having EMI problems in the frequency range 2 kHz - 150 kHz already cover a big amount of both domestic and public appliances. At the same time, related standards are still absent, which will need to be resolved as soon as possible. Thus, continuing the trend to study related issues under this frequency range in EMC as well as power electronics research fields will be unavoidable.

TDLs	Unintentional switching (between light steps, OFF, ON)
Street lighting	Unintentional switch-on and -off
Traffic control system	Malfunction
Traffic lights	Malfunction
Solid state meter	Displaying wrong meter register values
MCS	Temporary loss of data transmission function
Heat control through DCF77 signal	Malfunction
Heating systems	Incorrect alarms due to sensor faults
Contactless magnetic card reader	Fault of reading function
ADSL modem	Loss of link, CRC error
Routers	Loss of synchronization to network
Notebooks	Disturbed cursor position
Inductive train radio system	Audible noise
Ceramic hobs	Incorrect relay switching
Coffee machine	Incorrect control lamp function
Steam irons	Insufficient heat, water loss, incorrect control lamp blinking
Washing machines	Self-restart after end of operation phase
Automatic urinal water control	Switching to permanent operation
Broadcast standard time-signal systems	Electronic clocks: being fast (gaining up to 15 mins per day), malfunction of control circuits fed by the time-signal
TV and radio receiver	Audible noise
Amateur radio	Disturbed reception of distant transmitters

Table 1-1 Effects of EMI to equipment in the frequency range 2 - 150 kHz

1.2 Theoretical background and objectives

Great many efforts have been paid by those researchers working on this field and a big amount of progress has been achieved. Among all of those research teams, Professor M.H.J Bollen and his teammates have really made a great difference. They used short-time Fourier transform (STFT) to analyze the EMI effects in the frequency range 2 kHz - 150 kHz in frequency domain and applied different instruments to do the same analysis in time domain [3][10-12][19]. By doing so, it was possible to choose the better way to analyze signals dependent on diverse requirements. Meanwhile, they also found that the spectrum characteristic would vary according to the different locations [3]. However, there is no further explanation for this. Thus finding out whether this results from the source impedance difference is quite a great inheritance from their research. But measuring the source impedance is not simple, especially when it needs to be measured without interrupting the normal operation. As far as we know, seldom such measuring approach has been proposed except for one using two current probes to measure the noise source impedance of a switched mode power supply (SMPS) at 150 kHz – 30 MHz [20] and another one using Vector Network Analyzer (VNA) [21]. Unfortunately, both of these approaches are only verified at the frequency beyond 150 kHz. Therefore, some efforts may be paid to testify and improve them to make one or both methods adapt to the measurements with 2 kHz - 150 kHz. In addition, there is seldom research done on smart meter immunity test and even if it exists, it concerns only some simple tests [6]. Even if it came out by IEC testing that some smart meters got influenced during their immunity test at the discussed frequency range, the reason why still is not known yet. One possible reason would be the resonance of source impedance and the load impedance at some frequency points however no published researches have mentioned this assumption. Besides, even though it might not influence the smart meter itself, it could lead to other problems for electrical parameters measurements on other devices. Therefore, a synthesized immunity test will be included in this task which is related to the impact from different source and load impedance combinations on electrical parameters measurements and smart meter readings which will give more detailed information for further research in the future.

In summary, the aim of this task is first to propose an effective in-situ measurement method for source and load impedances measurements. This measurement method has to be easy to operate, duplicable and safe. The measurement equipment will be accessible for most of electric relevant laboratories and companies. Then, this research is aimed to find out the influences of different load and source impedances combinations on electrical parameters measurements such as current, voltage and power when they meet disturbances in the 2 k – 150 kHz range. As many as possible combinations need to be measured to simulate the situations that when different loads are connected with different power supplies. Furthermore, the question on whether this influence will affect some electrical devices such as smart meter needs to be concerned. The measurement results should be reported and explained to help other researchers in the further investigation in relevant aspects.

1.3 Thesis layout

Chapter 2 describes the measurement systems, the goals and challenges in details.
Chapter 3 presents some basic knowledge, analysis, characterization, transfer impedance measurements and modeling of different current probes.
Chapter 4 discusses two in-situ measurements of source and load impedance and their merits and shortcomings.
Chapter 5 presents the measurement results of source and load impedances from various supplies and loads respectively.
Chapter 6 investigates the disturbance influence on electrical parameters measurements and a smart meter.
Chapter 7 contains the conclusions and recommendations.

2 Methodological approach

2.1 Challenges

To investigate whether the resonance of source and load impedance will influence the electrical parameters measurements and whether it is the reason that causes the wrong reading for a smart meter, one appropriate noise source is necessary. This noise source needs to be able to inject 2 k – 150 kHz disturbances into the circuit under test. Besides, reaching the same amplitude of the noise signal on each frequency point is also necessary to simplify the analysis. Then, measuring source and load impedances at power-on situation needs to take into consideration the convenience and the safety, because this work needs to be accomplished with the grid connected. Therefore, finding an appropriate way to achieve the measurement is the most important step. Certainly, the selected method must be easy to install and manipulate, otherwise it is not be comparable to the normal measurement methods. At last, the measurement results should be transferred to computer to be processed. Thus, some software and subsequent programming may be needed.

2.2 Measurement systems

The main measurement system for the research of disturbance influence on smart meter as well as electrical parameters measurements is shown in Fig 2-1. It contains a signal generator used to inject noise, a power supply offering stable 230 V AC power, a reference meter which collects electrical parameters and transfers the data to a computer to analyze via a Labview platform, an electrical load and the EUT (e.g. smart meter). For the safety and convenience, current probe is selected as the noise injection instrument. In this case, an arbitrary waveform generator (AWG) is used as the noise source which is able to output the desired waveform uploaded from a computer. Fig 2-2 shows the injecting signal used in this test. It is an equal-amplitude multi-tone signal from 1 kHz to 150 kHz spaced 1 kHz and there is no significant signal above 150 kHz.

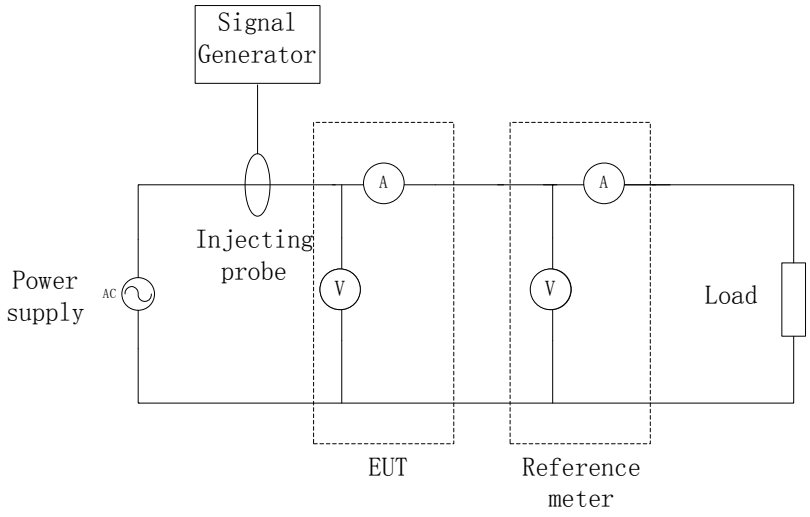

Fig 2-1 Main measurement system

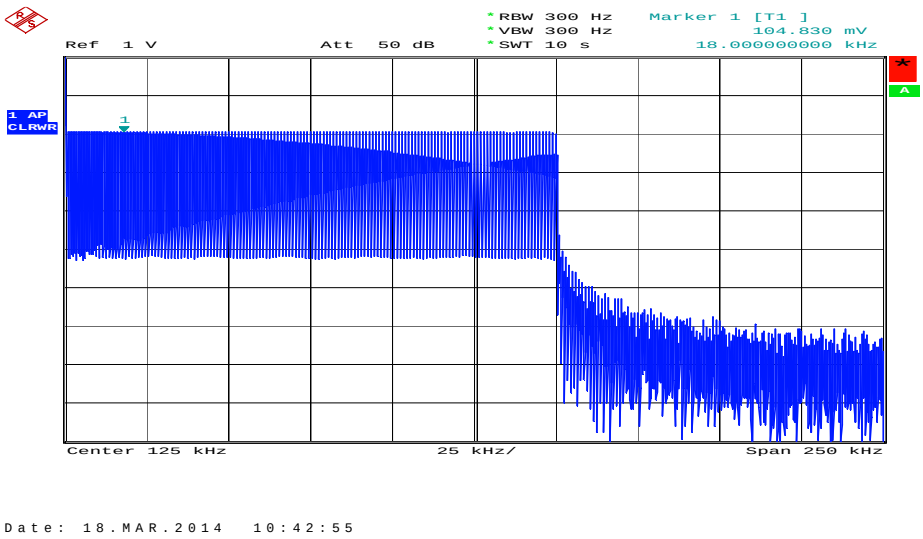

Fig 2-2 Injecting noise source

The interference is injected by the injecting probe and detected by the applicable receivers so that it is able to control the injection intensity. The smart meter is connected to the computer and the data will be received and analyzed using the applicable software. Then, other electrical parameters can be measured successfully with the “reference meter” and analyzed by the Labview platform.

Another measurement setup in this research is for the in-situ measurements of source and load impedances. In this part, current probes still play very important roles. As it is described in [20], a two-probe approach was validated to manage measuring of the noise source impedance at 150 kHz – 30 MHz. The basic setup consists of just two current probes, one signal generator and one spectrum analyzer as illustrated in Fig 2-3. The way to install a setup and collect the data is quite simple. Clamping two probes around the wire under test is easy and it is not necessary to interrupt the devices’ operation. Furthermore, it is galvanic isolated from the conductor to avoid electric shocks. For the reasons described above, the basic idea of this method using current probes to measure source and load impedance is applied to our measurements. However, the actual two-probe approach is used at frequency beyond 150 kHz. This means that some improvements are necessary to make this method applicable for the required frequency range.

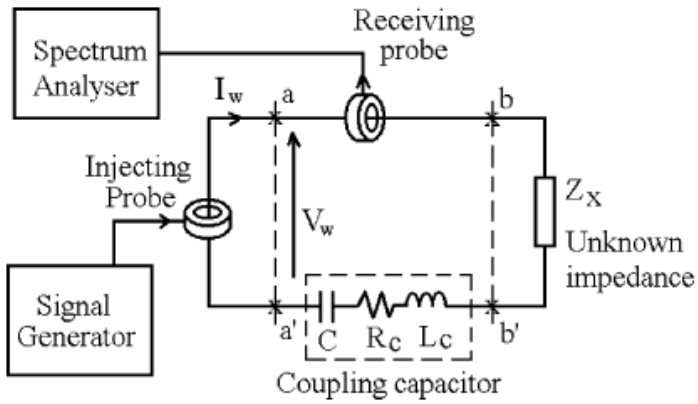

Fig 2-3 Basic setup of the two current probes approach

In fact, the method used in our research is called “three-probe” approach as Fig 2-4 illustrates. The difference between these two approaches is not only the addition of an extra current probe but also the changing of the analysis strategy. The signal is collected in time domain using a digitizer instead of being collected in frequency domain using a spectrum analyzer. By applying the circuit analysis, it is possible to find the relationship between the unknown impedance and two current probe measurements (detecting probe and receiving probe). The detailed characterization and mathematic deduction will be discussed in chapter 4.

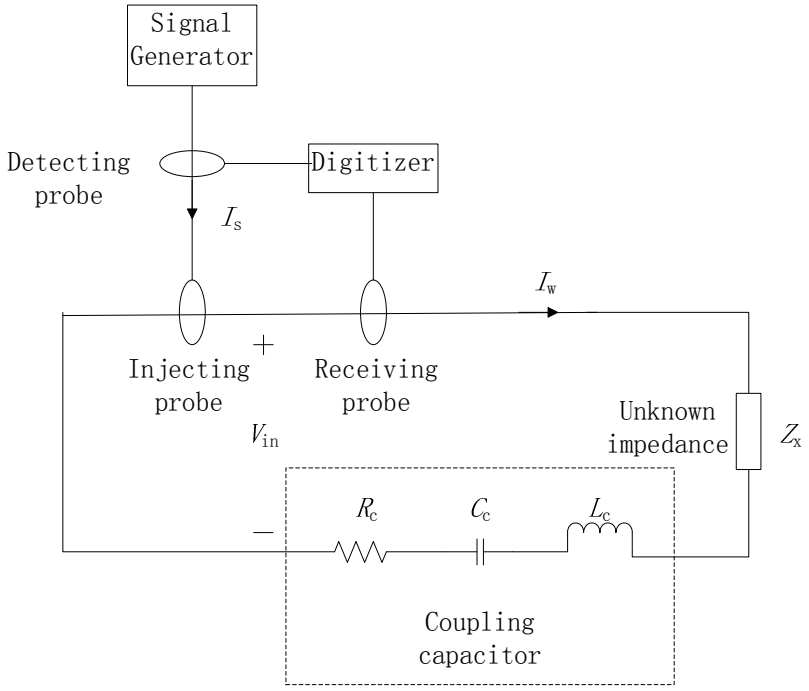

Fig 2-4 Impedance measurement system

To obtain a better understanding of the measurement circuit and find the way to solve the unknown impedance, accurate electric models for different probes are necessary. Therefore, a lot of effort has been paid to the current probe’s characterization and modeling. In this part, the spectrum analyzer and the VNA are both used as the signal receiver. Fig 2-5 illustrates the current probe measurement setup.

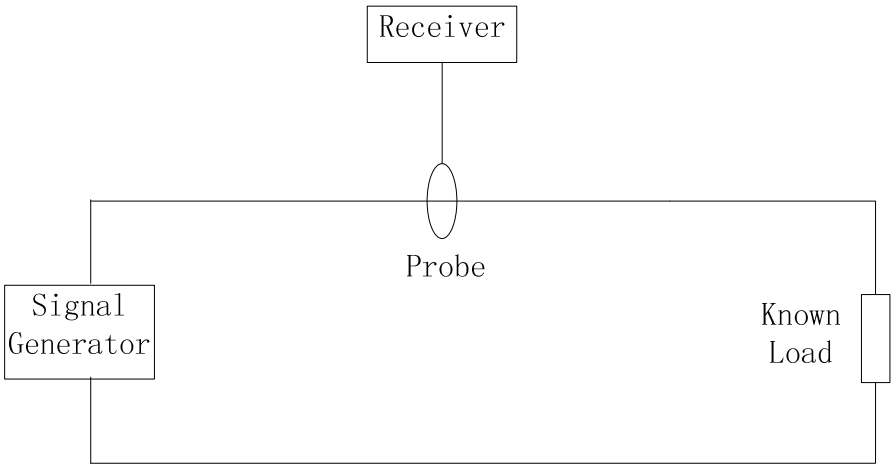

Fig 2-5 Current probe measurement system

3 Monitor probe and BCI probe analysis, modeling and characterization

The concept of measuring the magnitude of any unknown impedance using three current probes approach is proposed in chapter 2. As Fig 2-4 shows, in the setup, it involves an injecting current probe, a detecting probe and a receiving current probe. The functions of these three probes are just as their names indicate - injecting signal, detecting signal and receiving signal. However, as far as we know, there are two categories of current probes in the market, current monitor probes and bulk current injection probes. Both categories are widely applied to do the electric and magnetic measurements. Since the two different probes have distinctive properties which are significant for our further measurement and analysis, profound investigation of the properties of these probes is of importance.

In this chapter, four different current probes will be discussed in detail. First, a simple probe property test will be applied and we will find the measurement difference between using current probe and current shunt. Secondly, one of the most important parameters of a current monitor probe - transfer impedance - will be discussed, including the applicable fundamental knowledge, the testing method used, and a comparison with the data from a datasheet. Followed by the probes' SPICE model and verification based on previous information. Next, some specific discussions on the BCI probes will be given like electrical model and different transfer impedance test method. At last, several differences between the monitor probe and the BCI probe will be listed as a conclusion.

3.1 Current probe and current shunt

The idea of this experiment is to find a difference between using a current probe and a current shunt to measure the target current. By doing so, there will be a better understanding of current probe's property which is helpful for our further investigation.

3.1.1 Test setup

1. Power supply

Fig 3-1 Power supply

Model 108 AMX, as a member of Pacific Power's AMX series popular family of high performance Linear AC Power Sources, can offer a programmable output voltage (adding harmonics to test load impedance and influence to the load) with low distortion.

2. Current Probe ETS 94430-5

Fig 3-2 Current probe ETS 94430-5

Model 94430 Series Radio Frequency (RF) Current Probe is a clamp-on RF current transformer designed for use with Electromagnetic Interference (EMI) Test Receivers/Spectrum Analyzers, or with any similar instrument having a 50 Ω input impedance, to determine the intensity of RF current present in an electrical conductor or group of conductors. The circuit is that of a radio frequency transformer as illustrated below in Fig 3-3:

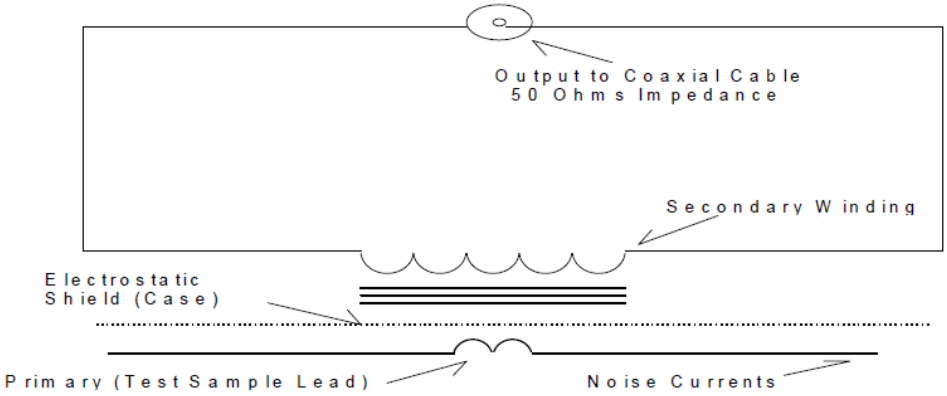

Fig 3-3 Basic current probe testing structure

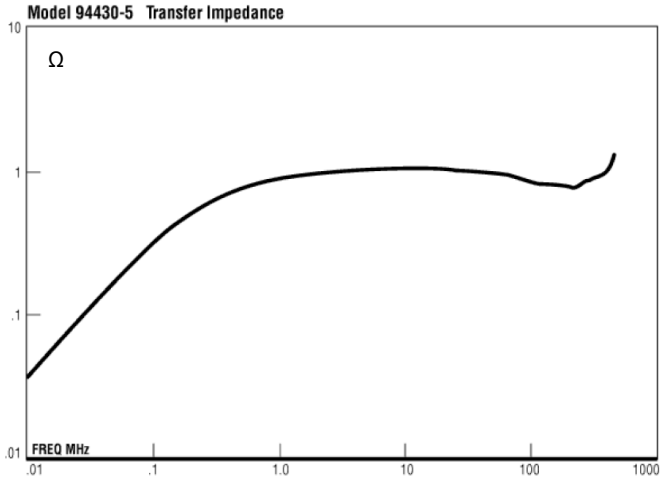

Fig 3-4 Typical transfer impedance variation with frequency for model 94430-5

3. Current shunt

The AC-DC current shunt provides a stable resistive property in the low frequency range. By measuring the voltage signal on the shunt, the current value can be obtained by simply applying Ohm's law.

Fig 3-5 Current shunt

4. NI PXI-1031DC

NI digitizer (NI5922, 24-bit resolution up to 500 ksamples/s, ranging to 16 bits at 15 Msamples/s) samples the voltage and current waveform in time domain. Subsequently the time domain information of signals will be sent to a computer to display or do further analysis like frequency domain conversion by using some analysis software such as Labview.

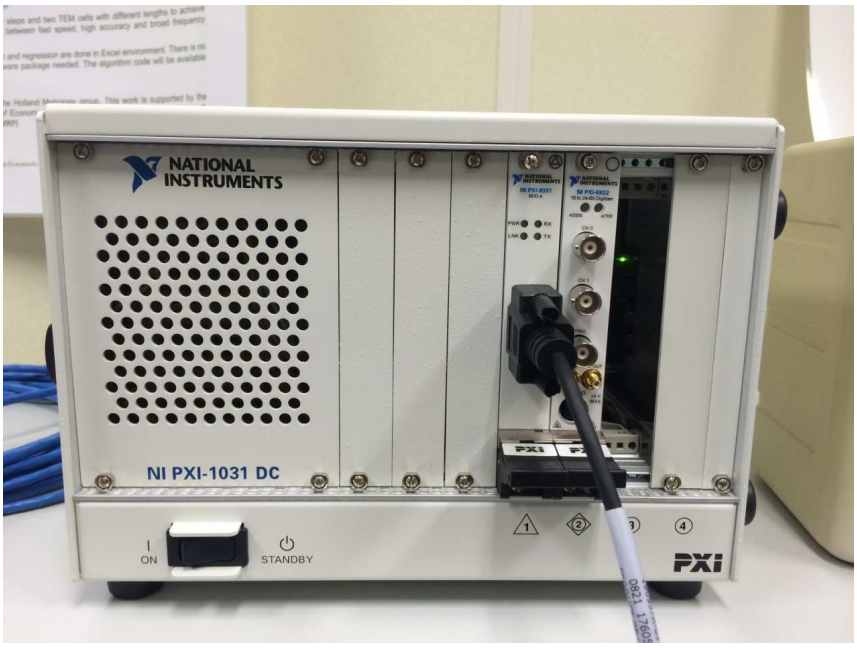

Fig 3-6 NI digitizer

3.1.2 Test circuit and results

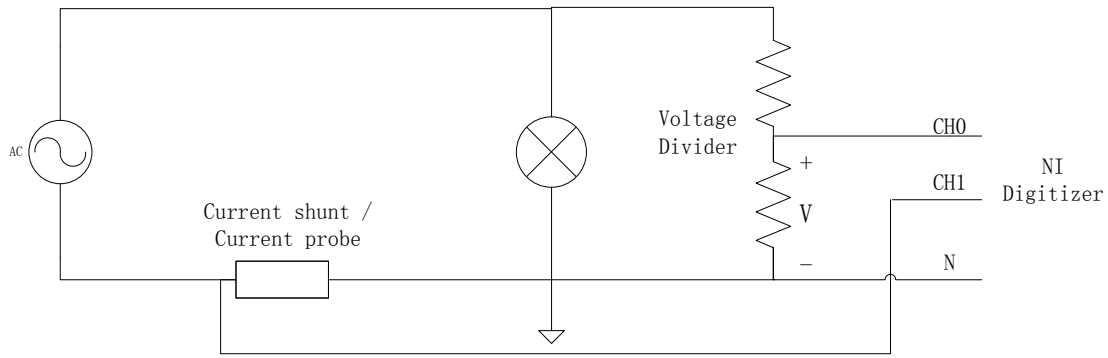

Fig 3-7 Current probe/shunt property test schematic

In this test, a nonlinear LED lamp is used as a load as shown in Fig 3-8. The NI digitizer samples the signals from the voltage divider and the current shunt/probe and then sends them to the PC where the sampled signals are analyzed via Fast Fourier Transformation (FFT). This process is executed by a Labview program platform. As a result, the frequency domain analysis will be presented.

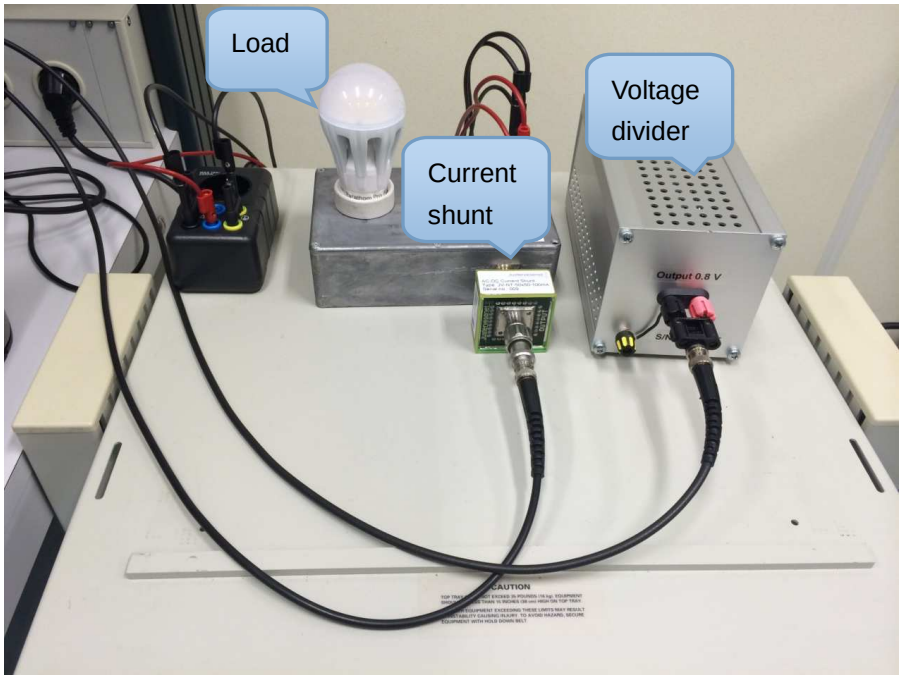

Fig 3-8 Current probe/shunt property test circuit

In Fig 3-9, an obvious difference to current measurements exists due to the variable transfer impedance (Z_t) of current probe. In this case, a constant Z_t was used in the program when testing both with the current shunt as well as with the probe. The value of Z_t is 0.028 Ω which as Fig 3-4 indicates is Z_t at 10 kHz. In such case when the program transfers voltage into current, it would treat the Z_t as a constant. This was true when current shunt was used. However, as Fig 3-4 demonstrates, the Z_t of this current probe is increasing linearly at this frequency range. So actually, when frequency is beyond nearly 10 kHz, the real Z_t is larger than applied in program. Higher current output is shown in the graph as a result according to Ohm's law. Similar things happen at frequencies below nearly 10 kHz. Therefore, when using

the current probe to measure the current, a correction factor is needed which is based on the exact Z_t variation. For this reason, obtaining an accurate Z_t variation curve is necessary.

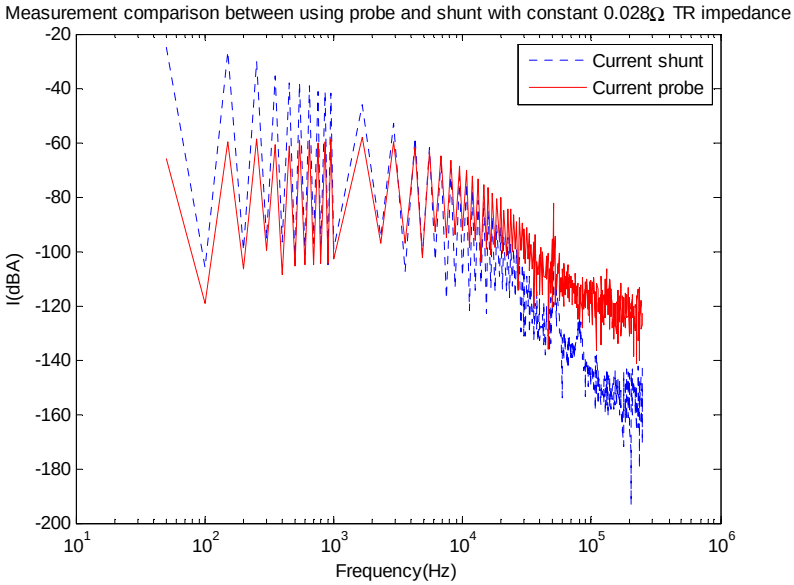

Fig 3-9 Results from using current probe and shunt

3.2 Transfer impedance measurement of monitor probes and their modeling

3.2.1 Basic theory of a current probe

Current probes are characterized by the parameter: “transfer impedance”, the ratio between the output voltage and the current flowing through the current probe. Since it is the ratio between voltage and current, the transfer impedance (Z_t) has units of ohms. But, one needs to note that the current in this case is not caused by the output voltage. It occurs in a different circuit.

Although the transfer impedance is measured in ohms, it is often plotted on a log-log scale such as presented in Fig 3-4. The unit of y-axis is normally labeled dBΩ. This is calculated by:

$$\text{dB ohms} = 20 \log (|Z_t|) \tag{3-1}$$

where $|Z_t|$ is the magnitude of the transfer impedance.

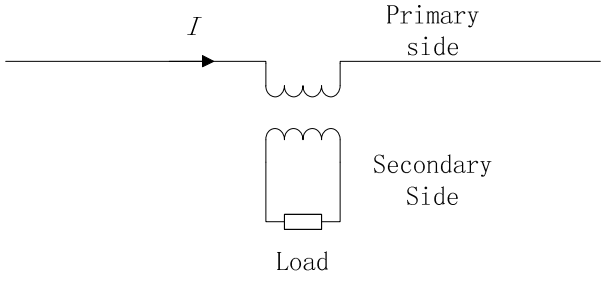

Fig 3-10 Simplified current transformer model

A current probe can be modeled as a current transformer as shown in Fig 3-10. The difference

is, in this case, the primary winding is a one-turn wire while the secondary winding is the coil around the probe core.

Fig 3-11 delivers us the Thevenin circuit of the secondary winding. The Thevenin equivalent voltage induced into the secondary winding is given by:

$$V_{\mathrm{s}} = M\frac{\mathrm{d}I_1}{\mathrm{d}t} = M\mathrm{j}\omega I_1 \tag{3-2}$$

Where $\omega = 2\pi f$ and M is the mutual inductance between the coil and the conductor through the probe.

Combined with Equation (3-2) and this equivalent circuit, the output voltage can easily be deducted by:

$$V_0 = M\mathrm{j}\omega I_1 \frac{Z_0}{Z_0 + \mathrm{j}\omega L_2} \tag{3-3}$$

Where V_0 is the output voltage delivered by the probe to the load and Z_0 is the load impedance, usually 50 Ω and L_2 is the self-inductance of the secondary side.

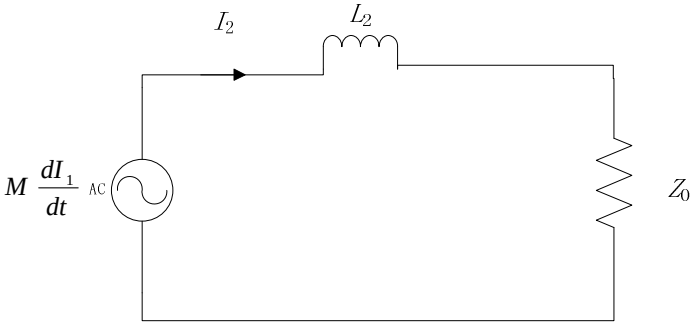

Fig 3-11 Thevenin equivalent circuit of secondary winding

By simply solving the Equation (3-3) for the transfer impedance Z_t, V_0/I_1, one yields the result:

$$Z_{\mathrm{t}} = \frac{\mathrm{j}\omega M}{1 + \mathrm{j}\omega L_2/Z_0} \tag{3-4}$$

Equation (3-4) shows that Z_t varies with frequency and can be divided into a low frequency part and a high frequency part with the boundary frequency F_c which leads to $\omega_{\mathrm{C}} L_2 = Z_0$ or $F_{\mathrm{c}} = \frac{Z_0}{2\pi L_2}$.

Below F_c, in the so called voltage region, Equation (3-4) can be reduced to:

$$Z_{\mathrm{t}} = \mathrm{j}\omega M \tag{3-5}$$

If M is constant, then the function of Z_t and frequency should be a monotonically increasing line. Equation (3-5) also tells us that the mutual inductance is the only factor that affects the performance of the Z_t at the lower frequencies.

Above F_c, in the so called current region, Equation (3-4) turns into:

$$Z_{\mathrm{t}} = \frac{M}{L_2}\mathrm{Z}_0 \tag{3-6}$$

As can be deducted from Equation (3-6), Z_t is constant at the higher frequency part when M and L_2 are both invariable.

3.2.2 Test setup

1. Signal generator

HP 33120A Function Generator is a versatile instrument capable of generating sine, square, and other waveforms with frequencies up to 15 MHz. The output resistance of the 33120A is 50 Ω, which means that we can model this device as an ideal internal voltage source with a 50-Ω resistor in series. Furthermore, it is able to inject – a user programmed signal into the generator, which makes this generator have wide application. Fig 3-12 gives the picture of HP 33120A in the lab.

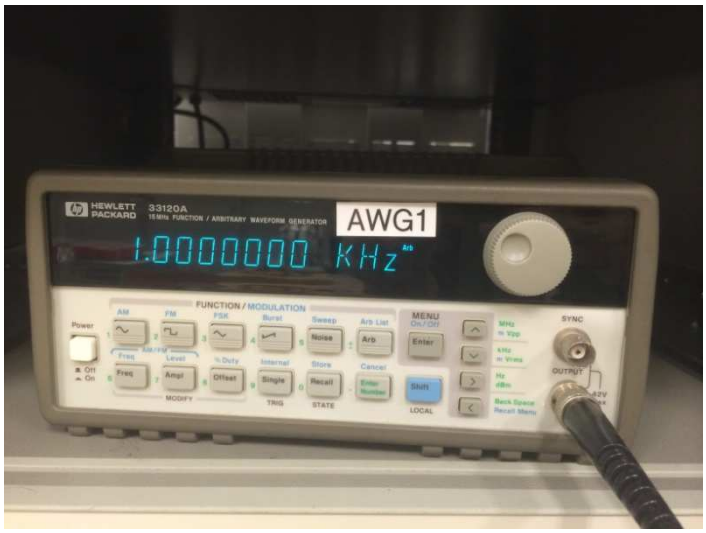

Fig 3-12 HP 33120A function generator

2. Spectrum analyzer

The Rohde & Schwarz (R&S) FSP40 spectrum analyzer is a wide band (9 kHz – 40 GHz), very sensitive receiver. The received frequency spectrum is slowly swept through a range of pre-selected frequencies, converting the selected frequency to a measurable DC level (usually logarithmic scale), and displaying the same on the screen. But there is a shortcoming that it can only show the magnitude information.

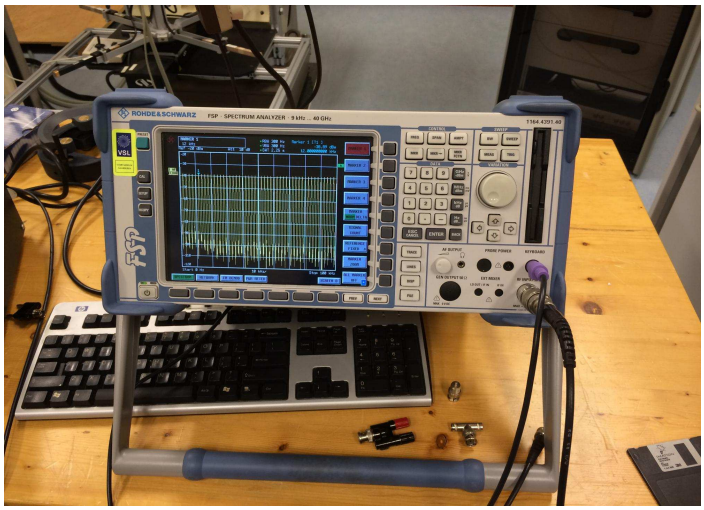

Fig 3-13 R&S spectrum analyzer

3. Vector network analyzer (VNA)

A VNA is a device which measures the *S* parameters of its two ports, Port 1 and Port 2. Usually, a VNA measurement result contains four *S* parameters. They are S_{11}, S_{12}, S_{21} and S_{22}, representation of forward reflection coefficient (input match), forward transmission coefficient (gain or loss), reverse transmission coefficient (isolation) and reverse reflection coefficient (output match) respectively, if we use Port 1 as injection port and Port 2 as output port. In this case, it is used to measure input/output impedance of probes as well as their transfer impedance at high frequency (above 300 kHz).

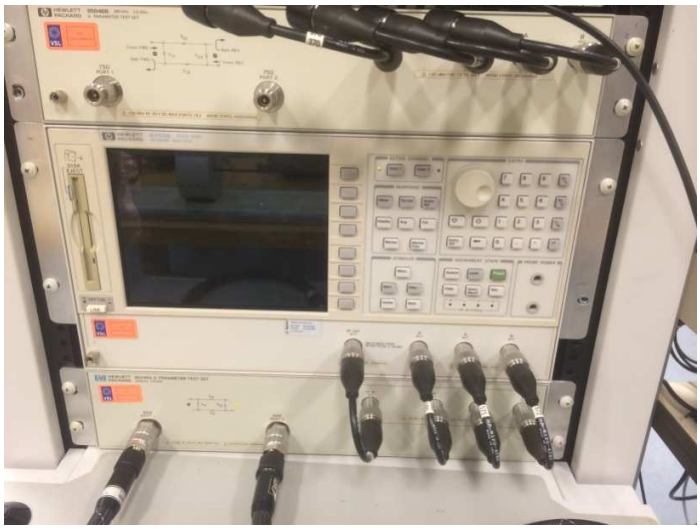

Fig 3-14 VNA

4. Calibration fixture (Jig)

Test jig is used to set current probes and its specific design can promise the impedance characteristic is as much as possible stabilized along the conductor at high frequency which is important to reduce the side effects.

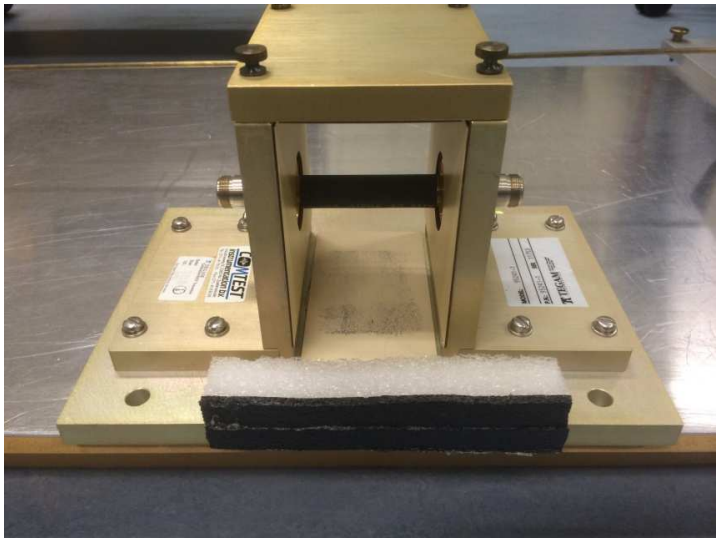

Fig 3-15 Jig

5. Monitor probes

There are 3 monitor probes in the experiment. One is Model 94430-5 used in section 3.2 as shown in Fig 3-2 and the two are both Fisher F75 probes. To distinguish between the two F75 probes, one of them was taped with a red mark and named “F75red” in the following text and the other one is still called F75 probe. Their pictures are shown in Fig 3-16.

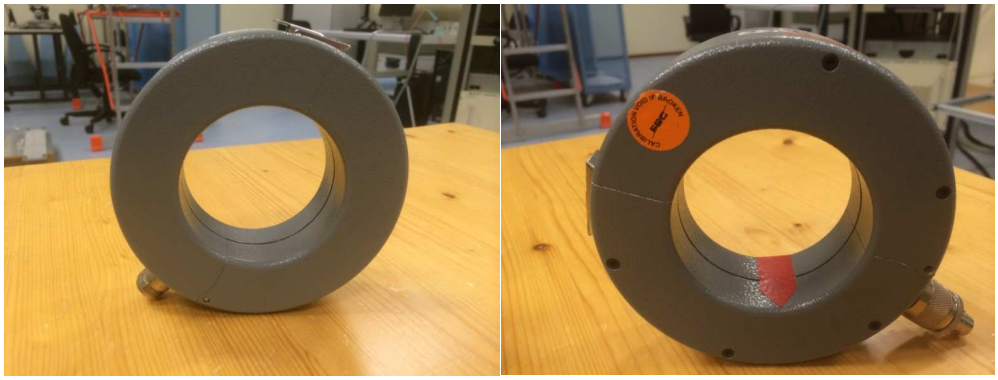

Fig 3-16 F75 (left) and F75red (right)

3.2.3 Test circuit

1. Low frequency (1 k – 150 kHz)

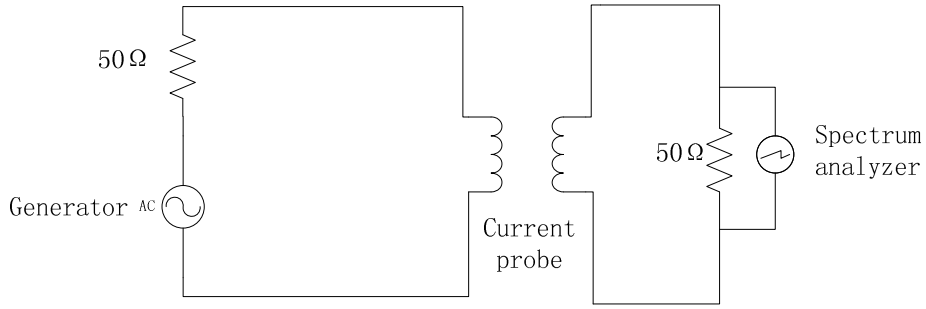

Fig 3-17 Transfer impedance measurement circuit at low frequency

For the low frequency test, the signal in Fig 2-2 is used as the source. By applying this signal, it is able to notice the current probe's response intensity at different frequency in the same time.

In Fig 3-17, on the primary side the current probe in clamped on a calibration jig to which a generator, is connected while the output port of the current probe is terminated by a spectrum analyzer on the secondary side.

What needs to be noticed is that the amplitude of the source is measured directly by spectrum analyzer. However, there are 50 Ω built-in impedances inside both the generator and the analyzer. Therefore, the direct measurement is just half of the actual open source value. This is clarified in the circuit shown in Fig 3-18.

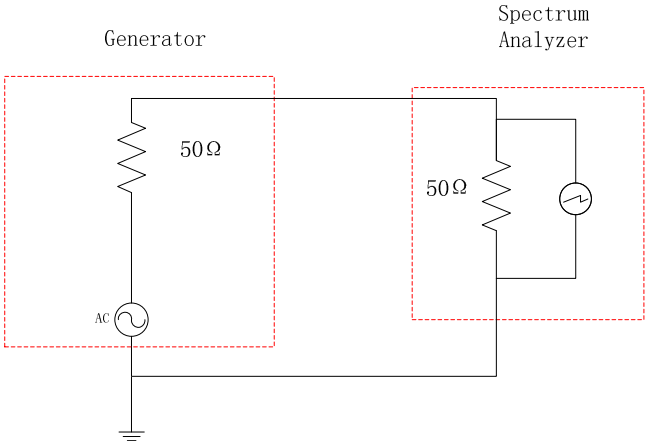

Fig 3-18 Source measurement circuit

According to the transfer impedance's definition, the ratio of between output voltage of the probe and the current on the conductor through the probe, spectrum analyzer is connected to output port to measure the amplitude of the voltage at 1 k – 150 kHz while generator injects signal into the conductor of the jig which goes through the probe under test. Fig 3-19 shows the measurement circuit and its implementation.

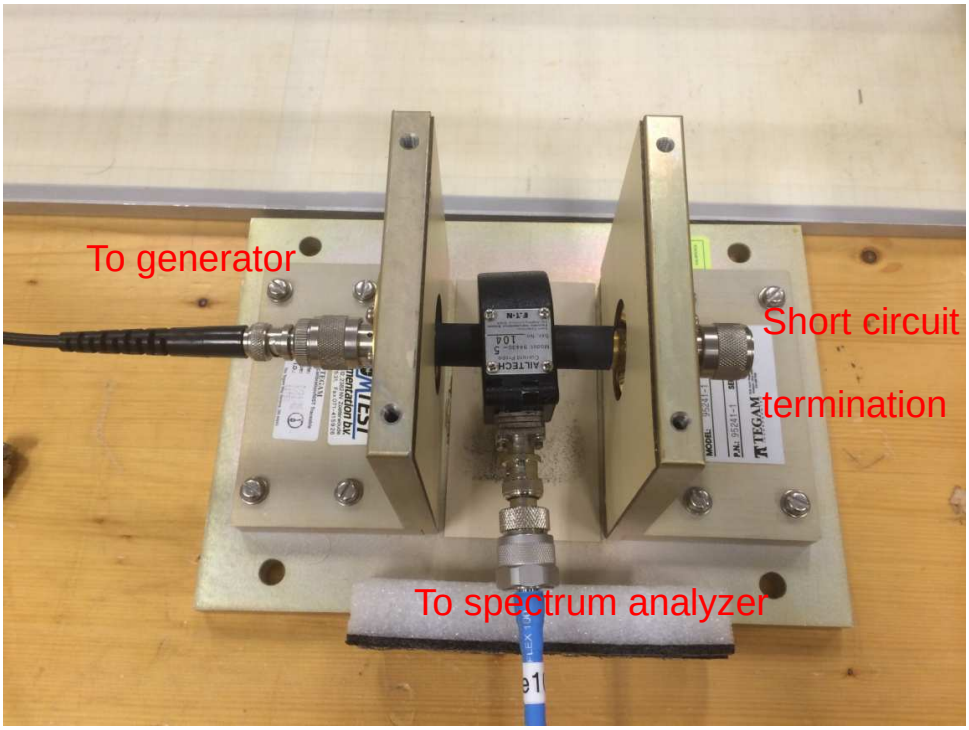

Fig 3-19 Implementation of Z_t measurement circuit at low frequency

2. High frequency (above 300 kHz)

Although this thesis mainly aims at the performances at 2 k – 150 kHz, high frequency analysis is also a good supplementary to examine our ideas on the probe's properties. Considering the frequency limitation of our source signal, in the thesis, the high frequency measurements were accomplished by VNA not spectrum analyzer.

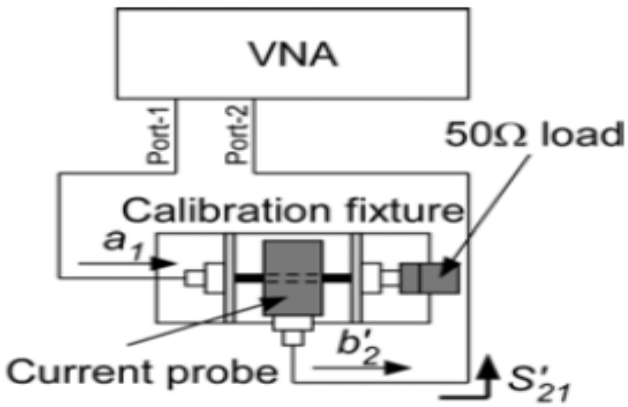

Fig 3-20 Zt measurement at high frequency

As shown in Fig 3-20, Port 1 injects signal into the conductor of calibration fixture (jig) and Port 2 receives the signal from probe's output. By making use of the definition of S_{21}, it is possible to figure out the transfer impedance of this probe.

3.2.4 Test results

As is described previously, measurements are divided into two parts, at low frequency and at high frequency. Therefore, the test results of each probe are also discussed separately.

1. Monitor probe Fisher F75

a) Low frequency

Based on the measurement approach, three steps are needed to obtain the transfer impedance. First, the value of injection voltage (V_{in}) from generator is required. This can be done by making use of circuit shown in Fig 3-18. But the value that spectrum analyzer displays (V_d) is half of V_{in} (V_d= V_{in}/2). Then another circuit as Fig 3-17 shows needs to be applied to find the probe output voltage (V_p). At last, the transfer impedance can be deducted by:

$$Z_t = \frac{V_p}{2V_d} Z_{SA} \tag{3-7}$$

where Z_{SA} is the built-in spectrum analyzer impedance, 50 Ω in this case.

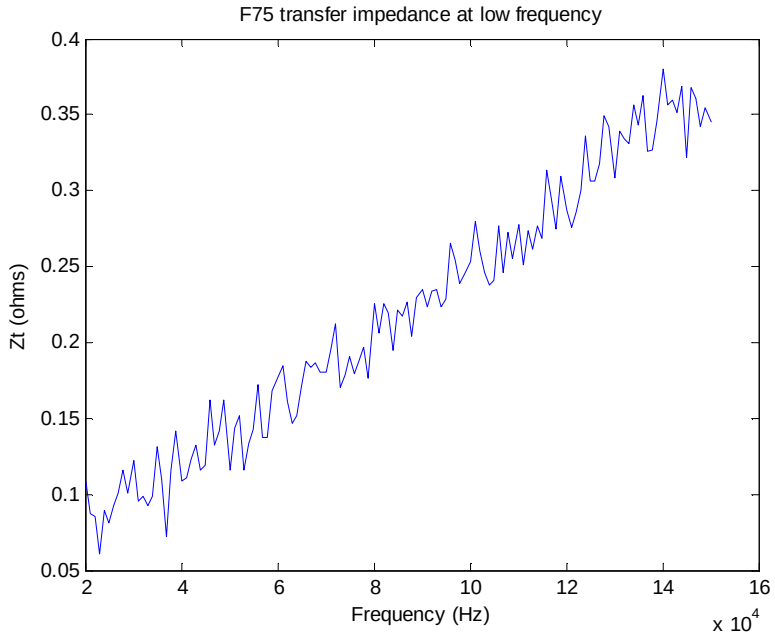

Fig 3-21 Z_t of F75 at low frequency

As Fig 3-21 illustrates, Z_t is a linearly increasing line with some fluctuations at low frequency, which is just as Equation (3-5) indicates. The fluctuations are inevitably caused by the background noise of spectrum analyzer which is also the reason that data starts at 20 kHz.

b) High frequency

As it has been demonstrated before, Z_t at high frequency is measured by VNA. From VNA, the ratio of V_p to V_{in} (voltage of Port 2 to Port 1) is indicated by the S_{21} in the unit of dB. In Fig 3-22, Z_t is V_p/I. To calculate current (I), Ohm's Law is used wherein I=V_{in}/50. So Z_t is therefore:

$$Z_t = \frac{V_p}{I} = \frac{V_p}{V_{in}} \times 50 \tag{3-8}$$

where Z_t is in units of ohms (Ω).

Z_t is often expressed in dBΩ . This can be accomplished by taking 20log of each side of the

above equation:

$$20\log(Z_t) = 20\log\left(\frac{V_p}{I}\right) \tag{3-9}$$

where 20 log (Z_t) is now in units of dBΩ

$$20\log(Z_t) = 20\log(V_p) - 20\log(I)$$

$$20\log(Z_t) = 20\log(V_p) - 20\log(V_{in}) + 20\log(50)$$

finally,

$$20\log(Z_t) = 20\log(V_p) - 20\log(V_{in}) + 34\text{dB}$$

or

$$20\log(Z_t) = S_{21} + 34\text{dB} \tag{3-10}$$

We see from the result above that 34 dB needs to be added to the S_{21} measurement made by the network analyzer if S_{21} is measured in dBV.

If we consider the case of a current probe that has a transfer impedance Z_t of 0 dBΩ (or 1 Ω in non-dB terms), the initial measurement from the network analyzer for S_{21} as described above would show a ratio of -34 dB. The 34 dB correction noted above would then be added to result in a Z_t of 0 dBΩ.

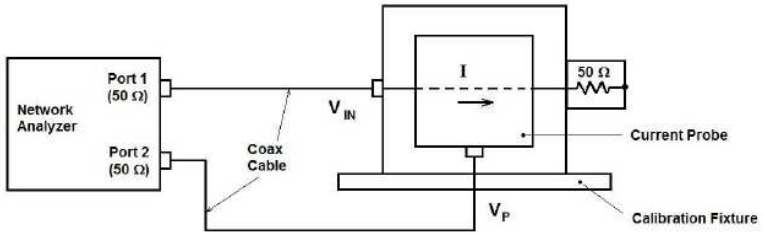

Fig 3-22 Z_t test structure via VNA

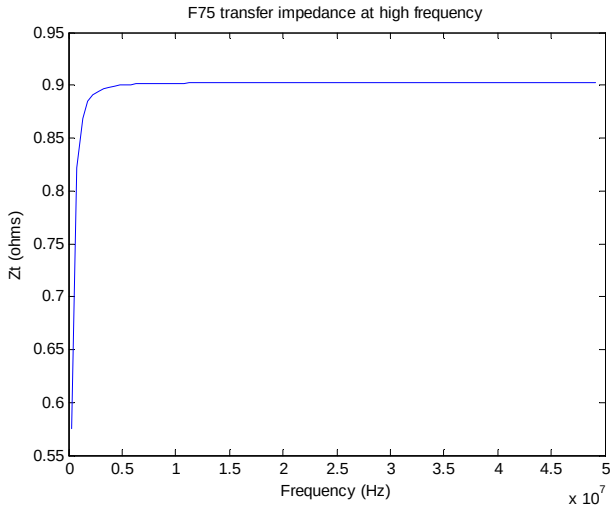

Fig 3-23 Z_t of F75 at high frequency

In this case, the transfer impedance has been represented in units of ohms via the reverse

transformation as mentioned above and the results are shown in Fig 3-23. Z_t stays constant (0.9 Ω) beyond 5 MHz which is just as Equation (3-6) denotes it would be.

2. Monitor probe Fisher F75red

a) Low frequency

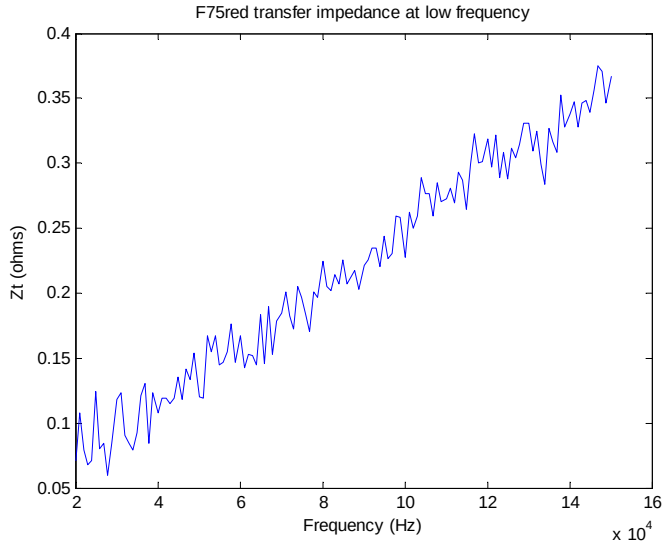

Fig 3-24 Z_t of F75red at low frequency

b) High frequency

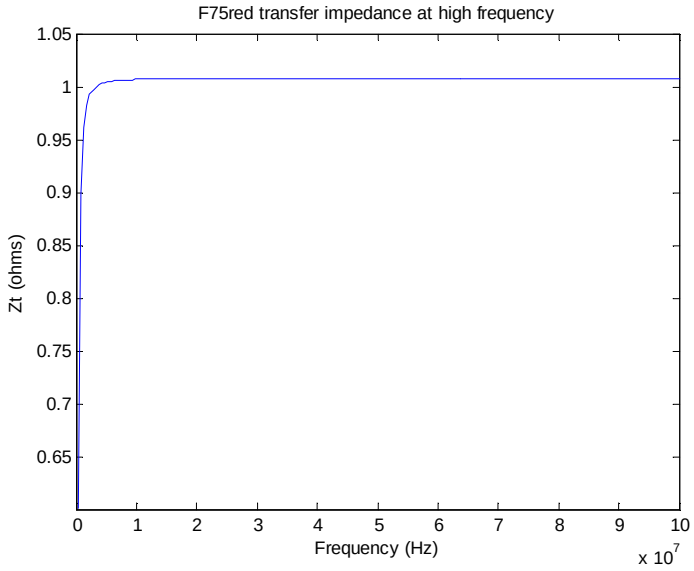

Fig 3-25 Z_t of F75red at high frequency

Obviously, F75 and F75red have similar performance, which is acceptable for they share the same product type. However, if we put Fig 3-23 and Fig 3-25 together, we would find that the values of Z_t in their current regions are not overlapping.

For current probes employing a magnetic core, the following relationship for the mutual inductance, M, holds:

$$M = k\sqrt[2]{L_1 L_2} \tag{3-11}$$

where k is the coupling coefficient, L_1 is the inductance of the primary (wire or conductor)

and L_2 is the inductance of the secondary (probe).

Then by substituting M from Equation (3-11) into Equation (3-6), it yields:

$$Z_t = \frac{M}{L_2} Z_0 = k^2 \sqrt{\frac{L_1}{L_2}} Z_0. \tag{3-12}$$

According to the theory of transformer, the inductance ratio equals to the square of turns ratio. Since L_1 represents the wire passing through the center of the current probe and usually represents one turn. Therefore Equation (3-12) can be written as:

$$Z_t = k \frac{Z_0}{N_2} \tag{3-13}$$

where N_2 is the turns number of the probe.

For our situation, load (Z_0) and turns number (N_2) are the same in both cases. Therefore the only variable becomes the coupling coefficient. It is the different k which may be caused by manufacturing deviations that result in the distinct performances at current region for these two “same” current monitor probes.

3. Monitor probe ETS 94430-5

a) Low frequency

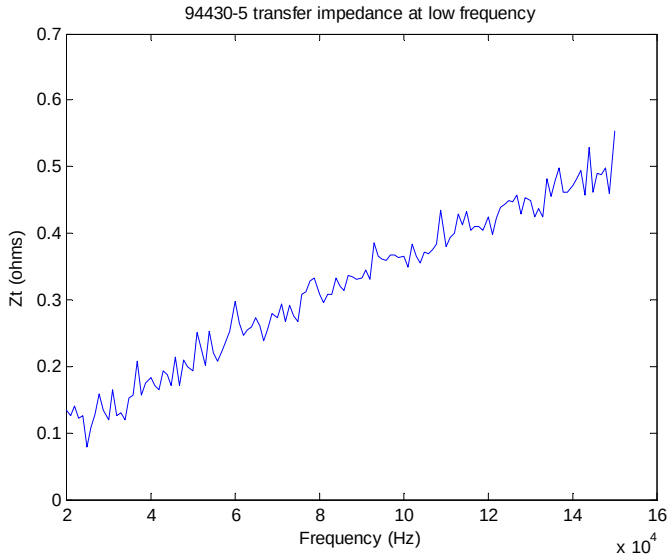

Fig 3-26 Z_t of 94430-5 at low frequency

Compared with F75, the higher slope resulted from higher mutual inductance and lower fluctuations caused by higher response intensity that spectrum analyzer receives from probe which implies that probe 94430-5 has better properties at the lower frequencies.

b) High frequency

According to Equation (3-6), in the current region, the transfer impedance should stay steady also as the datasheet shows it would be in Fig 3-4 while for this probe under test it turns out that it cannot hold true anymore. Instead, the Z_t reduces slowly from the peak slightly over 1 Ω at nearly 10 MHz to 0.85 Ω at 100 MHz.

Equation (3-6) which is derived from Equation (3-4) holds true only when the probe can be treated as an ideal current transformer. In other words, it does not take the stray parameters into account. When the stray parameters are insignificant when compared with their main parameters, the equation works quite well like in F75. However, in this case, the

volume of ETS 94430-5 is much smaller than F75 so that the stray capacitors between windings would be much larger in turn. Therefore, it would be more complex to some extent to model this current probe than the previous two.

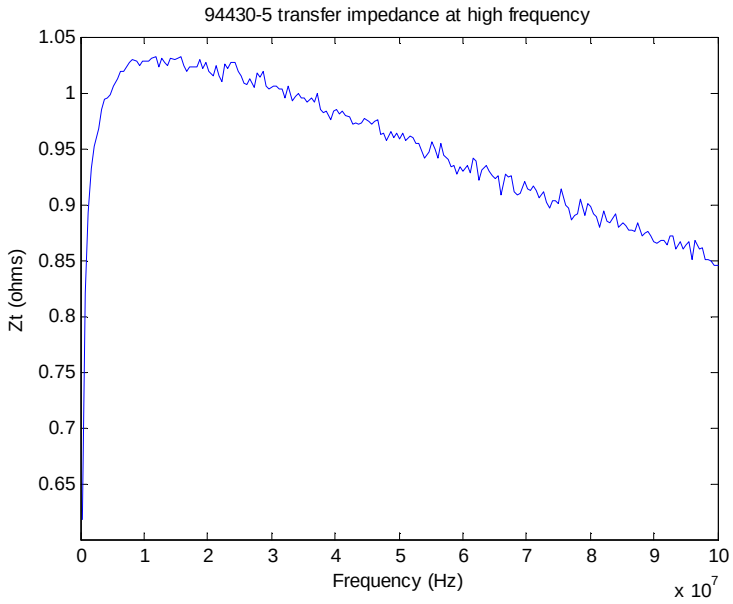

Fig 3-27 Z_t of 94430-5 at high frequency

3.2.5 Modeling

SPICE models for each of these probes are built according to the measurement results of their transfer impedances. The basic idea of building a SPICE model is following the current transformer's model then set the parameters relying on the experiment tools' property and test results. Combined with Equation (3-5), the mutual inductance can be calculated from the low-frequency Z_t curve's slope. Then using Equation (3-4) and some mathematic strategies, it is possible to solve the inductance of the secondary side. At last, applying Equation (3-11) and (3-13), the rest of the main parameters can be confirmed.

1. Modeling monitor probe F75

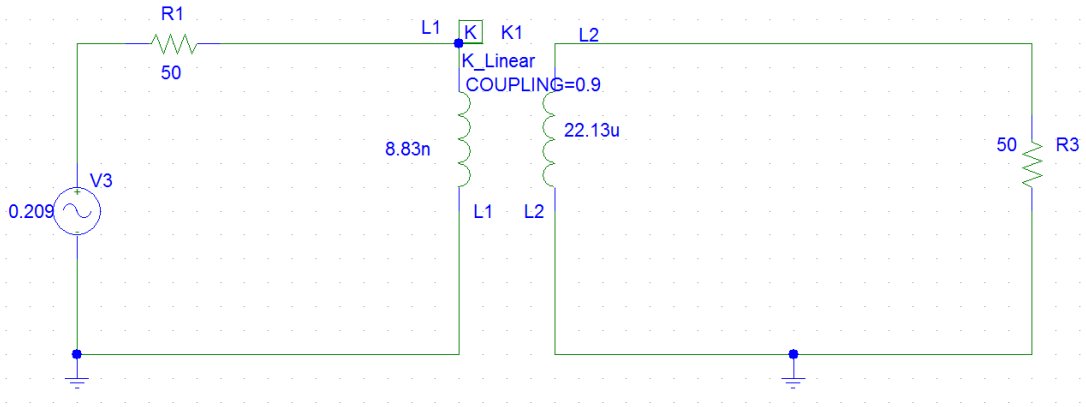

Fig 3-28 SPICE model of F75

In this model, R_1 represents the built-in impedance of signal generator while R_3 is referring to the impedance inside spectrum analyzer. L_1 and L_2 are the self-inductances of the primary and secondary side respectively.

The value of each parameter can be calculated as follows:

1) adding a trend line for the low-frequency Z_t curve and confirming the slope of the trend line which is equaling to $2\pi M$,

2) setting the coupling coefficient according to high-frequency Z_t curve and Equation (3-13), 0.9 in this case,

3) using Equation (3-4) as a function of frequency, by changing L_2, to solve a curve closest to the high-frequency curve,

4) and calculating L_1 based on Equation (3-11).

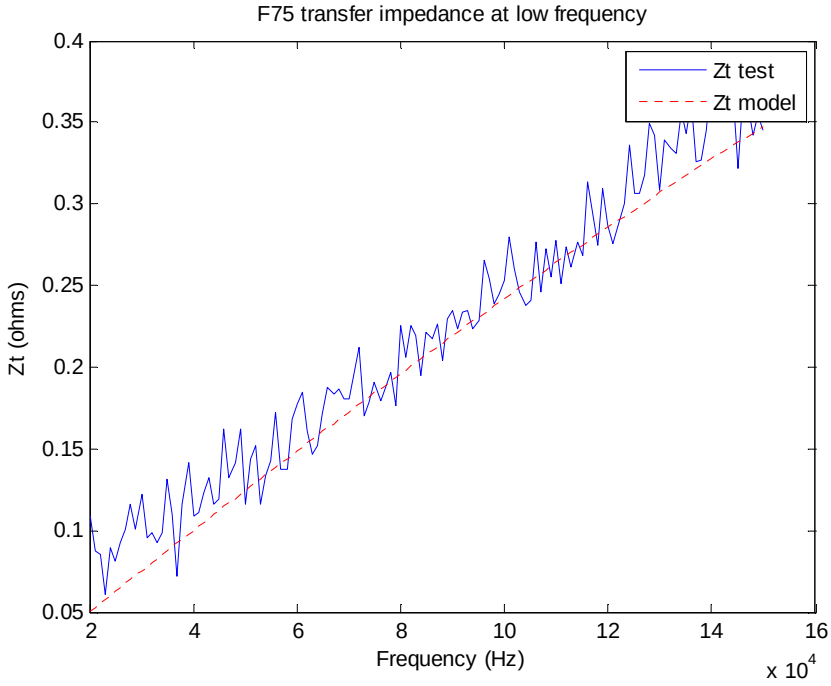

Fig 3-29 F75 Z_t comparison at low frequency

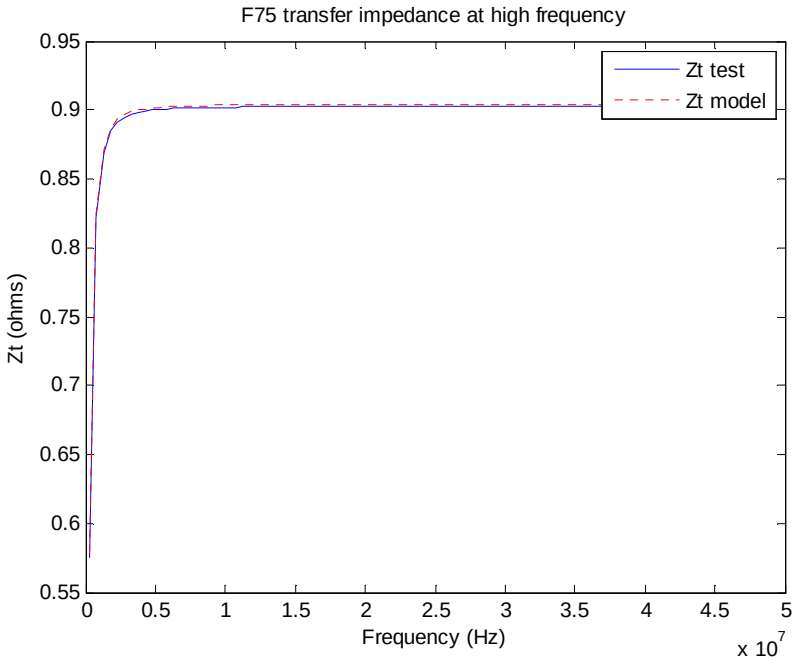

Fig 3-30 F75 Z_t comparison at high frequency

2. Modeling monitor probe F75red

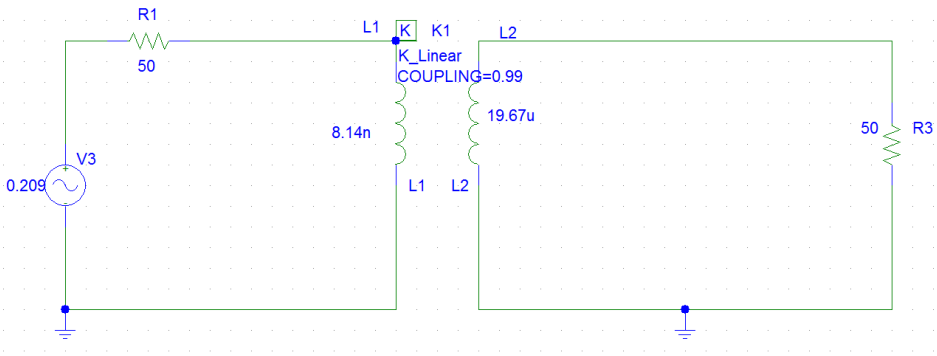

Fig 3-31 SPICE model of F75red

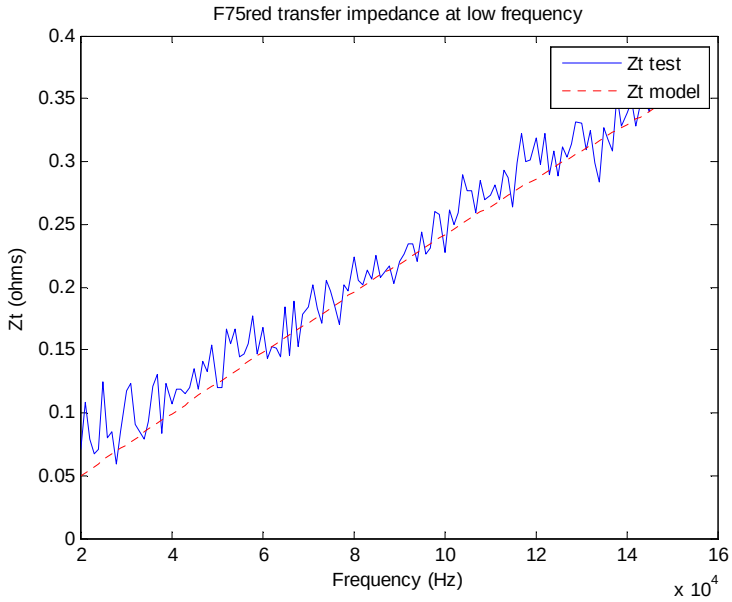

Fig 3-32 F75red Z_t comparison at low frequency

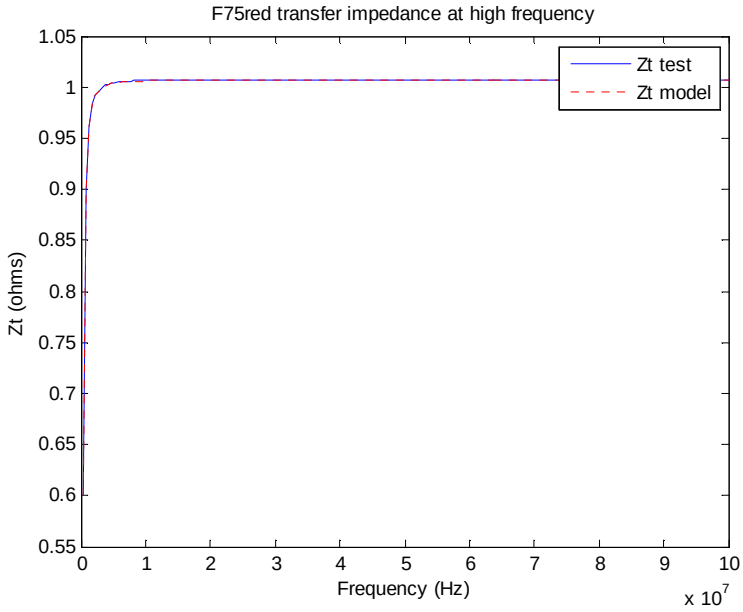

Fig 3-33 F75red Z_t comparison at high frequency

The difference is that F75red has a higher coupling coefficient which results in the different

value of L_1 and L_2.

3. Modeling monitor probe ETS 94430-5

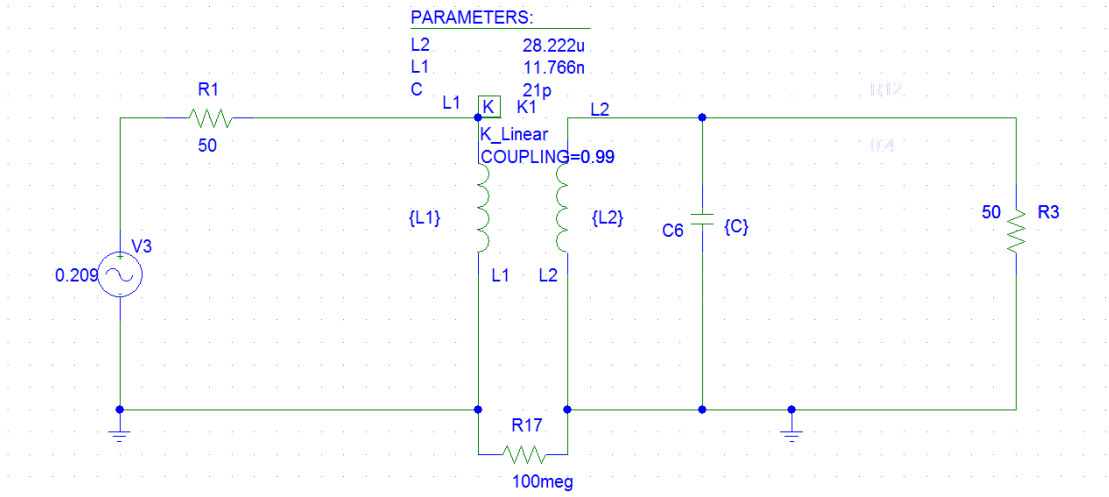

Fig 3-34 SPICE model of ETS 94430-5

Fig 3-34 illustrates the SPICE model of ETS 94430-5. Except for the different values of inductances, a capacitor acting as the stray capacitor between windings is added on the secondary of this circuit. For the reason of existence of this capacitor, at high frequency, it adds a parallel current route bypassing the load. Furthermore, this effect will enhance with the increase of frequency. Therefore, with gradual reduction of output voltage, the transfer impedance will fall as well.

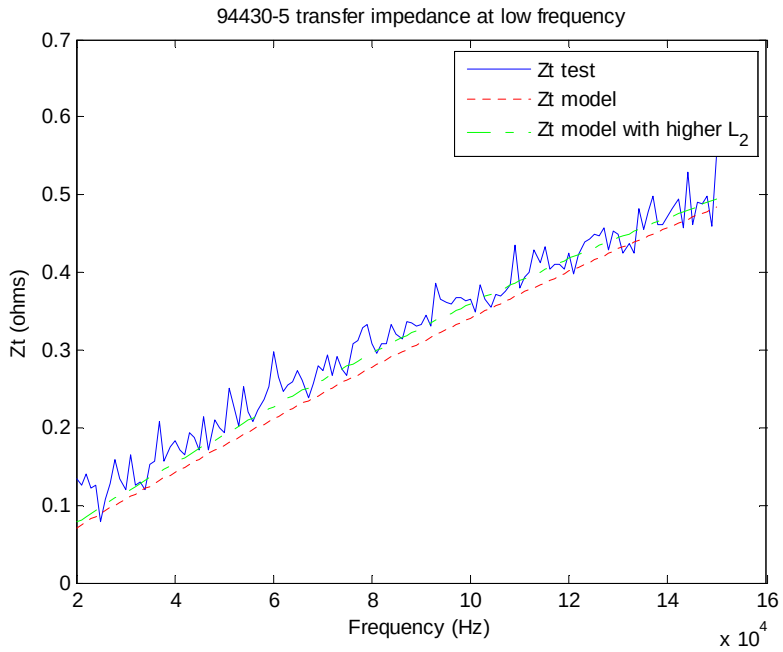

Fig 3-35 ETS 94430-5 Z_t comparison at low frequency

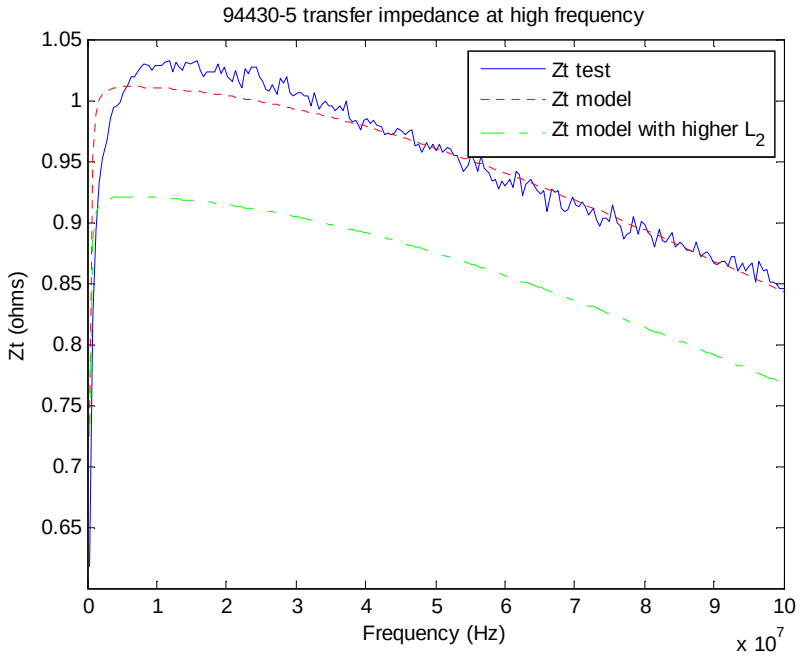

Fig 3-36 ETS 94430-5 Z_t comparison at high frequency

In the Fig 3-35 and Fig 3-36, curve "Z_t model" means it uses the value calculated following the process mentioned in section "Modeling monitor probe F75" while the curve, "Z_t model with higher L_2", is just using higher L_2 (34 μH) in the model. As we can see from Fig 3-35, higher L_2 gives the better simulation results at low frequencies. But, in the meanwhile, it reduces matching at high frequencies as shown in Fig 3-36.

The reason leading to this situation is that, as we discussed before, the current probe is essentially a transformer with a magnetic core inside. A probe or transformer's performance is highly depending on the core material, because the permeability of a magnetic core can be significantly distinct according to different type of magnetic material. What's more, there are lots of factors that can cause influences on permeability such as temperature and pressure. Then, in this case, the most significant factor is frequency. As Fig 3-35 and Fig 3-36 display obviously, the inductance reduces with frequency. From the basic inductance theory, both the self inductance and mutual inductance are proportional to the permeability as Equation (3-14) and Equation (3-15) describes below:

$$L = \frac{\mu N^2 A}{l} \tag{3-14}$$

and

$$M = \frac{k\mu NA}{l} \tag{3-15}$$

where μ is the permeability, k is coupling coefficient and N is the number of turns on the secondary side, A is the cross area of core and l is the average magnetic loop length. Although in our case, it is difficult to identify the cross area and loop length of the core, yet the trend of the inductance can also represent the variation of the permeability.

This situation also illustrates the shortcomings of modeling a non-linear magnetic component by SPICE. Therefore, in the future section, BCI modeling, one different modeling method using MATLAB will be discussed in detail.

3.3 Transfer impedance of BCI probe and its modeling

3.3.1 Test setup

Except for the same test setups as what have been used in monitor probe test such as VNA, spectrum analyzer, signal generator and calibration fixture, there are other special setups applied for some special purposes.

1. BCI probe CIP 9136A

The CIP 9136 probe (as Fig 3-37 shows) allows wide band performance from 10 kHz - 400 MHz, and above. The CIP 9136 core material is highly efficient and thermally rugged, thus allowing very high injected levels to be achieved with lower RF input power levels. Furthermore, the probe has 1:1 turn ratio so that the injection efficiency can be much higher than the normal current monitor probes.

Fig 3-37 BCI probe CIP 9136A

2. Impedance analyzer

1) QuadTech 7600 Precision LCR Meter

The 7600 Precision LCR Meter is an automatic, user programmable instrument for measuring a wide variety of impedance parameters. The 7600 covers a frequency range from 10 Hz to 2 MHz with basic measurement accuracy of 0.05%.

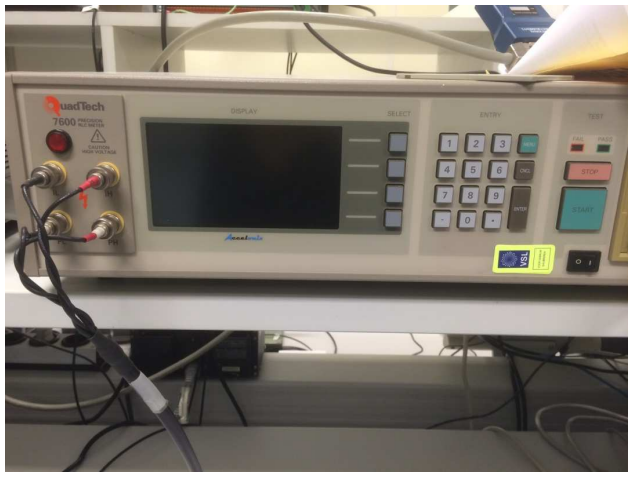

Fig 3-38 QuadTech 7600 precision LCR meter

2) Agilent E4980A Precision LCR Meter

The Agilent E4980A is a general-purpose LCR meter for inspection of incoming components, quality control, and laboratory use. The E4980A is used for evaluating LCR components, materials, and semiconductor devices over a wide range of frequencies (20 Hz to 20 MHz). It leads to better results compared with QuadTech 7600.

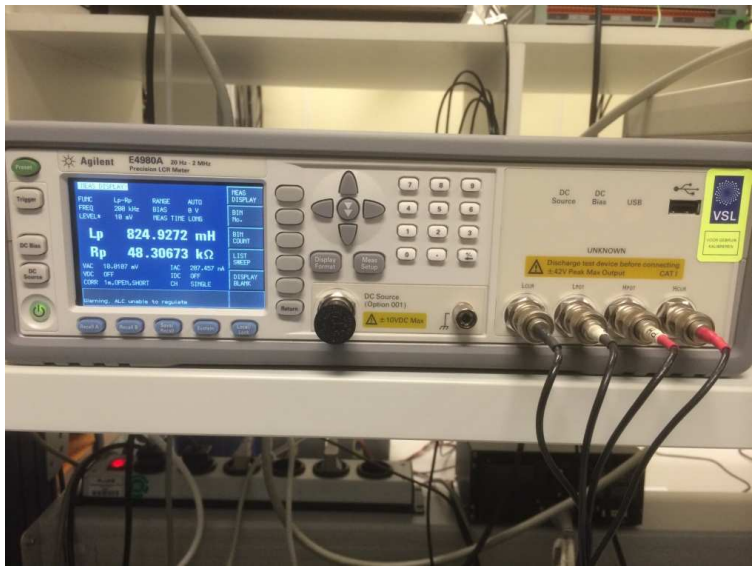

Fig 3-39 Agilent E4980A precision LCR meter

3.3.2 Transfer impedance test

1. Test circuit

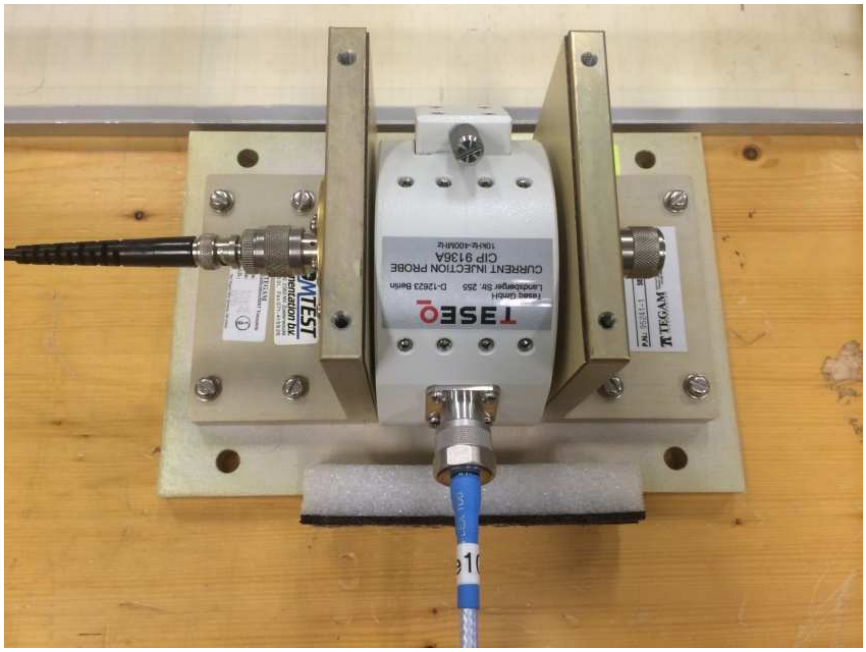

Fig 3-40 Implementation of Z_t measurement of BCI probe

The transfer impedance test circuit is the same as monitor probe's test. It is also accomplished separately by using signal generator and spectrum analyzer at low frequency and VNA at high frequency. The strategy of calculation is also similar as before.

2. Test results

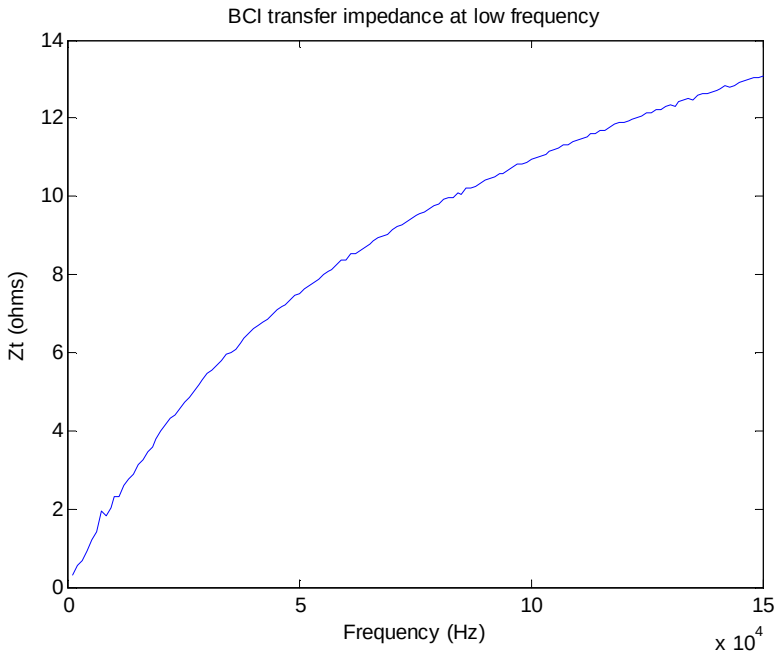

Fig 3-41 Z_t of BCI at low frequency

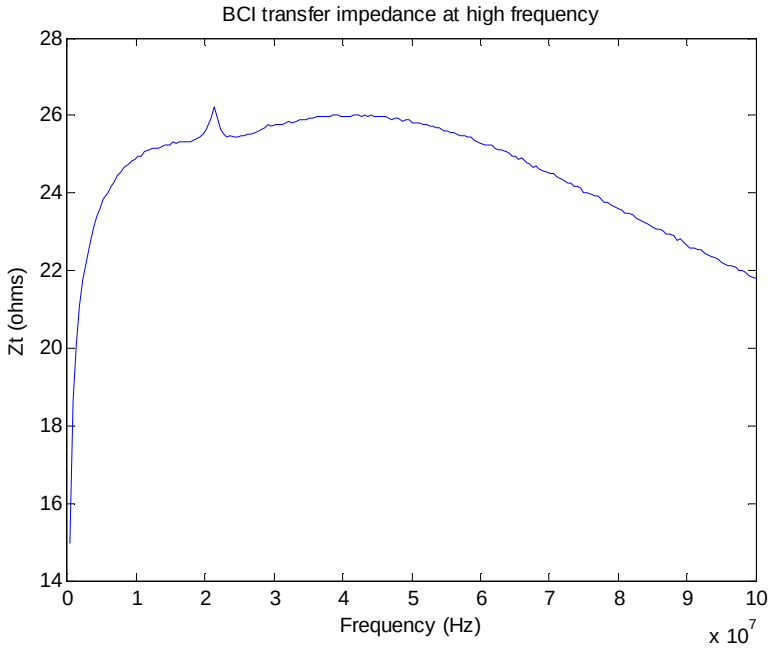

Fig 3-42 Z_t of BCI at high frequency

Fig 3-41 and Fig 3-42 illustrate the test results. Two important points obtained from these results are:

1) a gradual reduction of the slope of the low-frequency response, and

2) a transfer impedance at current region of near 25 Ω if ignoring the influence of the stray capacitor as is discussed before.

Regarding to the first fact - this is due to the decrease of permeability of the magnetic core as we discussed at ETS 94430-5 measurement.

For the second result, using Equation (3-13), it yields that the number of turns on the secondary side is 2. Therefore the turns ratio for this BCI probe should be 1:2. However, the truth is that the turns ratio is 1:1 according to the datasheet and confirmation from the employee of the manufacturing company. This means that our measurement method is not suitable anymore for this probe and it needs to be corrected.

3. Error analysis

Our measurement method was verified to be effective when we applied it to monitor probe. However, when it comes to BCI probe, the magic just fades away. To understand the reason behind this situation, one needs to distinguish between monitor probe and BCI probe. However their operating principles are the same – current transformer. Therefore the only difference can come from its manufacturing construction. When applying Equation (3-13) to the monitor probes, this leads to the number of the turns is 50, which means the turns ratio is 1:50.

Fig 3-43 is the equivalent current probe operating circuit. From this circuit, the transfer impedance is the ratio between V_0 and I_s depending on its definition. According the previous conclusion, Z_t can be derived by:

$$Z_t = \frac{V_0}{V_s} Z_s \tag{3-16}$$

However, Equation (3-16) is only effective for monitor probes not BCI probes.

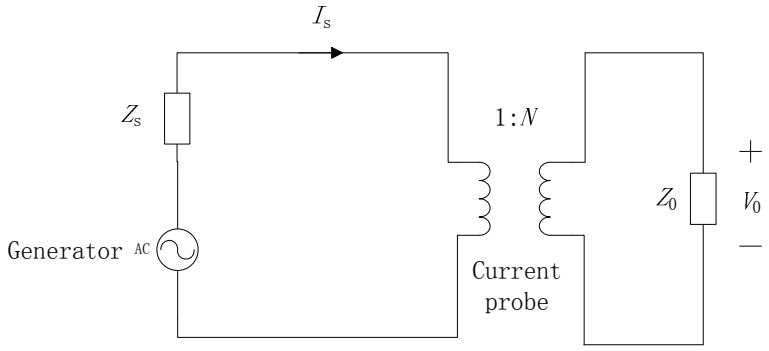

Fig 3-43 Equivalent current probe operating circuit

Applying the theory of transformer, Fig 3-43 can be redrawn into so called “T equivalent circuit” as Fig 3-44 illustrates.

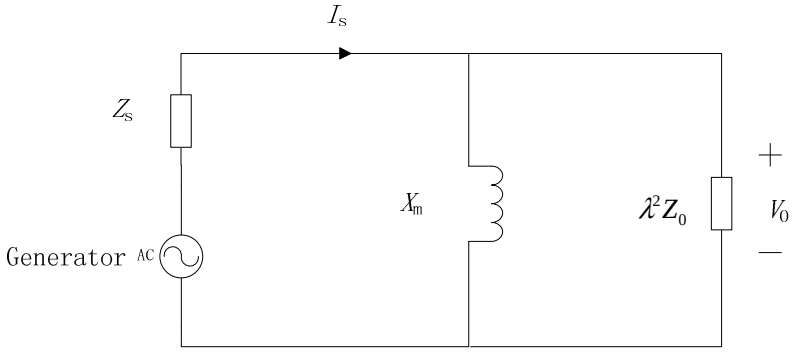

Fig 3-44 T Equivalent current probe operating circuit

In Fig 3-44, λ is referring to the turns ratio of the primary to the secondary, 1/N in this case. For monitor probes, the value of λ is 1/50, so ignorance of the secondary effects is no big deal. However, when the situation comes to the BCI probe where λ equals to 1, the load on the

secondary side will make a big difference for the input impedance on the first side so that it will result in a different I_s leading to a different transfer impedance. Therefore, to obtain a more accurate Z_t response, a correction factor needs to be considered.

4. Correction

To obtain the correct Z_t, the accurate input impedance of the primary needs to be confirmed. Before measurement, to verify our analysis, the following measurements were executed.

Fig 3-45 Implementation of Z_{in} measurement

As Fig 3-45 shows, a one-turn coil is added and the port of this coil is connected with impedance analyzer or a port of VNA depending on the test frequency range. To simulate the measurement situation, the output port of the BCI probe is terminated by a 50 Ω resistor. Besides, to make a comparison with other situations, the BCI port was also set to open circuit and short circuit. One group of test results, S_{22} reflection coefficients, by VNA is illustrated in Fig 3-46. Compared with short circuit case, a 50 Ω load on the secondary makes a difference on the primary input reflection coefficient so as the input impedance.

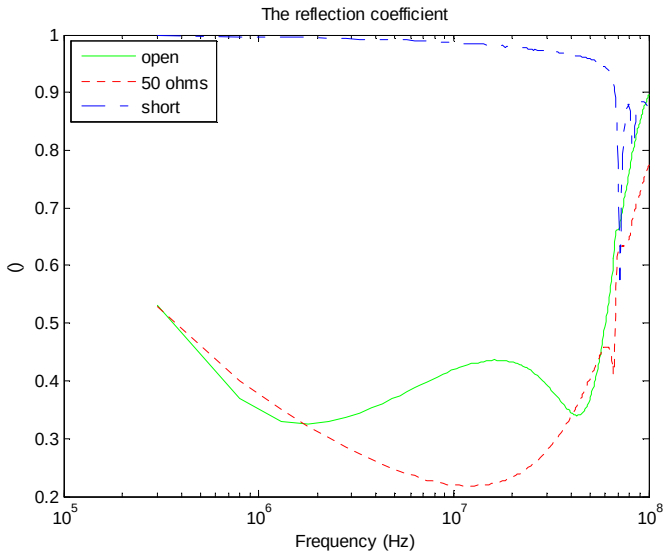

Fig 3-46 Reflection coefficient

At the lower frequencies (1 kHz – 1 MHz), the input impedance can be directly obtained from impedance analyzer while at the higher frequencies, this has to be calculated from the

reflection coefficient by:

$$Z_{\text{in}} = \frac{1+\tau}{1-\tau} Z_{\text{s}} \tag{3-17}$$

where Z_{in} is the input impedance of the primary, τ is the reflection coefficient S_{22} or S_{11} depending on which port is used as test port and Z_{s} is the built-in impedance of the VNA port.

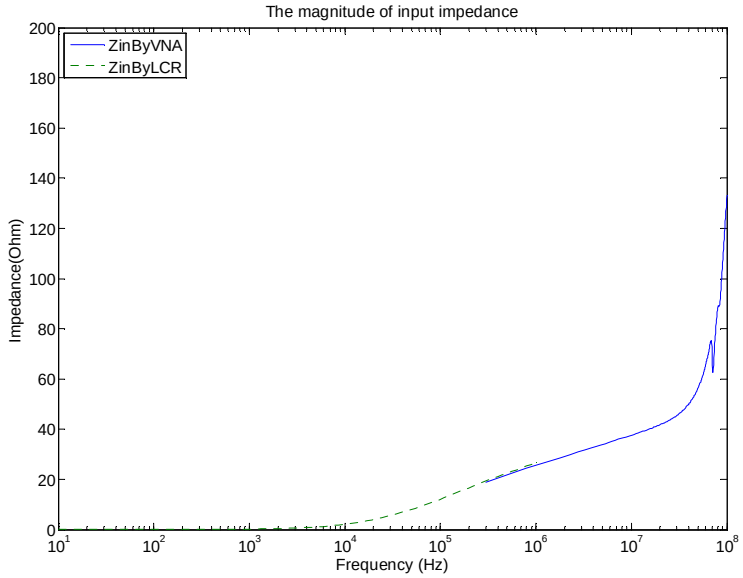

Fig 3-47 Input impedance

Fig 3-47 illustrates the input impedance from low frequency to high frequency. The Z_{in} needs to put into our transfer impedance calculation as a correction factor. After correction, the new transfer impedance at low frequency and high frequency are illustrated respectively in Fig 3-48 and Fig 3-49.

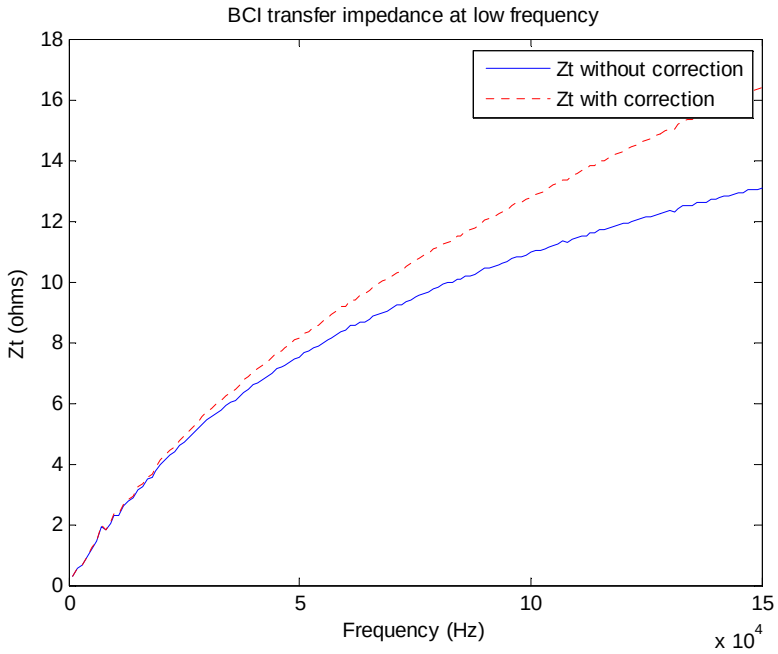

Fig 3-48 Z_{t} with correction at low frequency

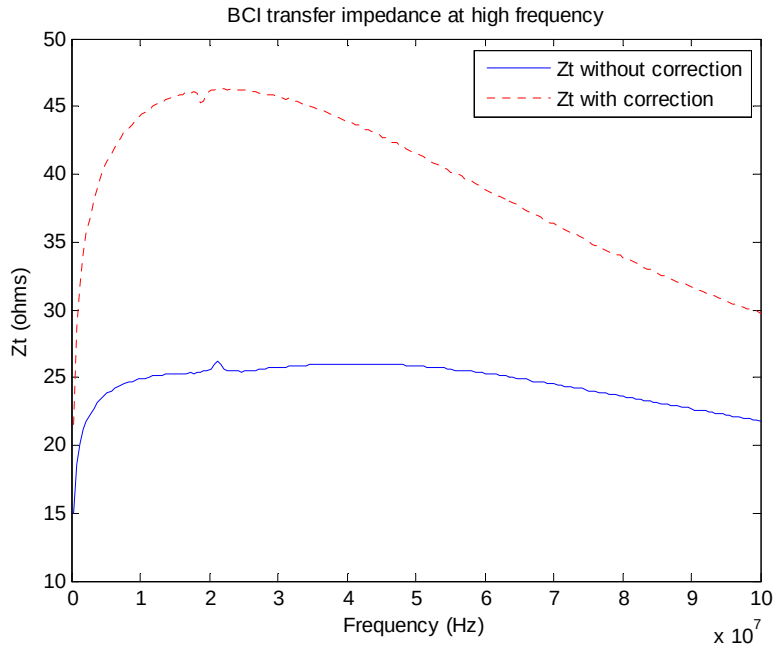

Fig 3-49 Z_t with correction at high frequency

Note that the transfer impedance at current region is 46 if ignoring the influence of stray capacitors. It does not equal to 50 Ω as we wish if the turns ratio is 1. However, it is just like the happened at F75 test where the coupling coefficient is lower than one. In this case, it should be approximately 0.925 as a result from 46 dividing by 50. Therefore, the turns ratio of 1 to 1 can still hold true.

5. Verification

To verify the secondary load will barely affect the Z_t calculation at monitor probe's test, similar correction test was applied to monitor probe F75red.

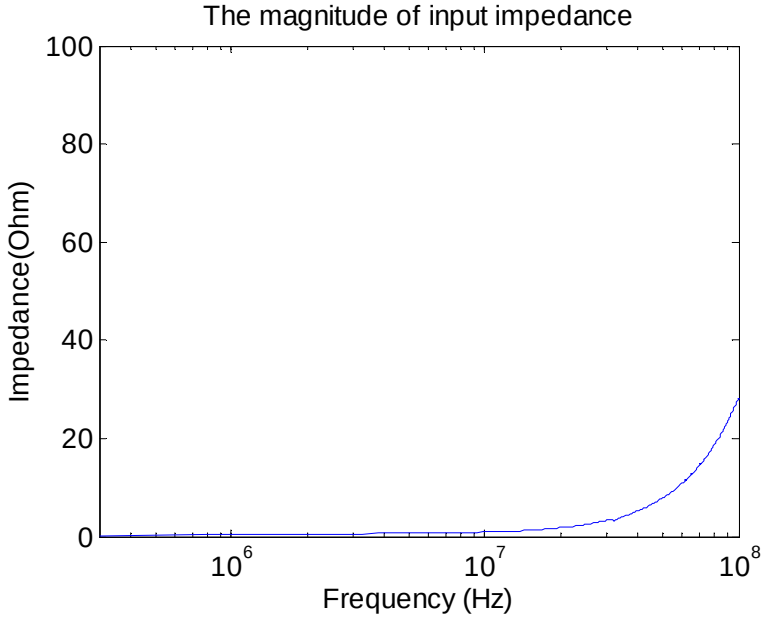

Fig 3-50 Z_{in} of F75red with a 50 Ω resistor

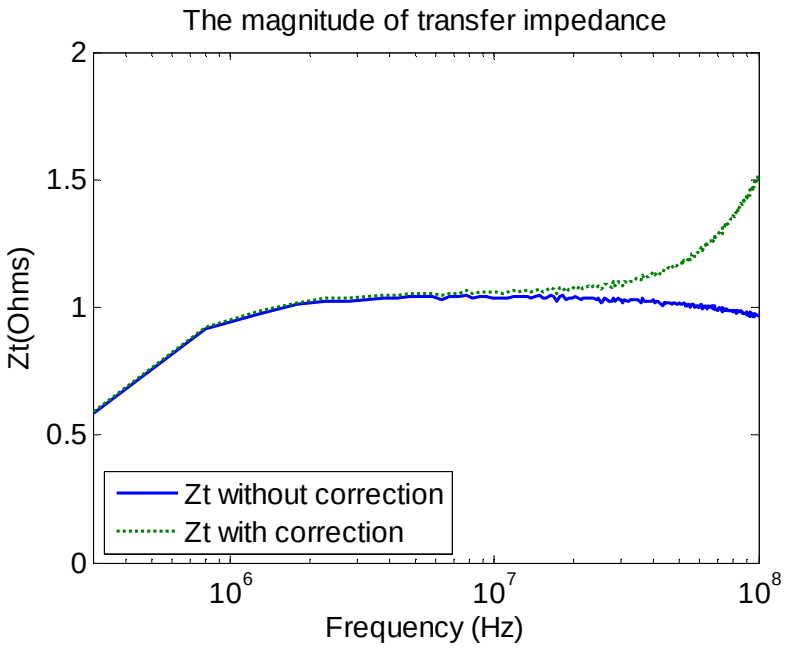

Fig 3-51 Z_t of F75red

As what is shown in Fig 3-50, the input impedance is constant and very limited except for that at the very high frequency part which is none of our concerns in this work. Therefore the calculation method in monitor probe has no effect on the performance of Z_t in the concerned frequency range which is just as Fig 3-51 shows.

3.3.3 Modeling

Considering the reduction of permeability at low frequency concluded from Fig 3-48 for the decreasing slope, it is not suitable to apply SPICE model in this case. Therefore circuit analysis will be the method combined with MATLAB to model this BCI probe.

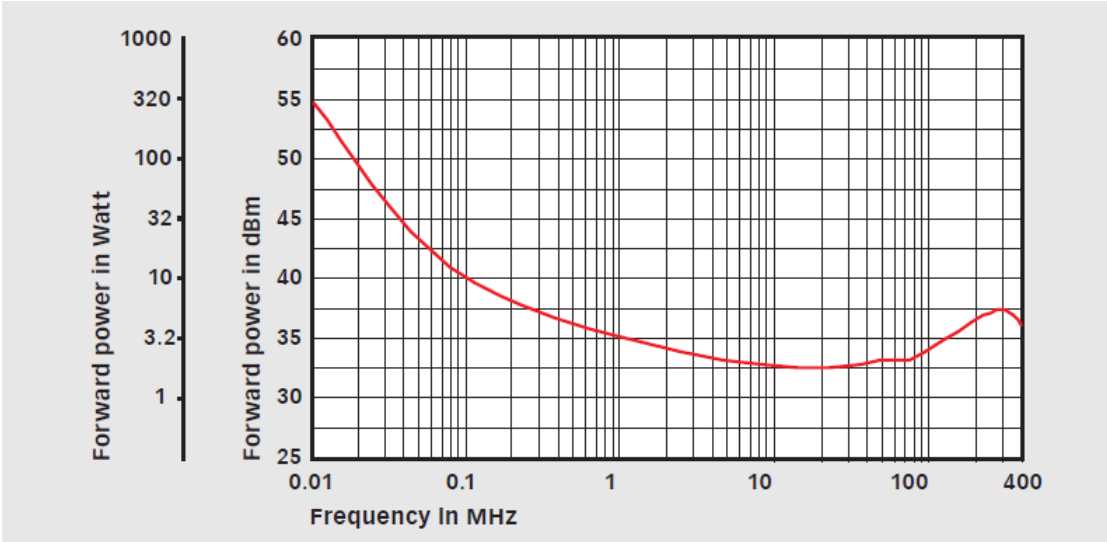

Fig 3-52 Typical required forward power to inject 100 mA

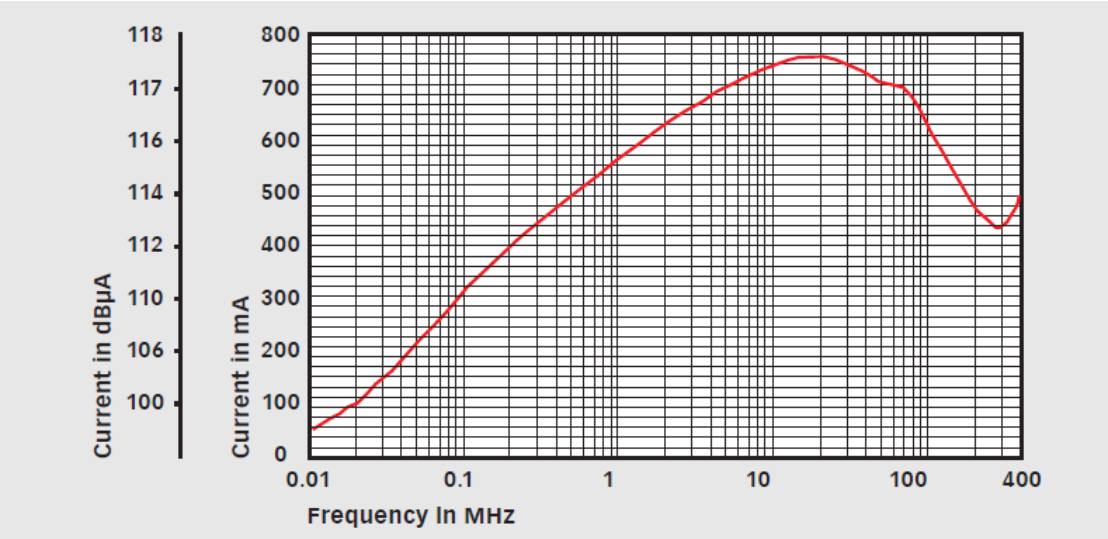

Fig 3-53 Typical injected current with 100 W forward power

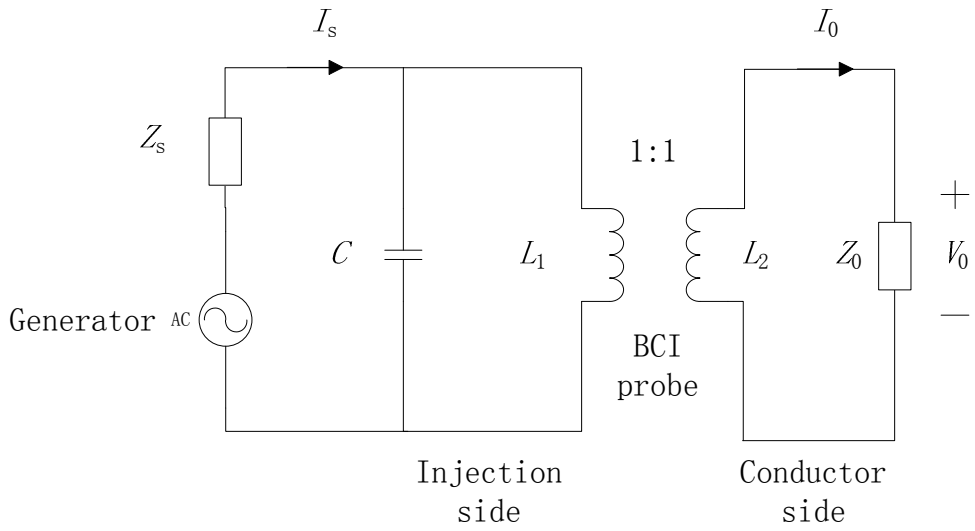

Fig 3-54 BCI probe modeling circuit

Fig 3-52 and Fig 3-53 illustrate the BCI probe's property curves which come from CIP 9136A's datasheet. In this case, the forward power indicates the power injected into the port of the probe, which is normally named "N port" similar as the output port of monitor probe. Then, the injected current is referring to the current induced on the conductor or wire through the center of the probe.

What needs to be noticed in the BCI probe modeling circuit in Fig 3-54 is that, since the source is on "N port" side, the primary indicates the probe side so not the conductor or wire side in the transfer impedance test. Besides, the capacitor refers to the stray capacitor between the windings in the BCI probe. However, what really is concerned is the performance at low frequency (especially at 2 k – 150 kHz) and in that case, the influence of the capacitance can be ignorable.

The main purpose is to find the relationship between forward power and injected current on the conductor. Thus, it could start with the forward power given by:

$$P = Re[V_s I_s] \tag{3-18}$$

where V_s is the forward injecting voltage indicated by

$$V_s = I_s Z_s + j\omega L_1 I_s - j\omega L_2 I_o \quad (3\text{-}19)$$

and I_o is the injected current on the conductor which has the relationship of

$$j\omega M I_s = j\omega L_2 I_o + Z_0 I_o \quad (3\text{-}20)$$

Substituting Equation (3-19) and Equation (3-20) into Equation (3-18) yields:

$$P = Re\{{I_o}^2[(\frac{j\omega L_2 + Z_o}{j\omega M})^2(Z_s + j\omega L_1) - (j\omega L_2 + Z_o)]\} \quad (3\text{-}21)$$

where L_1=L_2.

Although Equation (3-21) is capable to indicate the relationship between forward power and injected current, it is not enough to lead to the same response as Fig 3-53 and Fig 3-54 shows. It is due to the variable inductance for the mutative permeability as has been discussed before.

To solve this problem, one needs to add in the real inductance variation as a correction factor when using Equation (3-21) to draw the function.

The inductance can be deducted from the input impedance we have measured before. Since the impedance analyzer can not only provide the amplitude of Z_{in} but also offer the phase information. Therefore, the reactance as the imaginary part of Z_{in} will be given by:

$$X_{in} = |Z_{in}| \sin\theta \quad (3\text{-}22)$$

where

$$X_{in} = 2\pi f \cdot L \quad (3\text{-}23)$$

With the measured inductance and relevant parameter values, the results are illustrated in Fig 3-55 and Fig 3-56 respectively, as a verification of this model circuit at low frequency.

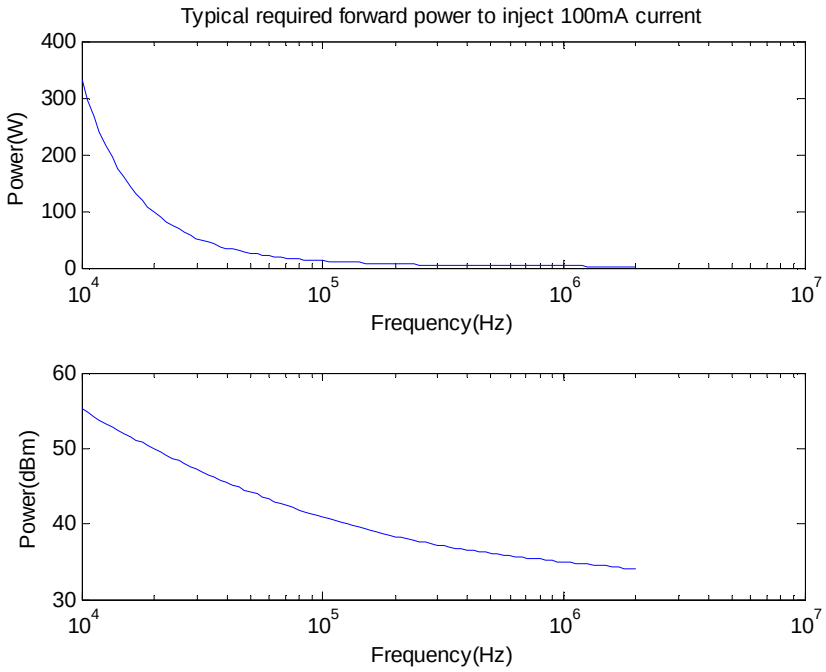

Fig 3-55 Modeling results of typical required forward power to inject 100 mA

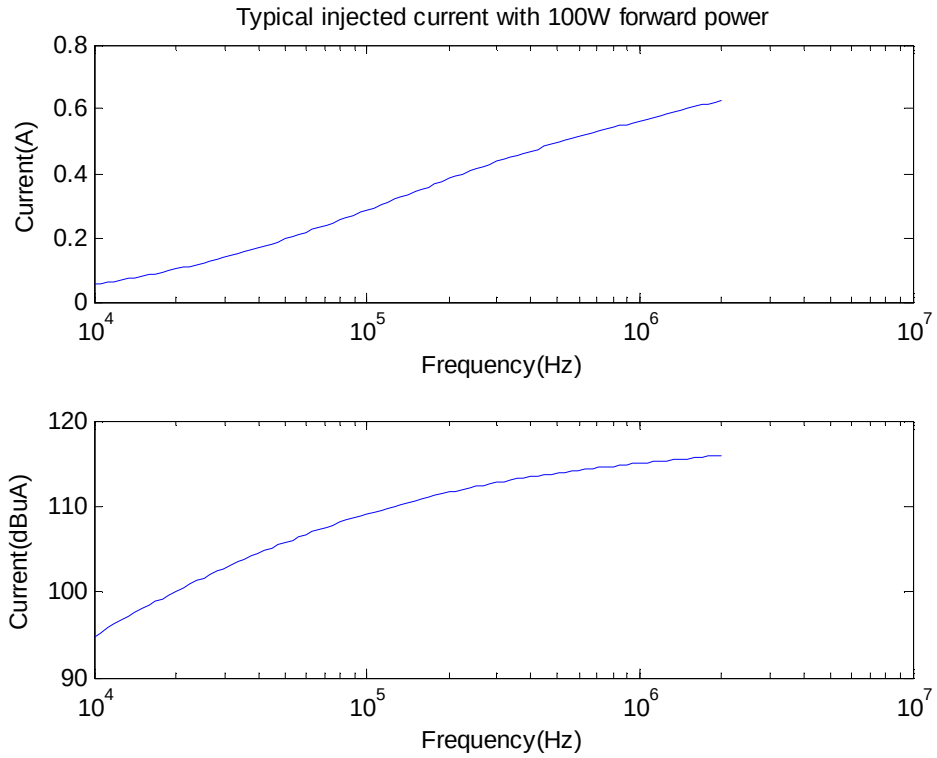

Fig 3-56 Modeling results of typical injected current with 100 W forward power

3.4 Summary

A simple experiment is done by comparing a current probe with a current shunt when they are applied to measure current of the same load.

Basic knowledge of current probe and transfer impedance is proposed. Then different measurement methods depending on the frequency range for transfer impedance are implemented. Next, usage of transfer impedance performances of monitor probes results in the SPICE models and the simulation results are compared with the measurements as verifications.

What's more, concerning the specific transfer impedance curves, the reasons causing their non-ideal performances is discussed like stray capacitance, coupling coefficient and variable magnetic permeability.

Specific attention is paid to a BCI probe's transfer impedance measurement. Especially, discussion on the differences between measuring monitor probe's transfer impedance and BCI probes' should be noticed. Also, the reason for causing this particularity is analyzed in detail with an experiment on F75red as a reference. At last, due to the particular magnetic core property (a continuous reduction of permeability), a different modeling or analysis method compared to the one on monitor probes is proposed and realized with a real inductance variation provided by an impedance analyzer.

In summary, the distinct turns ratio and core material which are designed for their own specific reasons are causing the measurement and modeling methods differences.

4 Discussion of source and load impedance measurement approach

4.1 The two-probe approach

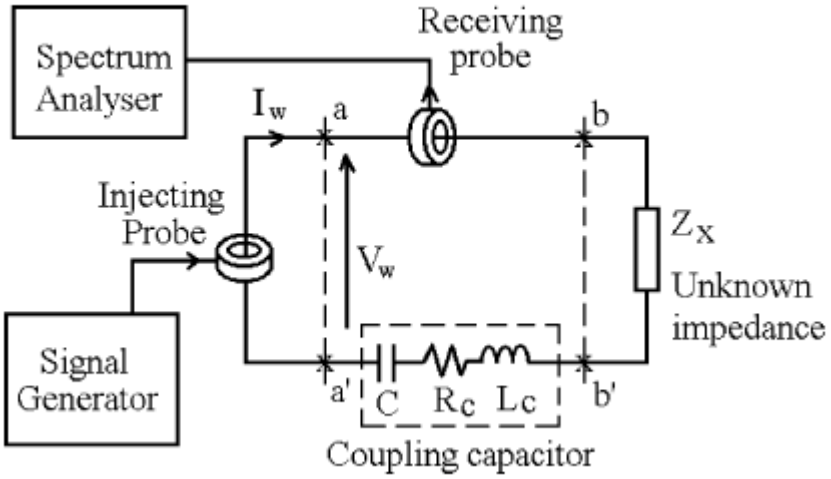

Fig 4-1 Basic structure of two-probe measurement

The method proposed by Dr. See and Dr. Deng has been successfully applied in the noise source impedance measurement at 150 kHz – 30 MHz according to [20]. In that case, the unknown impedance to be measured is represented by Z_x. The two current probes and a coupling capacitor form a radio frequency (RF) coupling circuit for the measurement of magnitude of Z_x. The signal generated by the generator is induced into the circuit through the injecting current probe. Through the receiving current probe, the spectrum analyzer measures the magnitude of the resultant current I_w in the wire of the coupling circuit.

4.1.1 Basic theory of the two-probe approach

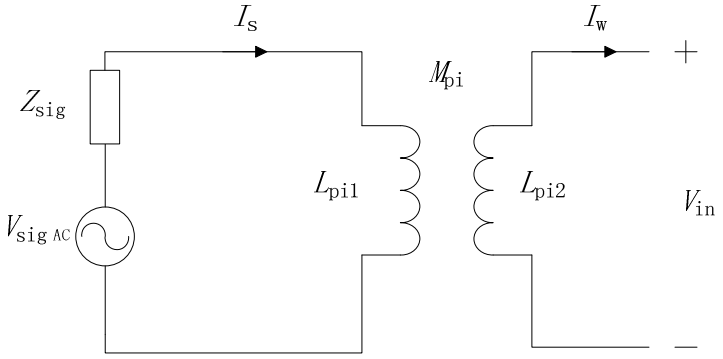

Fig 4-2 Equivalent circuit of the injection probe

In Fig 4-2, V_{sig} and Z_{sig} indicate the injection source and its source impedance respectively, while I_s represents the current flowing into the injecting port of the current injection probe and I_w

will be the induced current on the conductor through the probe. L_{pi1}, L_{pi2} and M_{pi} are the self-inductance on the primary (self-inductance of the probe) and the secondary (self-inductance of the wire loop of the coupling circuit) as well as the mutual inductance between them respectively. Therefore, it readily follows that

$$V_{\mathrm{sig}} = I_{\mathrm{s}} Z_{\mathrm{sig}} + \mathrm{j}\omega L_{\mathrm{pi1}} I_{\mathrm{s}} - \mathrm{j}\omega M_{\mathrm{pi}} I_{\mathrm{w}} \tag{4-1}$$

$$\mathrm{j}\omega M_{\mathrm{pi}} I_{\mathrm{s}} = \mathrm{j}\omega L_{\mathrm{pi2}} I_{\mathrm{w}} + V_{\mathrm{in}}. \tag{4-2}$$

Eliminating I_s from Equation (4-1) and (4-2), it yields

$$V_{\mathrm{in}} = V_1 - Z_1 I_{\mathrm{w}} \tag{4-3}$$

where

$$V_1 = \frac{\mathrm{j}\omega M_{\mathrm{pi}}}{\mathrm{j}\omega L_{\mathrm{pi1}} + Z_{\mathrm{sig}}} V_{\mathrm{sig}} \tag{4-4}$$

and

$$Z_1 = \mathrm{j}\omega L_{\mathrm{pi2}} + \frac{\omega^2 M_{\mathrm{pi}}^2}{\mathrm{j}\omega L_{\mathrm{pi1}} + Z_{\mathrm{sig}}} . \tag{4-5}$$

As Equation (4-3) suggests, the equivalent circuit of this two-probe approach setup can be simplified as Fig 4-3 illustrates. In Fig 4-3, Z_1 and Z_2 are the impedances in the coupling circuit caused by the injecting probe (BCI probe) and the receiving probe (monitor probe) respectively and Z_c referrers to the coupling impedance. Since the circuit is worked at low frequency, basic electric laws still hold true. Therefore, by simply applying Kirchhoff's law, V_1 is given by

$$V_1 = (Z_1 + Z_2 + Z_{\mathrm{c}}) I_{\mathrm{w}} + Z_{\mathrm{x}} I_{\mathrm{w}} . \tag{4-6}$$

Let $Z_{\mathrm{in}} = Z_1 + Z_2 + Z_{\mathrm{c}}$, then Equation (4-6) becomes

$$V_1 = (Z_{\mathrm{in}} + Z_{\mathrm{x}}) I_{\mathrm{w}} \tag{4-7}$$

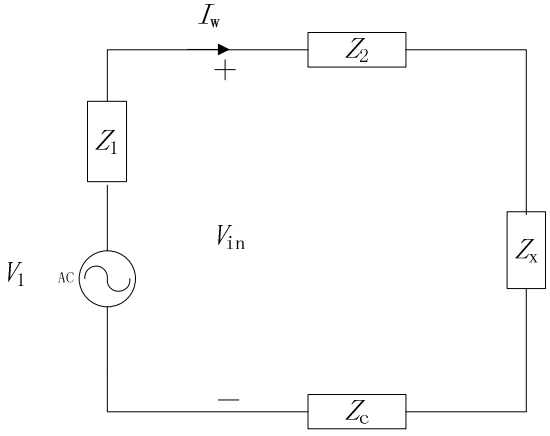

Fig 4-3 Equivalent circuit of the two-probe measurement setup

For the purpose of solving the unknown impedance Z_x, we rewrite Equation (4-7) to

$$Z_{\mathrm{x}} = \frac{V_1}{I_{\mathrm{w}}} - Z_{\mathrm{in}} . \tag{4-8}$$

As it has been demonstrated in the previous chapter, current probes are characterized by the

transfer impedance, the ratio of output voltage to current flowing through the current probe. Therefore, substituting

$$I_{\mathrm{w}} = \frac{V_{\mathrm{o}}}{Z_{\mathrm{t}}} \tag{4-9}$$

into Equation (4-8), it becomes

$$Z_{\mathrm{x}} = \frac{V_1}{V_{\mathrm{o}}} Z_{\mathrm{t}} - Z_{\mathrm{in}} \tag{4-10}$$

where V_{o} and Z_{t} is the output voltage and transfer impedance of the monitor probe.
If V_1 is replaced by Equation (4-4), then Equation (4-10) will change into

$$Z_{\mathrm{x}} = K \frac{V_{\mathrm{sig}}}{V_{\mathrm{o}}} - Z_{\mathrm{in}} \tag{4-11}$$

where $= \frac{\mathrm{j}\omega M_1 Z_{\mathrm{t}}}{\mathrm{j}\omega L_{\mathrm{p11}} + \mathrm{Z_{sig}}}$.

With the same V_{sig}, KV_{sig} stay constant for a given frequency. If the unknown impedance is replaced by a standard resistance R_{std} and the condition $R_{\mathrm{std}} \gg Z_{\mathrm{in}}$ holds true, then it is reasonable to obtain

$$R_{\mathrm{std}} \approx K \frac{V_{\mathrm{sig}}}{V_{\mathrm{o}}|_{Z_{\mathrm{x}}=R_{\mathrm{std}}}} \ . \tag{4-12}$$

Equation (4-11) suggests that if Z_{x} becomes zero which is known as short circuit then Z_{in} is able to be given by

$$Z_{\mathrm{in}} = K \frac{V_{\mathrm{sig}}}{V_{\mathrm{o}}|_{Z_{\mathrm{x}}=0}} \approx R_{\mathrm{std}} \frac{V_{\mathrm{o}}|_{Z_{\mathrm{x}}=R_{\mathrm{std}}}}{V_{\mathrm{o}}|_{Z_{\mathrm{x}}=0}} \ . \tag{4-13}$$

Finally, the Z_{x} can be calculated by

$$Z_{\mathrm{x}} = R_{\mathrm{std}} \frac{V_{\mathrm{o}}|_{Z_{\mathrm{x}}=R_{\mathrm{std}}}}{V_{\mathrm{o}}|_{Z_{\mathrm{x}}=Z_{\mathrm{x}}}} - R_{\mathrm{std}} \frac{V_{\mathrm{o}}|_{Z_{\mathrm{x}}=R_{\mathrm{std}}}}{V_{\mathrm{o}}|_{Z_{\mathrm{x}}=0}} \ . \tag{4-14}$$

To check whether the selected R_{std} can meet the requirement or not, it can be achieved by comparing the output voltages with $Z_{\mathrm{x}}=R_{\mathrm{std}}$ and $Z_{\mathrm{x}}=0$. Since the output voltages measured through the receiving probe can be represented by

$$V_{\mathrm{o}}|_{Z_{\mathrm{x}}=R_{\mathrm{std}}} = K \frac{V_{\mathrm{sig}}}{R_{\mathrm{std}}+Z_{\mathrm{in}}} \tag{4-15}$$

$$V_{\mathrm{o}}|_{Z_{\mathrm{x}}=0} = K \frac{V_{\mathrm{sig}}}{Z_{\mathrm{in}}} \ . \tag{4-16}$$

Thus if KV_{sig} keeps constant and $V_{\mathrm{o}}|_{Zx=R\mathrm{std}}$ is much less than $V_{\mathrm{o}}|_{Zx=0}$, it can prove that the situation $R_{\mathrm{std}} \gg Z_{\mathrm{in}}$ holds true.

4.1.2 Performances of the two-probe approach at 2 kHz – 150 kHz

To verify whether this method can also be performed at low frequency as well as at high frequency as [20] implies, a 1 Ω resistor is used as the unknown impedance to measure. The source is the same source which was used at the current probe transfer impedance test - the 1 k – 150 kHz “flat” signal as illustrated in Fig 4-4.

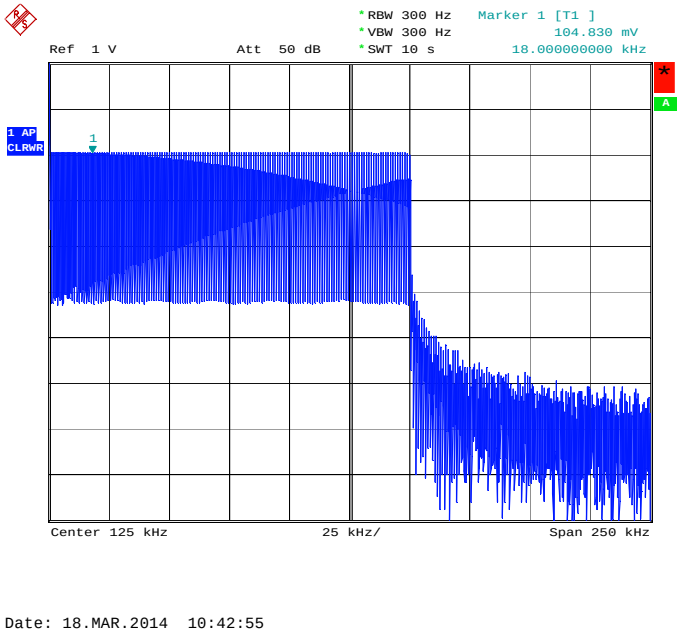

Fig 4-4 Source in frequency domain

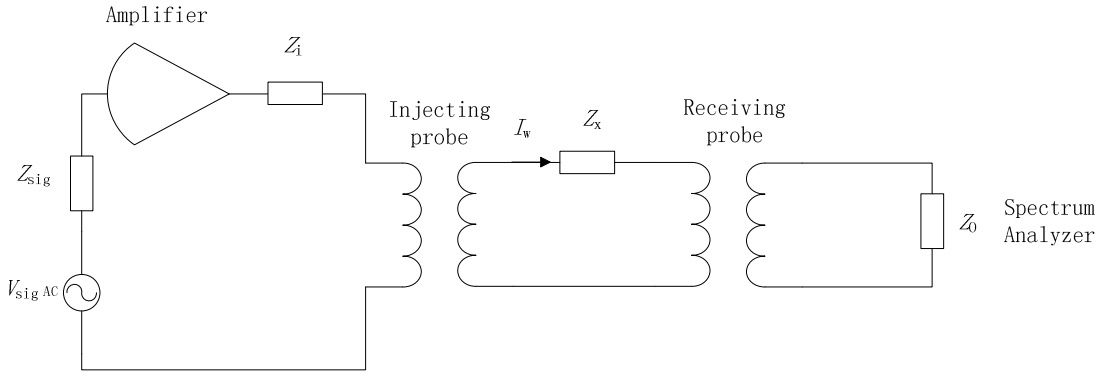

Fig 4-5 Test circuit for the 2-probe approach

The signal from the source injects into the injecting probe through an amplifier and protecting impedance (Z_i in Fig 4-5), then the resultant current will flow on the conductor which passing through the center of both injecting probe and receiving probe. In this case, the conductor loop is formed by the calibration fixture used at the current probe tests and the impedance under test (or the standard resistor and short circuit). Finally, the spectrum analyzer will detect the signal via the receiving probe. After the necessary calculation, the results are illustrated in Fig 4-6 and Fig 4-7.

The performance of the measurement improves with the increase of frequency as shown in Fig 4-6. However, what Fig 4-7 shows indicates that it still oscillates with relatively high amplitudes. Therefore, this 2-probe approach is not able to provide the accurate measurement at the targeted frequency domain.

The reasons why this method performs poorly in this case compared with its success in [20] are:

1. The BCI probe is used in the experiment as the injecting probe to increase the injection level, while in [20] monitor probes with much lower output/input impedances than BCI probes as described in previous chapter are used both as the injecting and receiving probes so that the

Z_{in} matches the requirement $R_{\text{std}} \gg Z_{\text{in}}$ better.

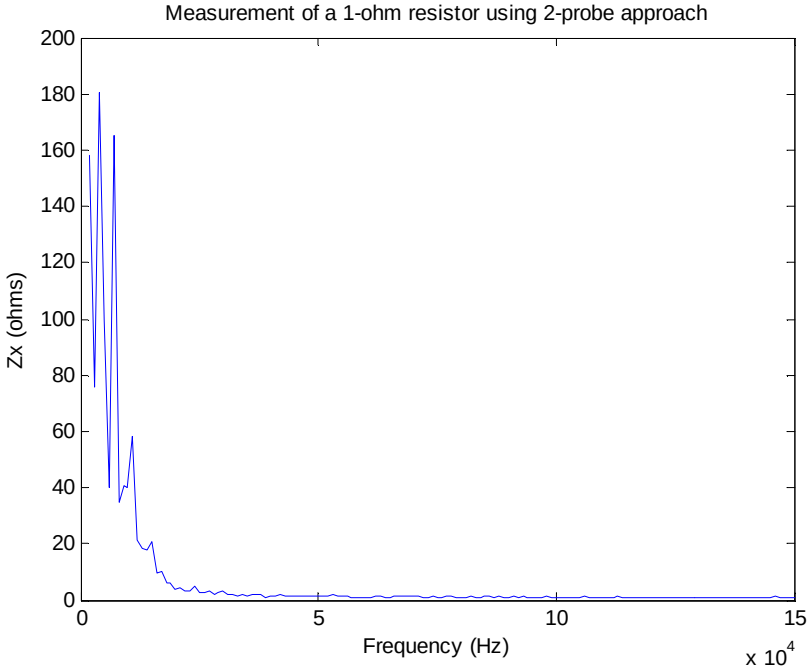

Fig 4-6 Measurement by the 2-probe approach

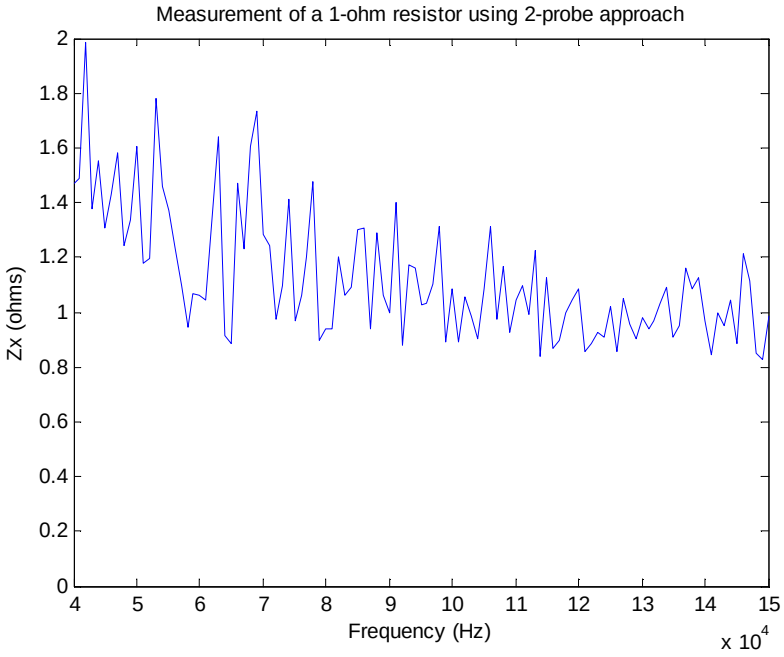

Fig 4-7 Measurement (zoom in above 40 kHz) by the 2-probe approach

2. With relatively low injecting and receiving efficiency at low frequency, the measurements are comparable with the background noise. This fact will highly affect the value's accuracy. Therefore, the lower frequency is, then the less accurate results are.

3. The deduction is only concerning the amplitude of the measurement and the phase information is missing. At high frequency the resistance is ignorable compared with the reactance while at low frequency the resistance is comparable to the reactance. Therefore, it leads to significant errors by using this method.

4.2 The three-probe approach

Considering the significant errors resulting from the two-probe approach in the low frequency measurement, a new approach is proposed which is improved on the basis of the two-probe approach. A new monitor probe called detecting probe is inserted between the protecting impedance Z_i and injecting probe which is illustrated in Fig 4-8.

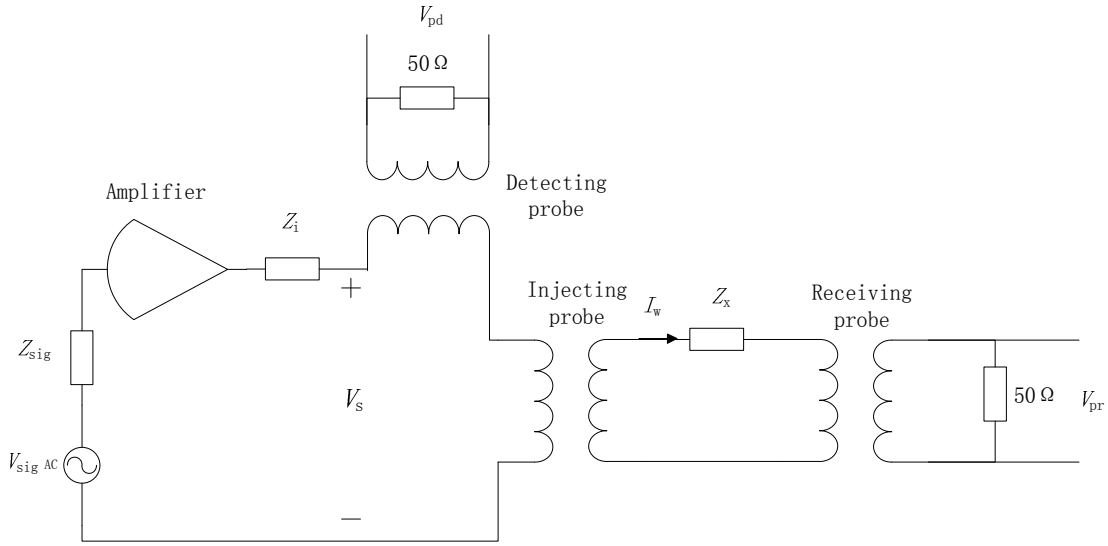

Fig 4-8 Test circuit for the 3-probe approach

4.2.1 Basic theory of the three-probe approach

To simplify the deduction, the Thevenin theory is applied and output voltage V_s and equivalent impedance Z_s are used to replace the source, amplifier and the impedances in Fig 4-8. Then, subscripts of “pd”, “pi” and “pr” are used to indicate the parameters of the detecting probe, injecting probe and receiving probe respectively. Thus, the circuit is redrawn in Fig 4-9.

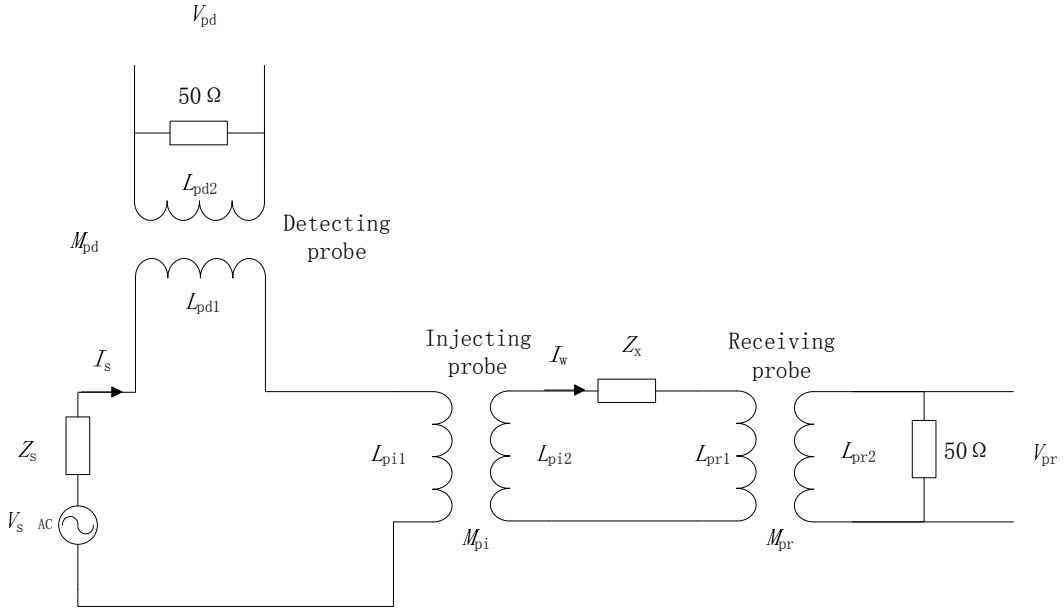

Fig 4-9 Test circuit (simplified) for the 3-probe approach

In Fig 4-9, V_{pd} and V_{pr} are the output voltage of the detecting probe and the receiving probe respectively. According to the character of a current probe, the current on the wire through each of the two probes, I_w and I_s, can be given by

$$I_{\mathrm{w}} = \frac{V_{\mathrm{pr}}}{Z_{\mathrm{tr}}} \tag{4-17}$$

$$I_{\mathrm{s}} = \frac{V_{\mathrm{pd}}}{Z_{\mathrm{td}}} \tag{4-18}$$

where Z_{tr} and Z_{td} are the transfer impedance of the detecting probe and the receiving probe respectively.

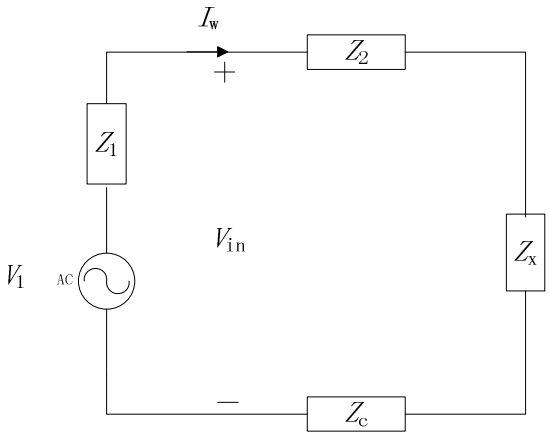

Fig 4-10 Thevenin equivalent circuit of the three-probe measurement setup

Because there are no changes on the secondary side of the circuit compared with the two-probe setup, both the Thevenin equivalent circuit as shown in Fig 4-10 and the mathematic deduction applied in the two-probe approach still hold true in the three-probe approach. Therefore, it has no problem to rewrite Equation (4-10) below as Equation (4-19):

$$Z_{\mathrm{x}} = \frac{V_1}{V_{\mathrm{pr}}} Z_{\mathrm{tr}} - Z_{\mathrm{in}} \tag{4-19}$$

where all the parameters have the same meanings as before.

V_1 is the induced voltage on the secondary side of the injecting probe. Therefore it can be represented by

$$V_1 = \mathrm{j}\omega M_{\mathrm{pi}} I_{\mathrm{s}} \quad . \tag{4-20}$$

Substituting Equation (4-18) and (4-20) into Equation (4-19), one yields

$$Z_{\mathrm{x}} = \frac{\mathrm{j}\omega M_{\mathrm{pi}} Z_{\mathrm{tr}}}{Z_{\mathrm{td}}} \frac{V_{\mathrm{pd}}}{V_{\mathrm{pr}}} - Z_{\mathrm{in}} \quad . \tag{4-21}$$

Similarly, let $K = \frac{\mathrm{j}\omega M_{\mathrm{pi}} Z_{\mathrm{tr}}}{Z_{\mathrm{td}}}$, then it becomes

$$Z_{\mathrm{x}} = K \frac{V_{\mathrm{pd}}}{V_{\mathrm{pr}}} - Z_{\mathrm{in}} \quad . \tag{4-22}$$

To obtain the unknown impedance, it is necessary to identify the values of K and Z_{in}. As these two parameters will keep constant at the certain frequency when the source is invariable, it is possible to determine their values by using two different standard resistors R_1 and R_2 (or short circuit) to replace Z_x respectively. Then Equation (4-22) becomes

$$R_1 = K\frac{V_{\mathrm{pd}}|_{Z_{\mathrm{X}}=R_1}}{V_{\mathrm{pr}}|_{Z_{\mathrm{X}}=R_1}} - Z_{\mathrm{in}} \quad (4\text{-}23)$$

$$R_2 = K\frac{V_{\mathrm{pd}}|_{Z_{\mathrm{X}}=R_2}}{V_{\mathrm{pr}}|_{Z_{\mathrm{X}}=R_2}} - Z_{\mathrm{in}} \quad . \quad (4\text{-}24)$$

By solving Equation (4-23) and (4-24), the values of K and Z_{in} can be confirmed. Finally, the unknown impedance can be determined via Equation (4-22).

This three-probe approach simplifies the mathematic deduction and takes no approximate calculation. What is of the paramount importance is that all of the values used in Equation (4-22) to (4-24) are complex. However, the spectrum analyzer still cannot provide the phase information yet. Therefore, a different analysis strategy is needed.

4.2.2 Performances of the three-probe approach at 2 kHz – 150 kHz

To obtain both of the amplitude and phase information, FFT is a good choice. Similarly as the test in section 3.1, the NI digitizer is used to sample the signal in time domain and the result will be sent to the PC where the FFT will be applied via a Labview platform. Furthermore, not like the spectrum analyzer containing significant background noise, signal processed in this way can effectively avoid this problem to lead to more accurate result.

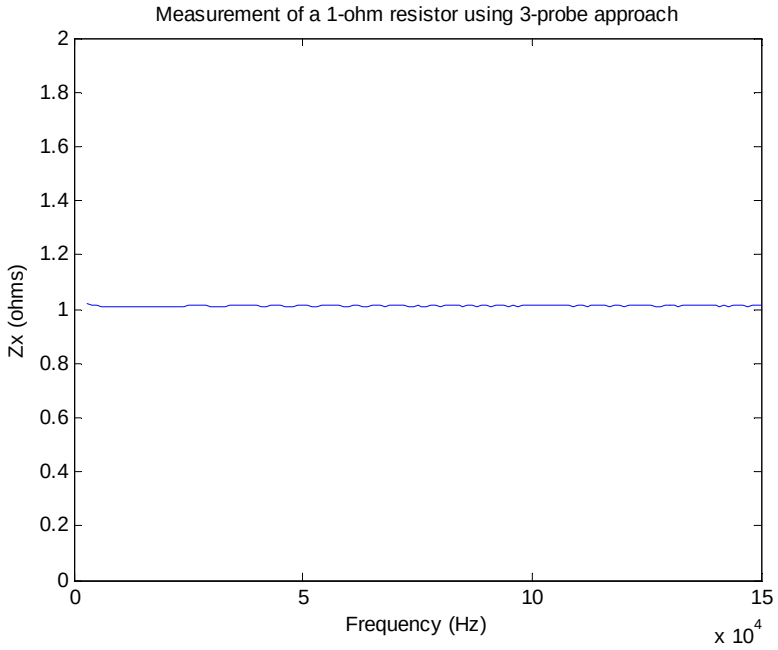

Fig 4-11 Measurement of a 1 Ω resistor using three-probe approach

The measurement of the same 1 Ω resistor using the three-probe approach is much more accurate compared with the one using the two-probe approach as shown in Fig 4-11. Additionally, Fig 4-12 illustrates the comparison between the measurements with and without phase information when applying the three-probe approach. This proves the importance of phase information in the measurement processing.

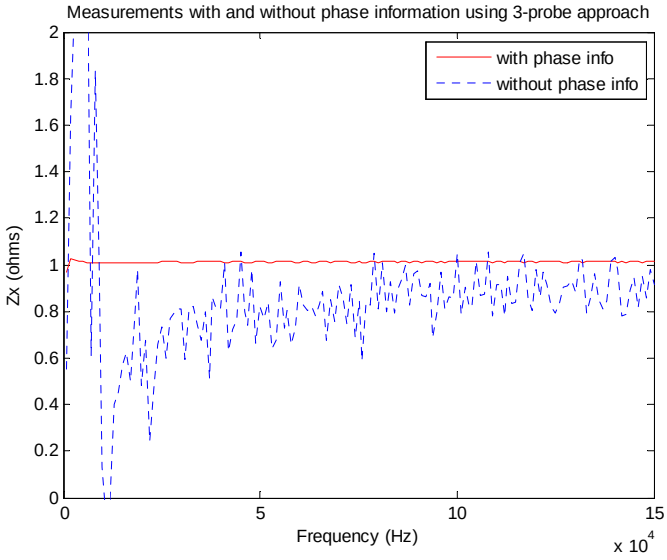

Fig 4-12 Comparison between measurements with and without phase information

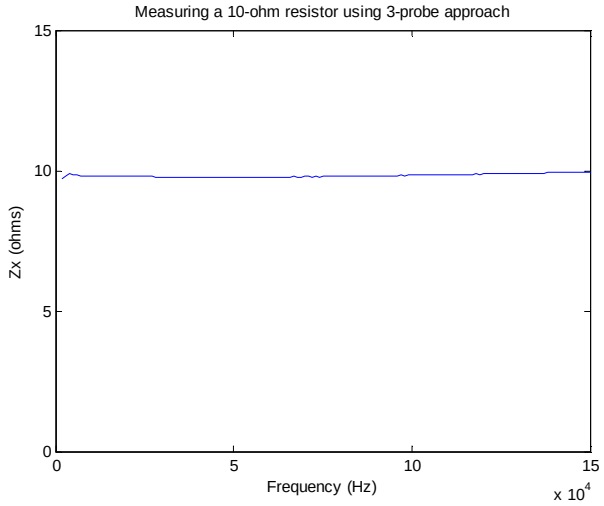

Fig 4-13 Measurement of a 10 Ω resistor using three-probe approach

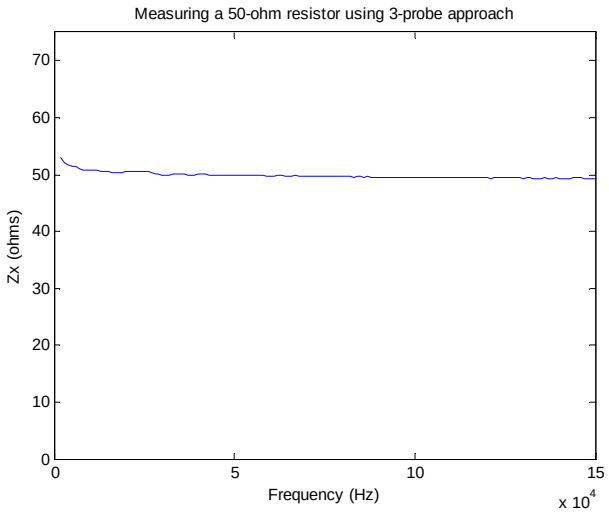

Fig 4-14 Measurement of a 50 Ω resistor using three-probe approach

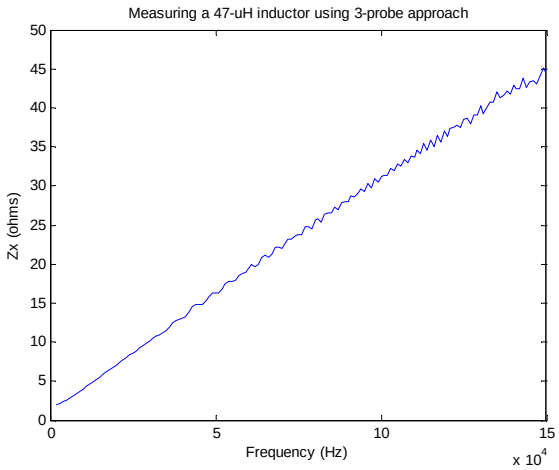

Fig 4-15 Measurement of a 47 μH inductor using three-probe approach

From Fig 4-13 to Fig 4-15, they illustrate the other three measurements using the three-probe approach. These measurements show that using the three-probe approach is possible to obtain the accurate impedance value regardless of its electric property (resistive, inductive or capacitive).

4.3 Summary

Measuring source or load impedance accurately contributes to understanding the circuit construction better and is important for EMI filter designs. Using current probes is a simple way to measure the unknown impedance accurately. At the high frequencies over 150 kHz, the reactance of the impedance is much higher than its resistance so that the phase information may not be that important. Thus the two-probe method is capable of leading to the correct measurement result in that case. However, when it comes to the measurement at low frequencies, the resistance is normally comparable to the reactance which means that the resistance should no longer be ignored. Using the three-probe method with FFT analysis in the computer is able to collect both the amplitude and the phase information precisely. With this information, the accurate source or load impedance can be easily deducted by applying the mathematical strategy mentioned in this chapter.

5 Source impedance and load impedance measurements

In this chapter, the three-probe approach is applied to measure the source impedances in different wall sockets at the laboratory and in the smart power supply Model 108 AMX mentioned in chapter 3. Furthermore, the various lamps and fans are used as the loads in the experimental circuit and their load impedances are also identified through this experiment.

5.1 Source impedance measurements

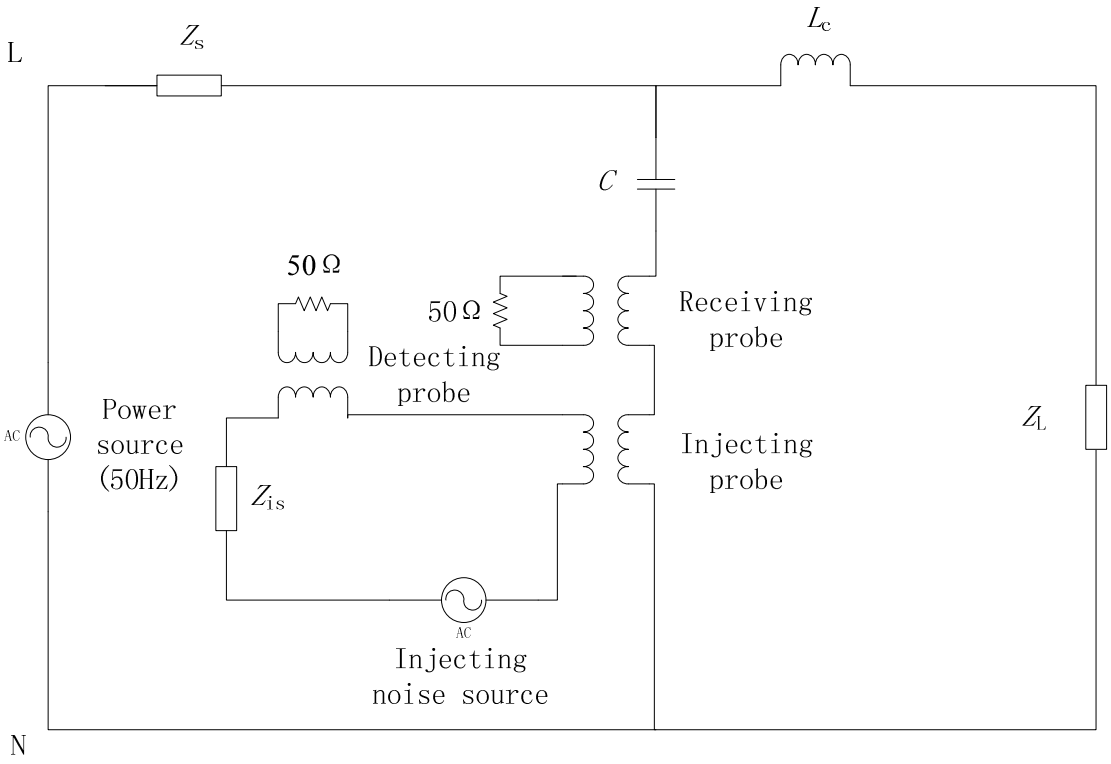

Fig 5-1 Source impedance measurement equivalent circuit

Fig 5-1 shows the equivalent circuit for the source impedance measurement. The capacitor C (5 of 2.2 μF capacitors connected in parallel) with the injecting probe and the receiving probe form the coupling circuit. To measure the source impedance Z_s, an inductor (or a choke) L_c is needed as shown in Fig 5-1 to shield the possible influence from the load side. Because actually the three-probe measurement setup is to measure the parallel impedance of Z_L and Z_s, so if the condition $Z_L \gg Z_s$ holds true, then the parallel impedance can be treated as the source impedance ($Z_L // Z_s \approx Z_s$). For this reason, a choke (8.7mH) is used to increase the impedance on the load side during the measurement. The actual implementation of the test circuit is shown in Fig 5-2.

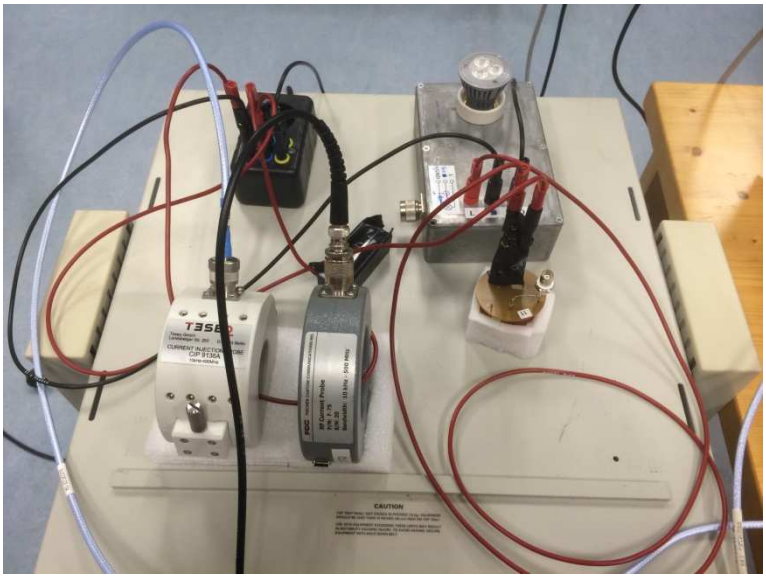

Fig 5-2 Implementation of source impedance measurement circuit

5.1.1 Source impedances in different wall sockets

In this section, two different wall sockets No. 9 and No. 11 in the lab are used as the power sources respectively. Furthermore, to minimize the irrelevant disturbances, the same load - OSRAM 4.5 W LED lamp (L1) as displayed in Fig 5-3 is applied in both measurements.

Fig 5-3 Load 1 – OSRAM 4.5 W LED lamp

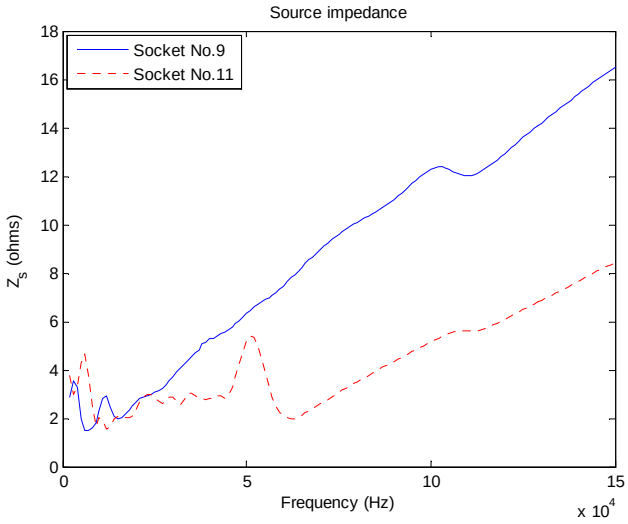

Fig 5-4 Grid source impedance measurement

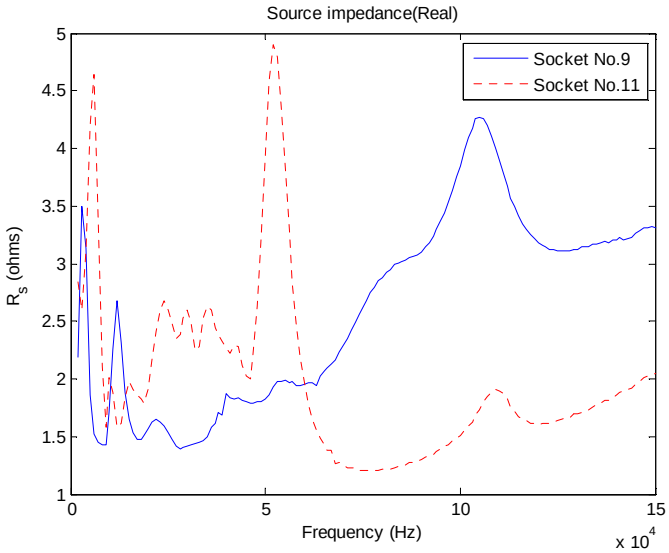

Fig 5-5 Grid source impedance measurement (real)

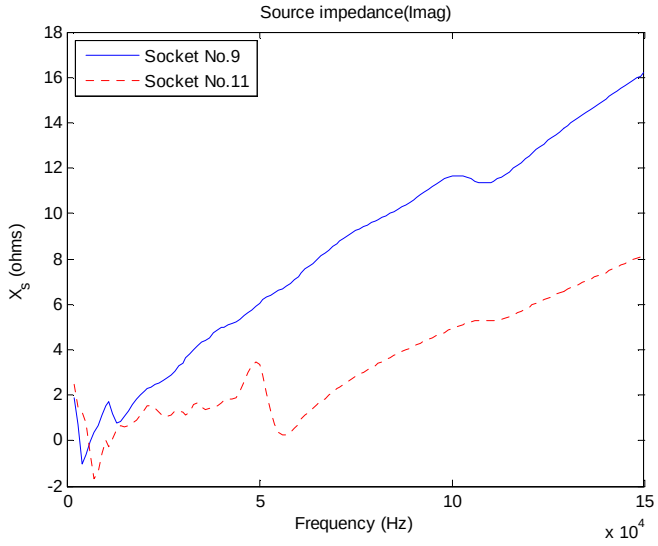

Fig 5-6 Grid source impedance measurement (imaginary)

Fig 5-4 to Fig 5-6 illustrate that the measurements of the source impedance of socket No.9 and No.11 (impedance, resistance and reactance respectively). Overall, the trends of the source impedance variations in both cases show the fact that they are inductive sources. What's more, this also indicates that the power source impedance does vary with the location.
Based on this measurement, the source impedances can be simply represented by a resistor and an inductor in series in electric circuit models.

5.1.2 Source impedance in smart power supply

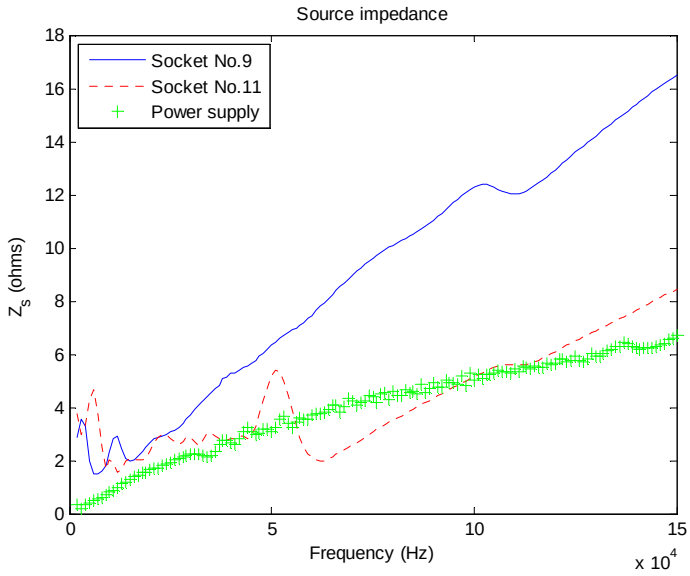

Fig 5-7 Source impedance comparison between wall sockets' and power supply's

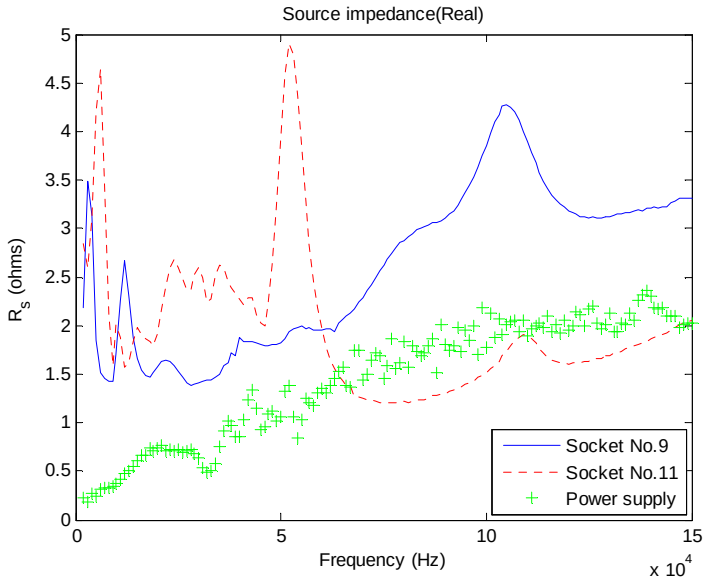

Fig 5-8 Source impedance (real) comparison between wall sockets' and power supply's

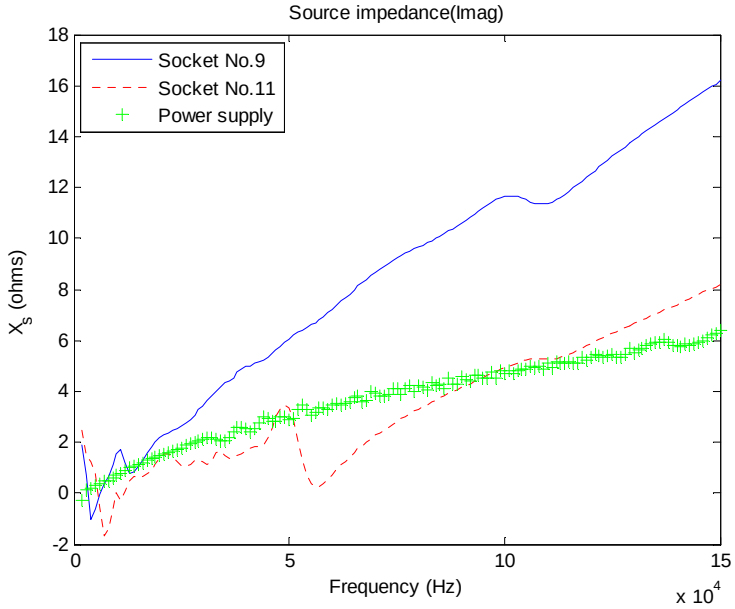

Fig 5-9 Source impedance (imaginary) comparison between wall sockets' and power supply's

Source impedance of the power supply shows a smoother increasing tendency compared with the ones in those wall sockets and the inductive property can still hold true for it.

5.2 Load impedance measurements

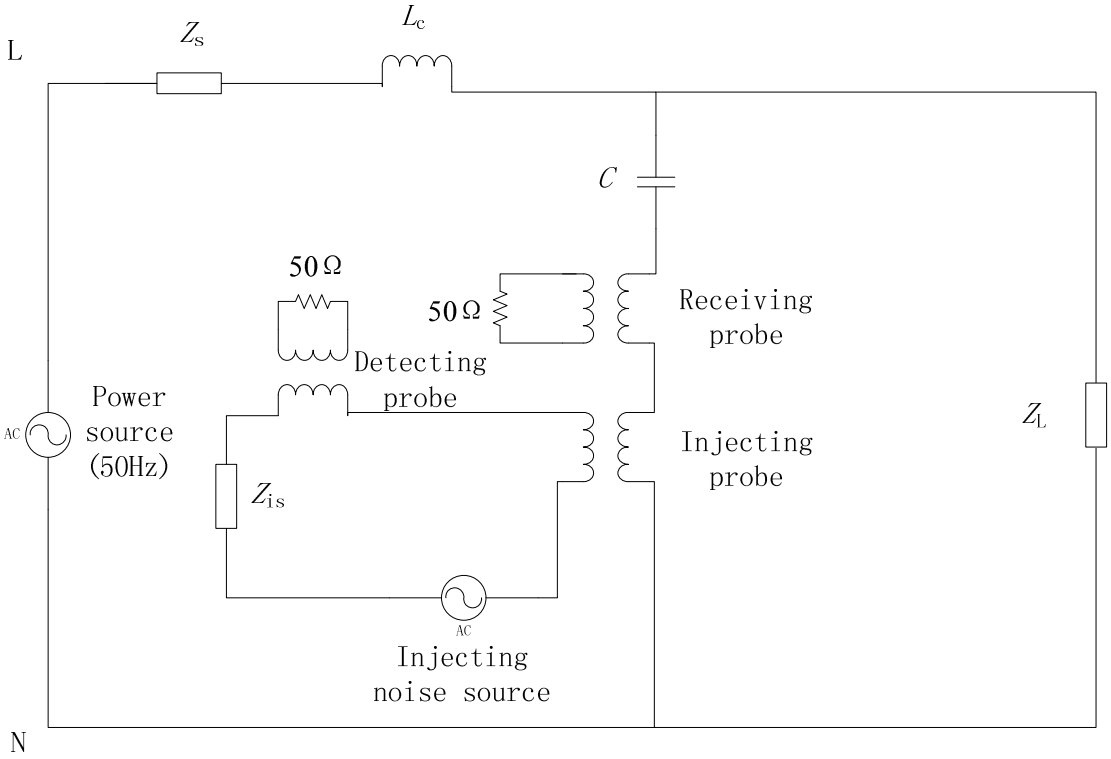

Fig 5-10 Load impedance measurement equivalent circuit

Similarly, this three-probe method can be applied to measure the load impedances. The only difference from measuring source impedance is that the choke is laid on the source side

instead of the load side in this case as illustrated in Fig 5-10.

In this case, measurements are implemented on 14 different loads including 11 distinct LED lamps, 1 compact fluorescent lamp (CFL) and 2 fans with different rated working power. The loads are shown in Fig 5-11 and Fig 5-12.

Fig 5-11 Lamps

Fig 5-12 Fans

For the purpose of simplification, the lamps are numbered from L1 to L6 and L11 to L16. Then they are divided into two experiment groups with the equal number of lamps. Specifically, L6 is the CLF lamp and the rest are LED lamps.

Group 1 (L1 to L6):

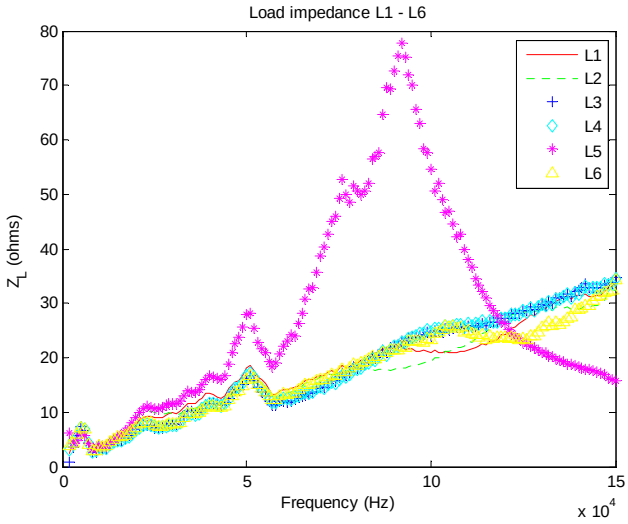

Fig 5-13 Load impedance comparison (L1 to L6)

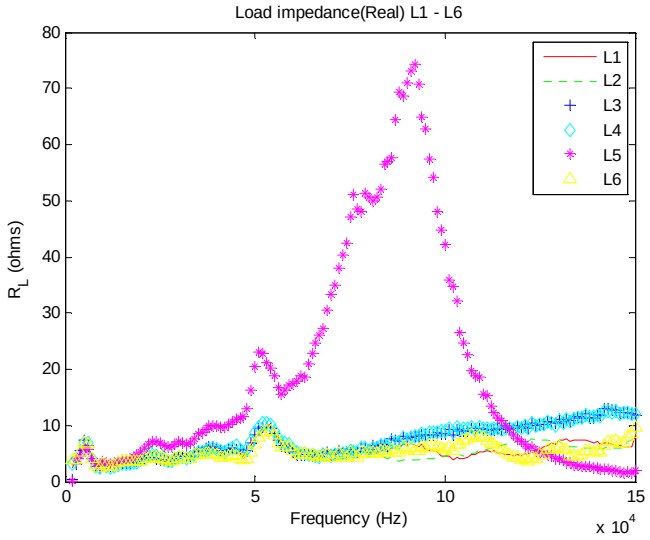

Fig 5-14 Load impedance comparison (real) (L1 to L6)

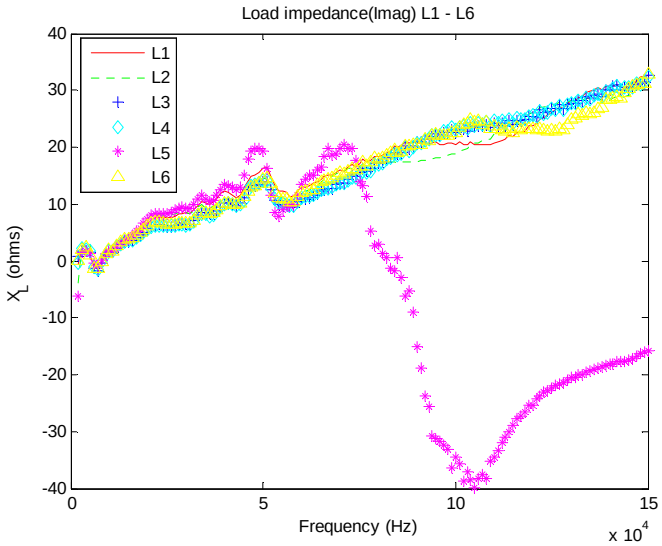

Fig 5-15 Load impedance comparison (imaginary) (L1 to L6)

Group 2 (L11 to L16):

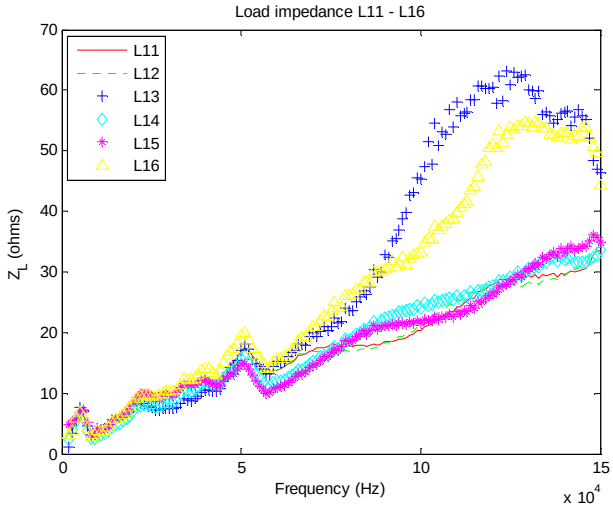

Fig 5-16 Load impedance comparison (L11 to L16)

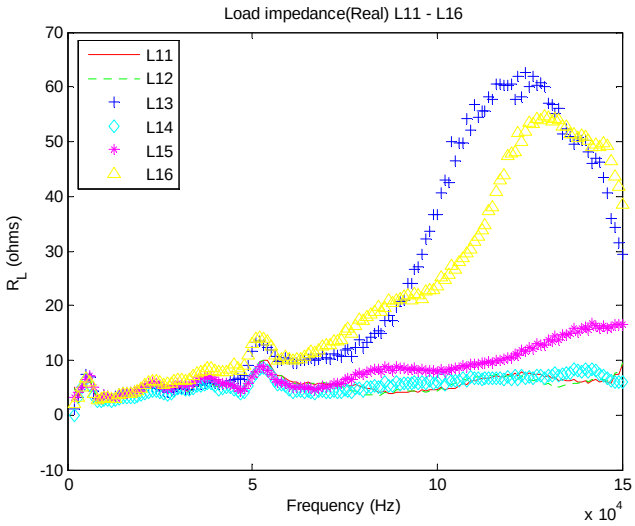

Fig 5-17 Load impedance comparison (real) (L11 to L16)

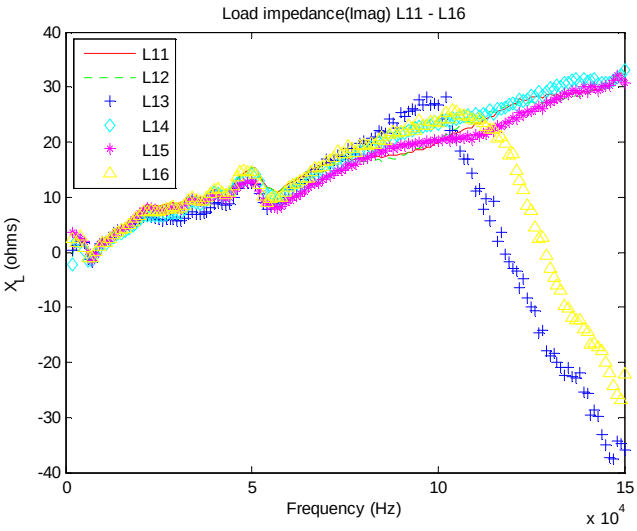

Fig 5-18 Load impedance comparison (imaginary) (L11 to L16)

The results of both experiment groups as shown from Fig 5-13 to Fig 5-18 indicate that the lamps have the distinctive impedances and some of them even change their electric properties from inductive to capacitive at certain frequency such as the L5 in group 1 as well as the L13 and the L16 in group 2.

In addition, since these lamps are unstable and nonlinear loads, the measurement results vary in a certain range. Fig 5-19 and Fig 5-20 show the 10 times measurements of L1 impedance and the range of its variation.

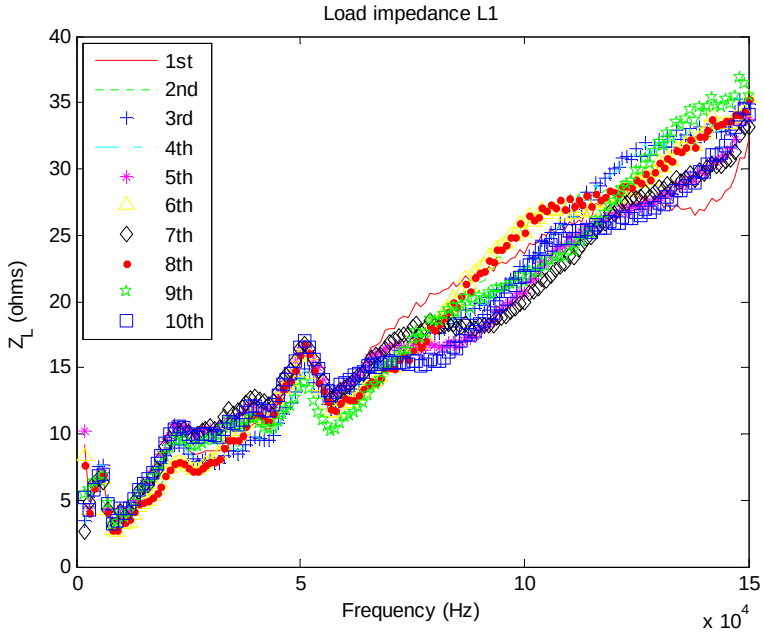

Fig 5-19 10 times measurements of L1 impedance

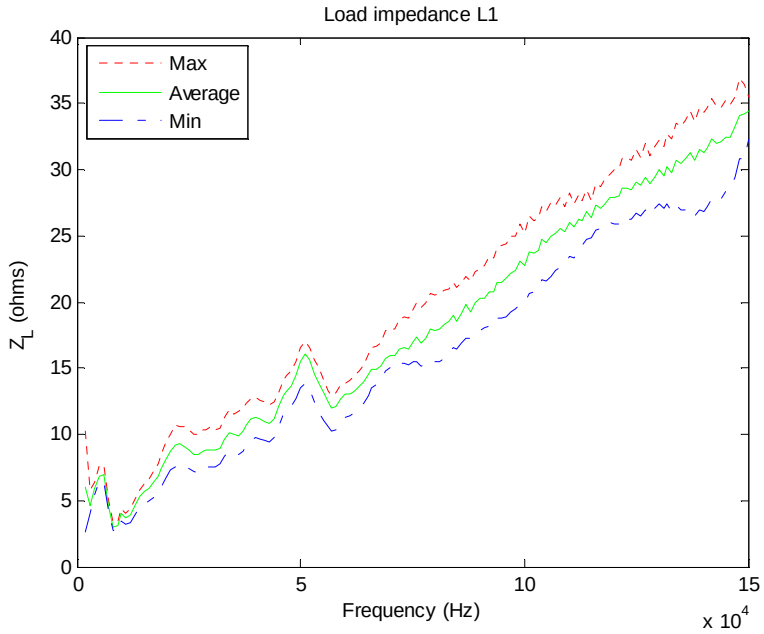

Fig 5-20 Range of L1 impedance variation

The similar measurements are applied to the electric fans. For the same reason, the fans are called by F1 (the fan of 12.5 W rated power) and F2 (the fan of 30 W rated power). The results are displayed in Fig 5-21 to Fig 5-23.

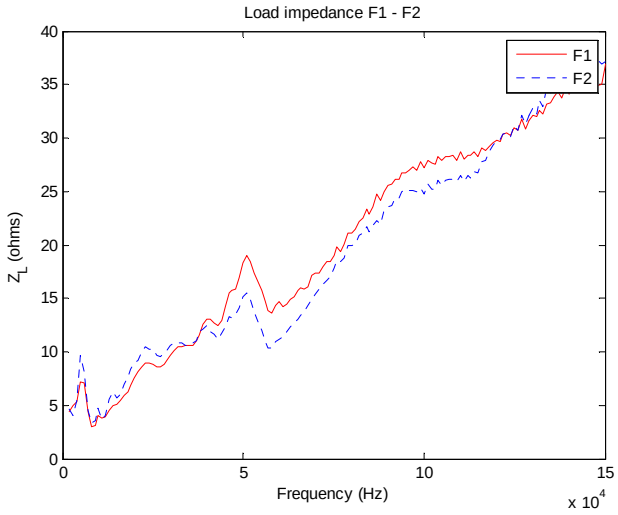

Fig 5-21 Load impedance comparison (F1 and F2)

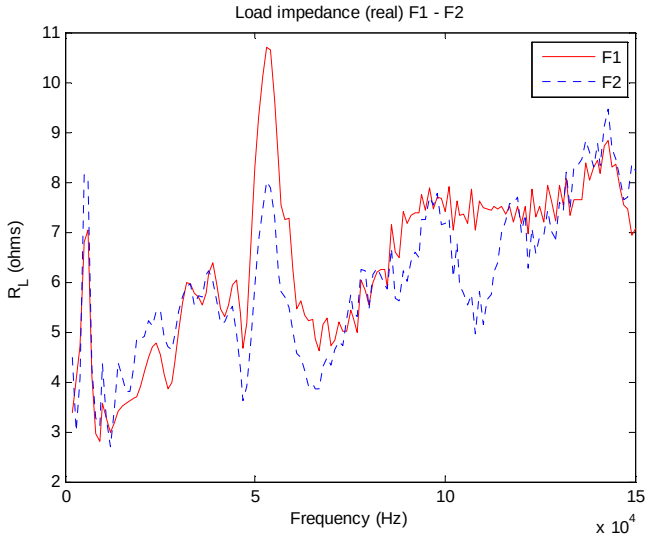

Fig 5-22 Load impedance comparison (real) (F1 and F2)

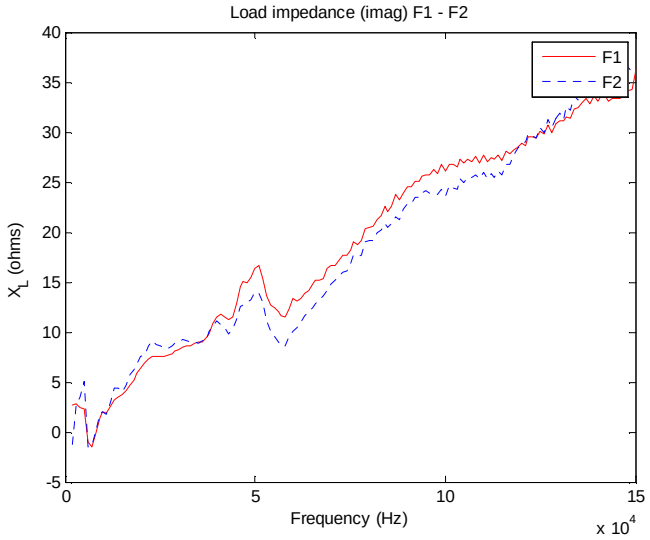

Fig 5-23 Load impedance comparison (imaginary) (F1 and F2)

5.3 Comparison between L1 and L16

The previous measurements imply that the lamps have two different sorts of impedances, inductive and capacitive. To further investigate these two sorts of lamps, L1 and L16 are chosen in this research.

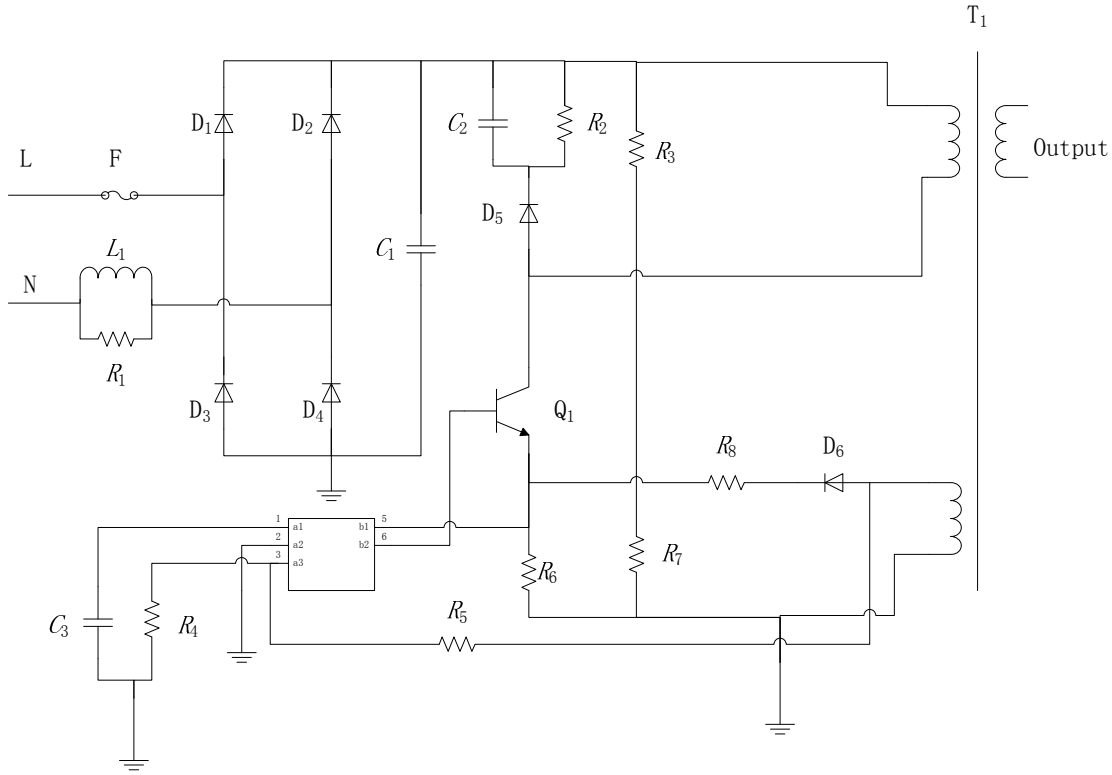

Fig 5-24 Schematics of L1

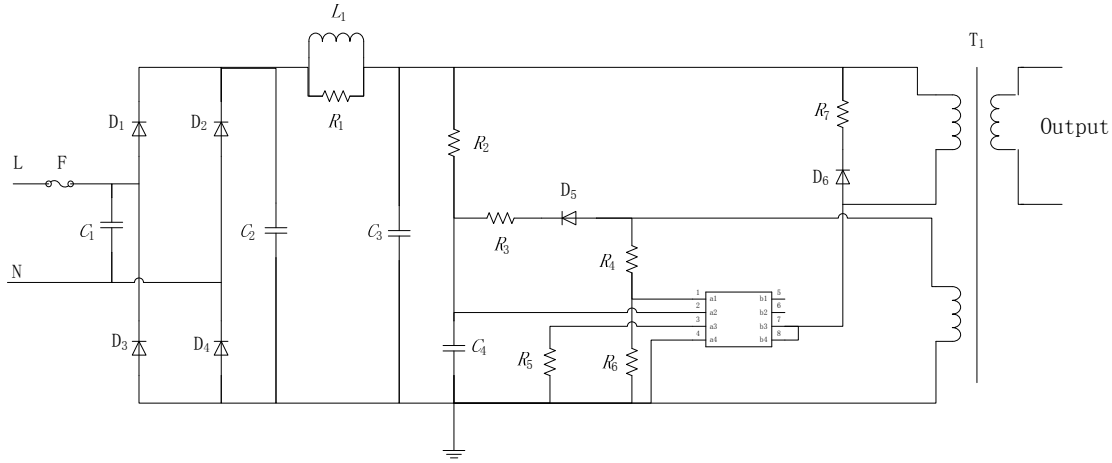

Fig 5-25 Schematics of L16

Fig 5-24 and Fig 5-25 show the schematics of L1 and L16 respectively. Apparently, the inductor before rectifier, named "L_1" in Fig 5-24 and the capacitor "C_1" in Fig 5-25 are supposed to be the main elements resulting in the differences. Using the impedance measurement result of L1, its schematics can be simplified into a simple RL circuit as shown in Fig 5-26.

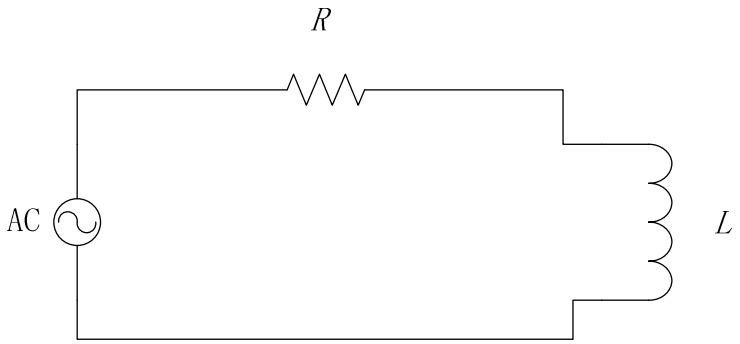

Fig 5-26 Equivalent model of L1

With $R = 5\,\Omega$ and $L = 35\,\mu\text{H}$ which can be derived from the impedance measurement of L1 easily, it shows the calculated impedance in Fig 5-27 using Pspice.

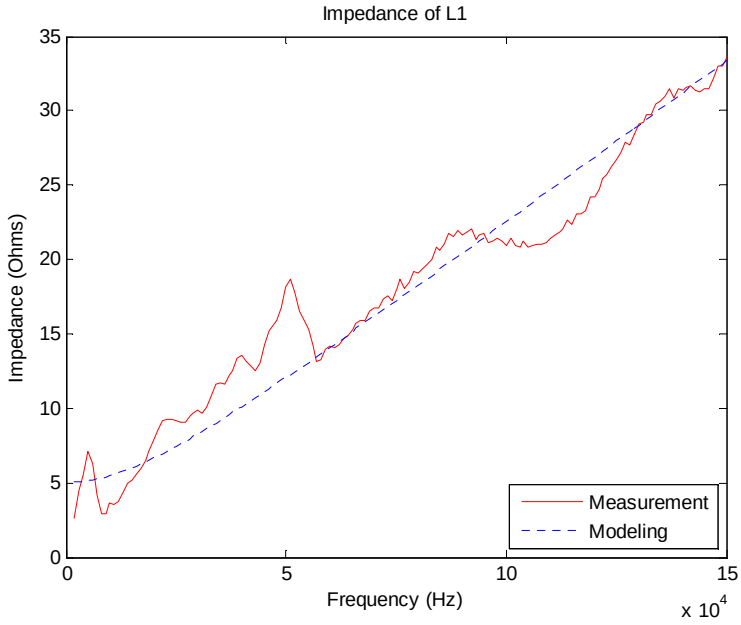

Fig 5-27 Modeling results of L1

Similarly, the schematics of L16 can be also simplified into a simple RLC circuit which is illustrated in Fig 5-28 where $R_1 = 5\,\Omega$, $C = 40\,\text{nF}$, $L = 35\,\mu\text{H}$ and $R_2 = 50\,\Omega$. Then the modeling result is shown in Fig 5-29.

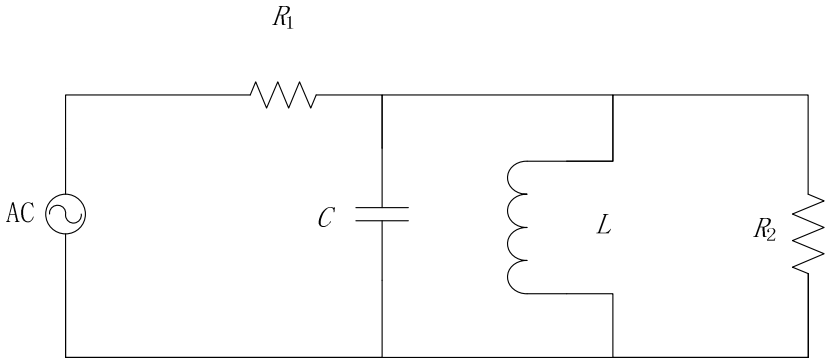

Fig 5-28 Equivalent circuit of L16

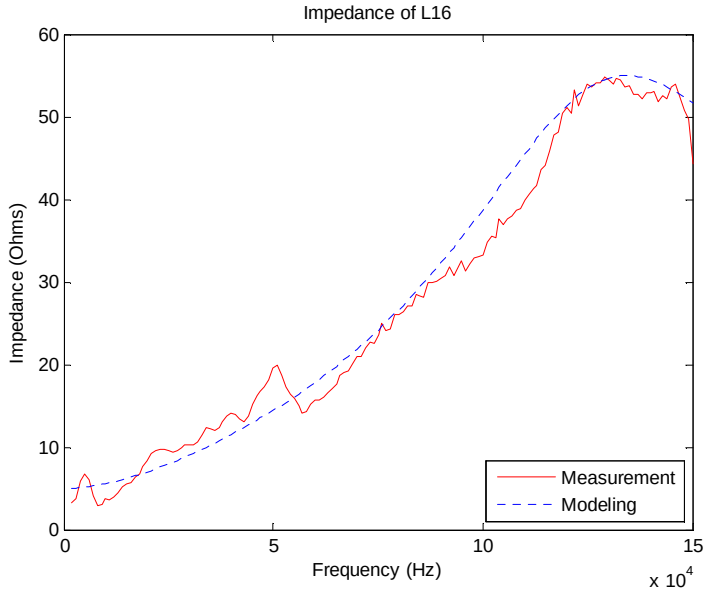

Fig 5-29 Modeling results of L16

The 40 nF capacitor used in modeling can be treated as the C_1 (47 nF) in Fig 5-25. However, the 35 μH inductors in both cases are not able to be located in their schematics. Actually, the inductors "L_1" in Fig 5-24 and in Fig 5-25 are the same, which are both confirmed to be 4.7 mH by a LCR meter. Then, to verify the measurement method again, this three-probe setup is used to measure this 4.7 mH inductor and Fig 5-30 illustrates the measurement results.

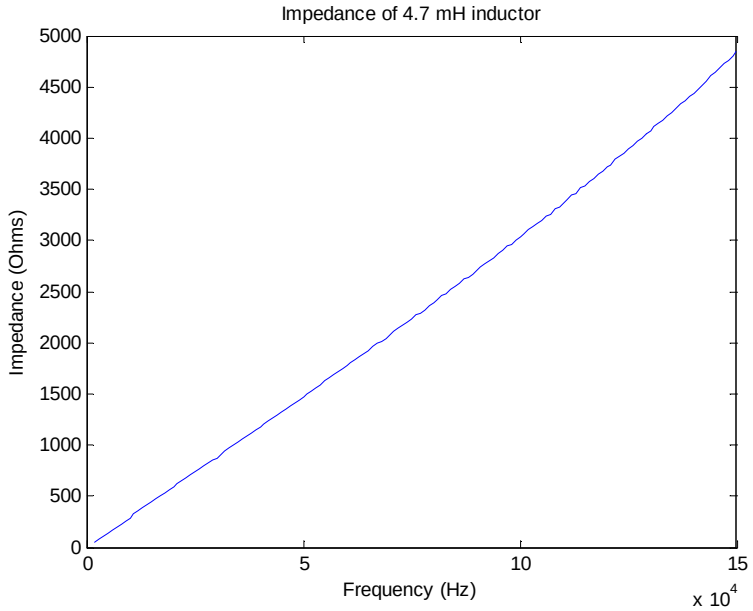

Fig 5-30 Result of using three-probe method to measure a 4.7 mH inductor

In Fig 5-30, it proves again that the three-probe method is capable to lead to the correct measurement result. Therefore, this value of 4.7 mH inductor indeed becomes 35 μH during the measurement. In fact, it is the saturation that degrades the magnetic core's performances during the measurement. As far as we know, most of the inductors have a limit for the flowing current. And for the inductors in this test, the value is about 200 mA. However, in most of immunity tests, the high injection current is sometimes unavoidable. In fact, the test level is at

least 500 mA in root mean square (RMS) value according to the standard [8].
In this case, even though the amplitude of the injection current on each harmonics is low, the summation of the harmonics is significant. Furthermore, the load is measured under its normal operation which means the AC operating current also needs to be counted. Therefore, the contributions of operating and injection current are large enough to saturate the magnetic core. In fact, the amplitude of the current is over 400 mA under the measurement.

5.4 Summary

This three-probe approaching is capable of measuring both the load and the source impedances. Moreover, it is able to successfully distinguish the impedance properties. A choke is necessary for this measurement to separate the part of the circuit under test from the rest of circuit. The result of the power-on measurement may lead to a great difference from the power-off measurement due to the saturation problem. However, it is meaningless to use the power-off measurement result, because sometimes the standard injection results in saturation.

6 Disturbance influences on the measurement of electrical parameters and the smart meter

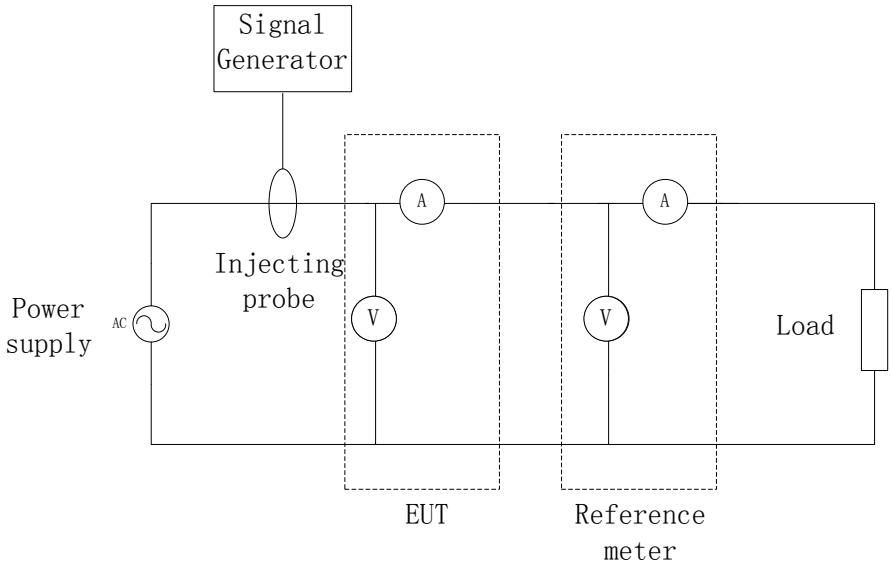

Fig 6-1 Main test circuit

In this case, the smart meter as the equipment under test (EUT) is set into the measurement circuit as illustrated in Fig 6-1. The disturbances are injected into the phase line via the injecting probe. Since the source and load impedances have been measured successfully in the previous part, it is possible to calculate their circuit resonance frequencies. Then by intentionally injecting noise at the certain frequencies, it is able to find whether the resonance will affect the accuracy of the smart meter or not.

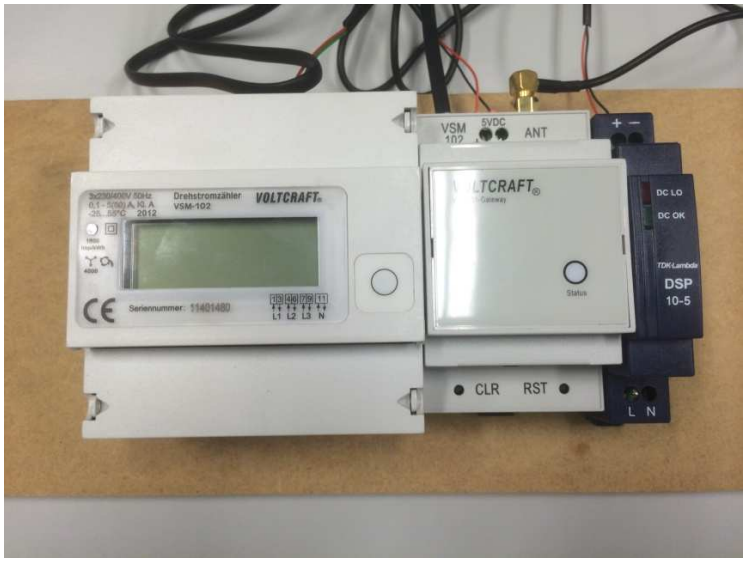

Fig 6-2 Smart meter setup

The VOLTCRAFT VSM-101 smart meter which is a normal home appliance is used in this case. The screen of this meter can display the real time power consuming when it is connected

into the circuit under test. The data measured by the smart meter is able to send via an antenna then PC can receive the data by a USB wireless receiver and process the data graphically. Therefore, it is very convenient to observe the performance of the meter when noise is injected.

In this research, the smart power supply Pacific Power Model 108 AMX is used again as the main supply for its stability. From chapter 5, it is noticed that there are 3 LEDs (L5, L13 and L16) which perform distinctly from the others. Thus these three LEDs are used as the loads under tests. In addition, as L1 has been investigated in detail, it is chosen to represent the other LEDs. These four LEDs are shown in Fig 6-3. Then, unlike the current probes, the current shunt has a stable transfer impedance performance, which makes it easier to realize in programming than using current probe. Thus, in this case, the BCI probe is used to inject noise and the current shunt, the voltage divider and the NI digitizer are used to form a reference meter. After necessary analysis, the results obtained from the reference meter are compared with the data received from smart meter to find difference.

Fig 6-3 Load L1 (upper-left), L5 (upper-right), L13 (down-left) and L16 (down-right)

To make the source impedance variable, either a variable-inductance box connected in series or a variable-capacitance box connected in parallel between the power source and the smart meter is used in this case. In this way, it is able to simulate the several combinations of sources and loads. However, since smart power supply has certain built-in source impedance itself and it is inductive as displayed from Fig 5-7 to Fig 5-9, it is not able to simulate the situation that a source with lower inductive impedance than this residual inductance.

In the following content, the performances of different loads with or without injecting noise are discussed first. Their current and voltage harmonics, power and RMS current are the main measured electrical parameters. Then the influence of the disturbances on the smart meter's display is presented and compared with the readings of the reference meter. At last, some analysis and possible explanations are given.

6.1 Measurement with the variable-inductance box

In this case, a variable-inductance box is connected in series with the smart power supply and the smart meter as shown in Fig 6-4. By switching the knobs, it is able to simulate the different inductive source impedance. Here, the values of 0 H, 10 μH, 50 μH, 100 μH, 200 μH, 300 μH and 400 μH are used to investigate.

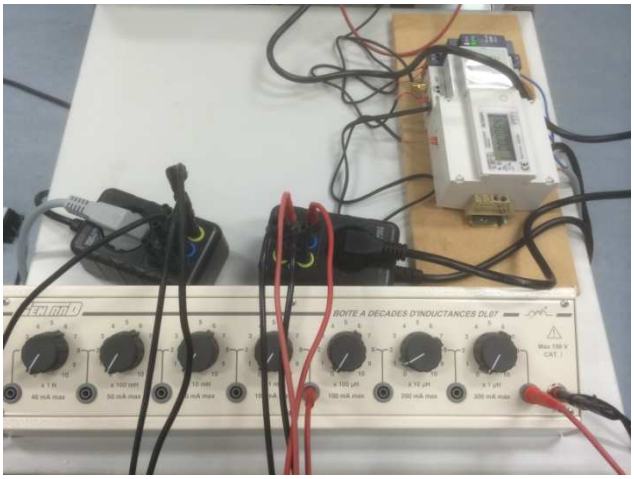

Fig 6-4 The variable-inductance box

The experiment is done under two different situations that system works without injection and with 1 k – 150 kHz injection. The source of injection (or noise source) is the same as before – the 1 k – 150 kHz "flat" source produced by HP 33120A Function Generator. The advantage of using this noise source here is that it covers all the needed frequencies so that it is not necessary to calculate the specific resonance frequency. When resonance occurs in this frequency range, it can be observed clearly. Nevertheless, due to the inconstant transfer impedance of BCI probe, the resultant signal from the injecting probe will not be flat anymore at the frequency domain.

From Fig 6-5 to Fig 6-20, they illustrate the receiving current and voltage of the reference meter both in log-log (left) and in linear axis (zoom in range 1 k – 150 kHz) (right) for L1, L5, L13 and L16 when there is or is not injection respectively.

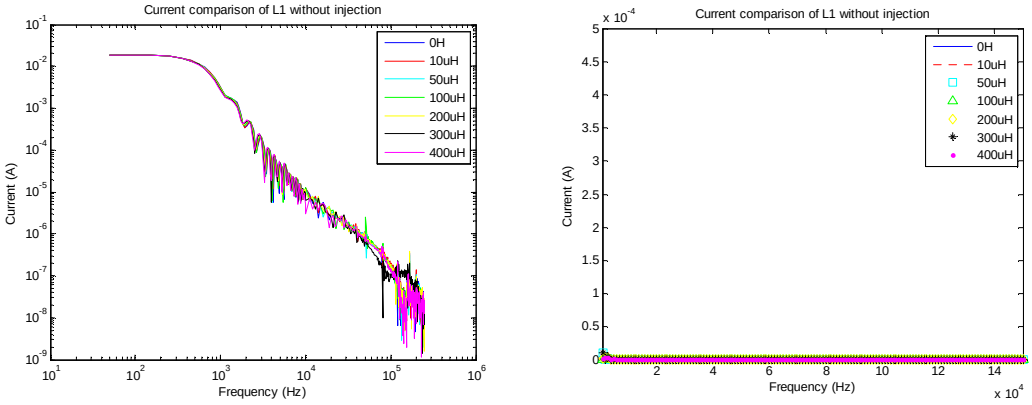

Fig 6-5 Current comparison of L1 without injection using inductance box

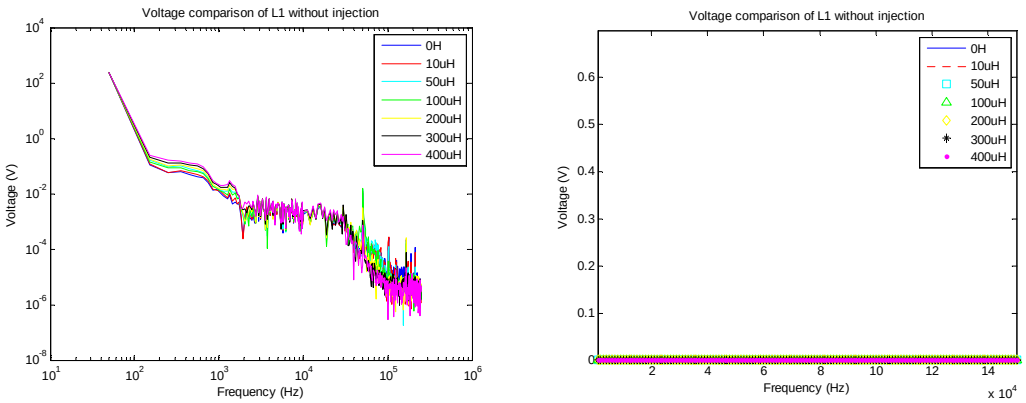

Fig 6-6 Voltage comparison of L1 without injection using inductance box

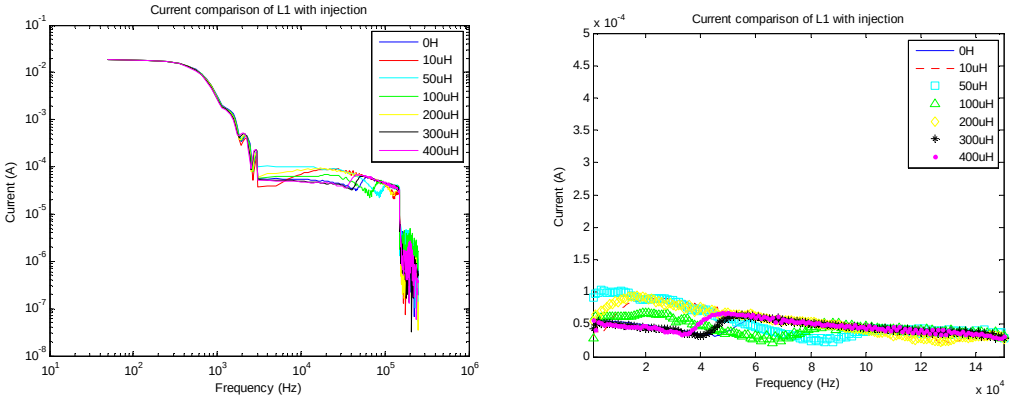

Fig 6-7 Current comparison of L1 with injection using inductance box

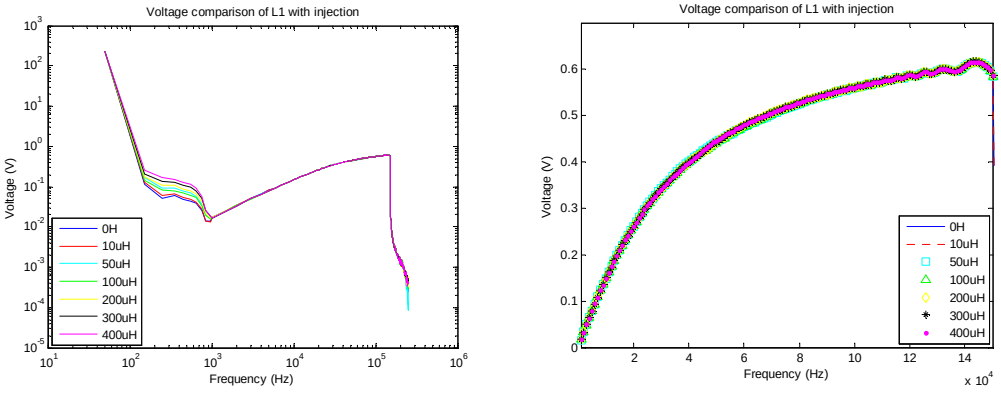

Fig 6-8 Voltage comparison of L1 with injection using inductance box

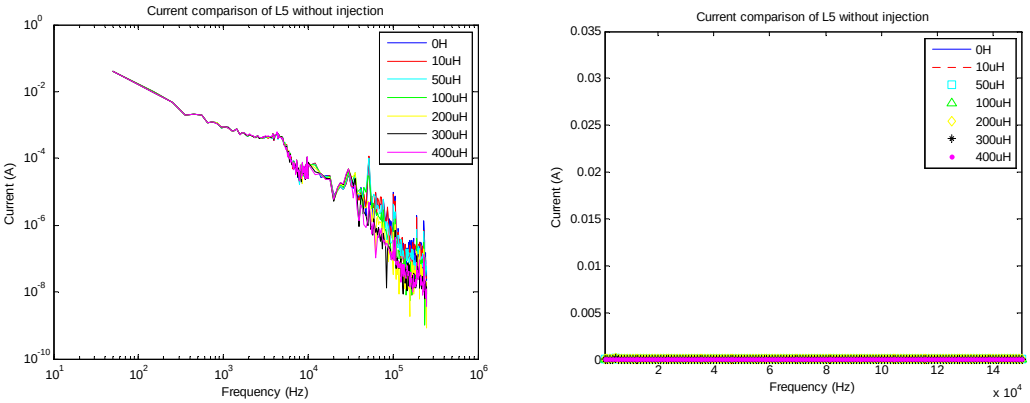

Fig 6-9 Current comparison of L5 without injection using inductance box

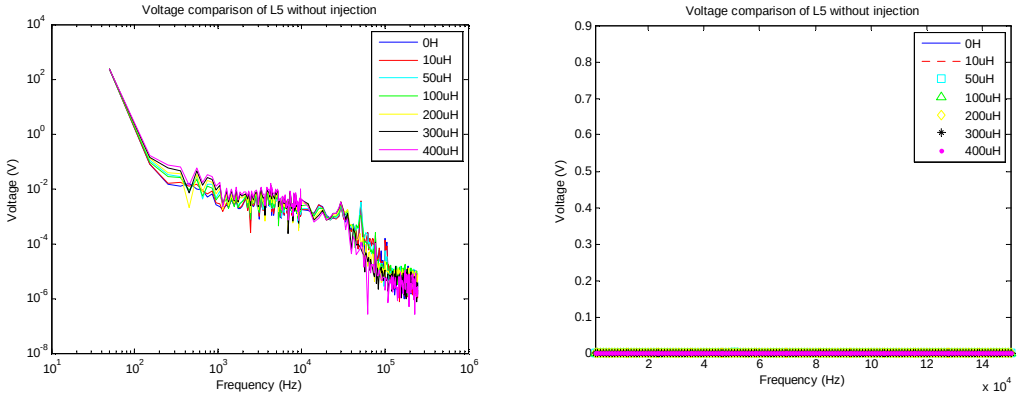

Fig 6-10 Voltage comparison of L5 without injection using inductance box

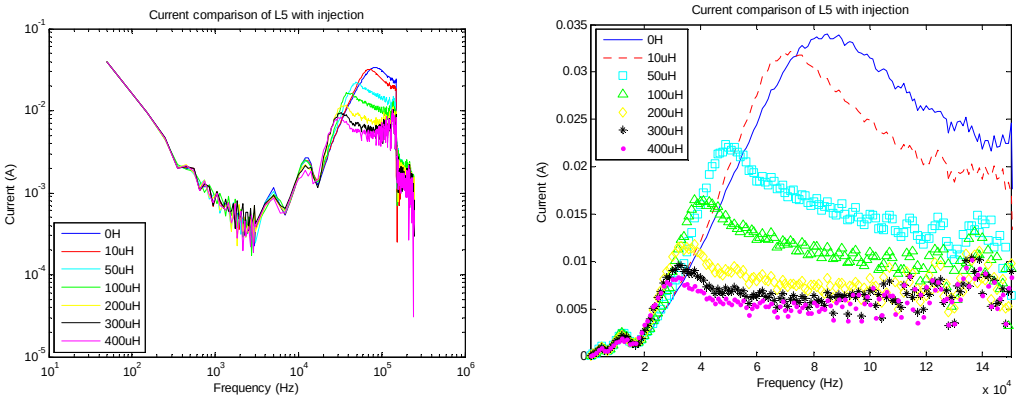

Fig 6-11 Current comparison of L5 with injection using inductance box

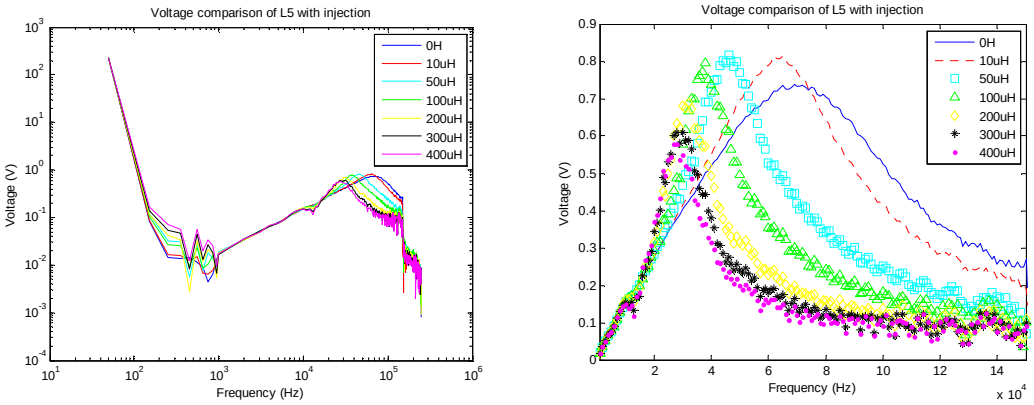

Fig 6-12 Voltage comparison of L5 with injection using inductance box

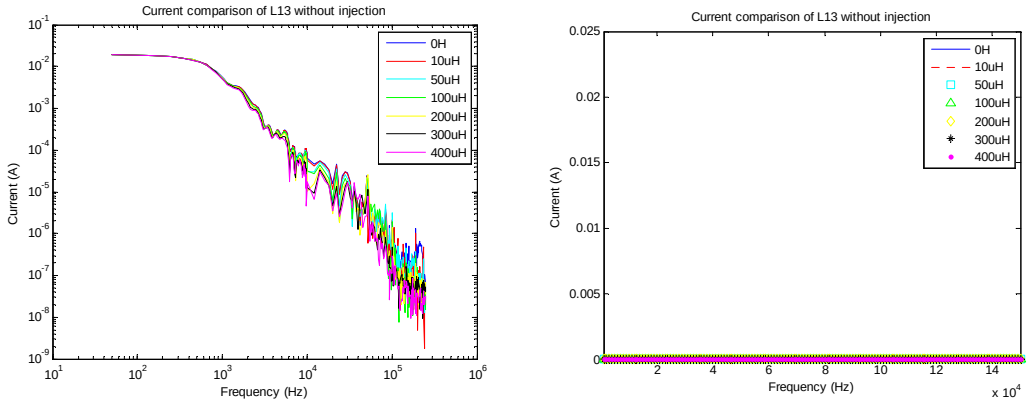

Fig 6-13 Current comparison of L13 without injection using inductance box

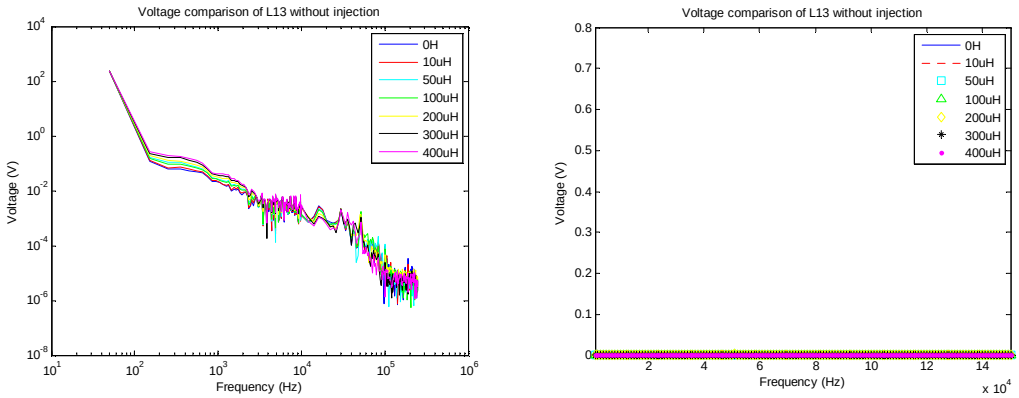

Fig 6-14 Voltage comparison of L13 without injection using inductance box

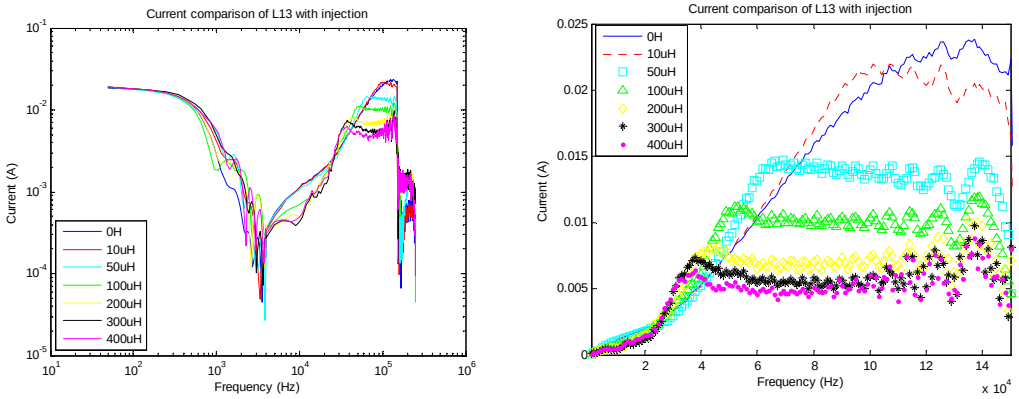

Fig 6-15 Current comparison of L13 with injection using inductance box

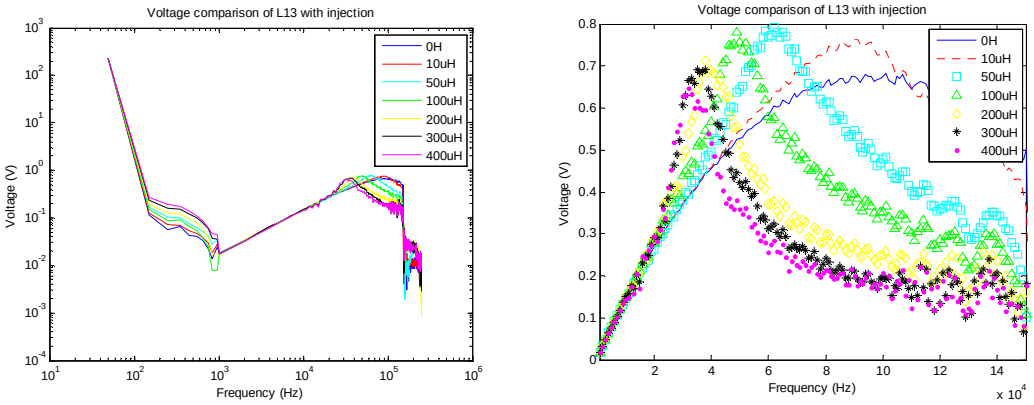

Fig 6-16 Voltage comparison of L13 with injection using inductance box

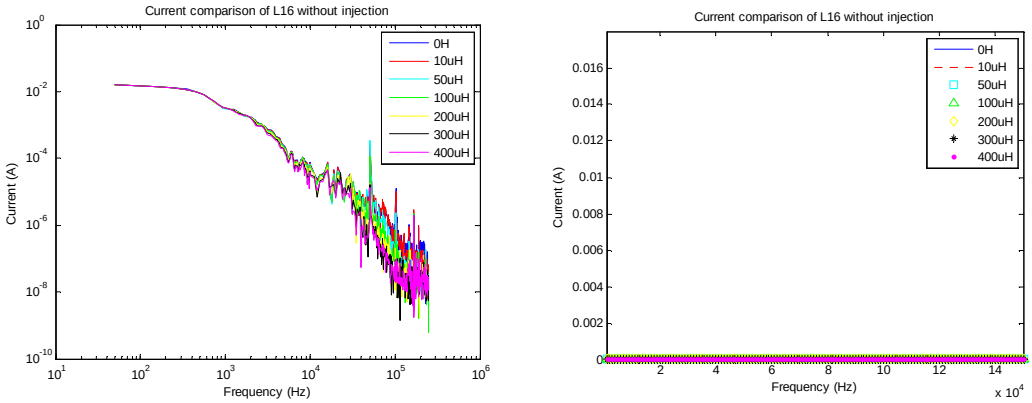

Fig 6-17 Current comparison of L16 without injection using inductance box

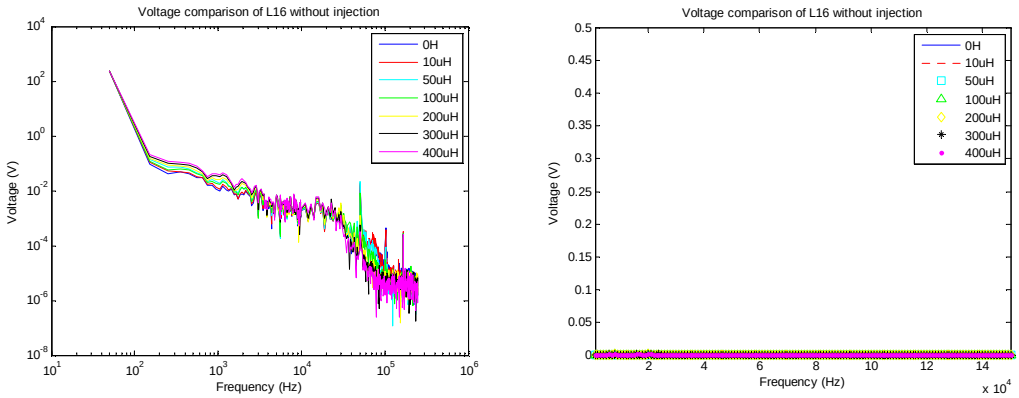

Fig 6-18 Voltage comparison of L16 without injection using inductance box

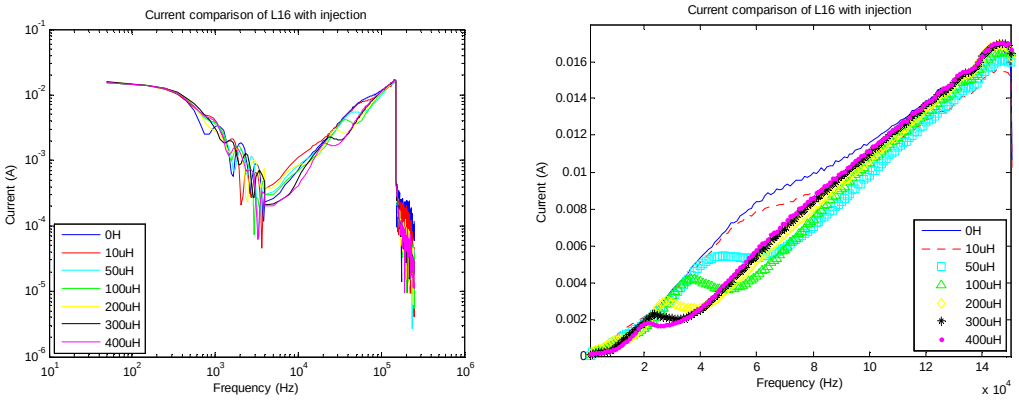

Fig 6-19 Current comparison of L16 with injection using inductance box

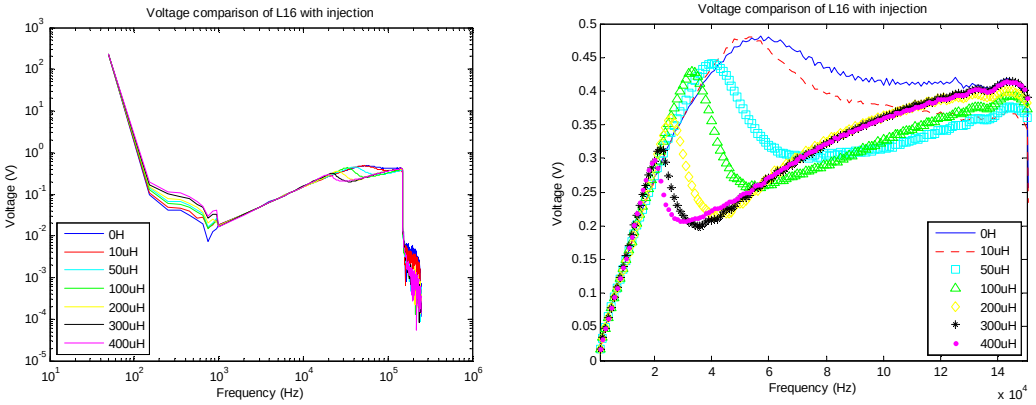

Fig 6-20 Voltage comparison of L16 with injection using inductance box

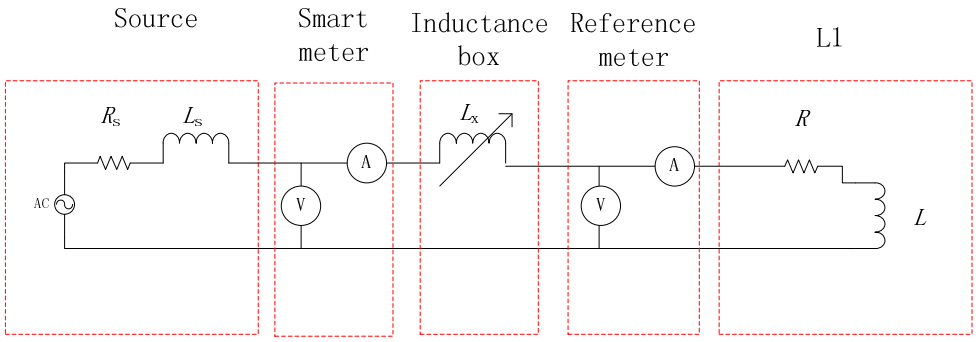

Fig 6-21 Equivalent circuit of measurement with L1 using inductance box

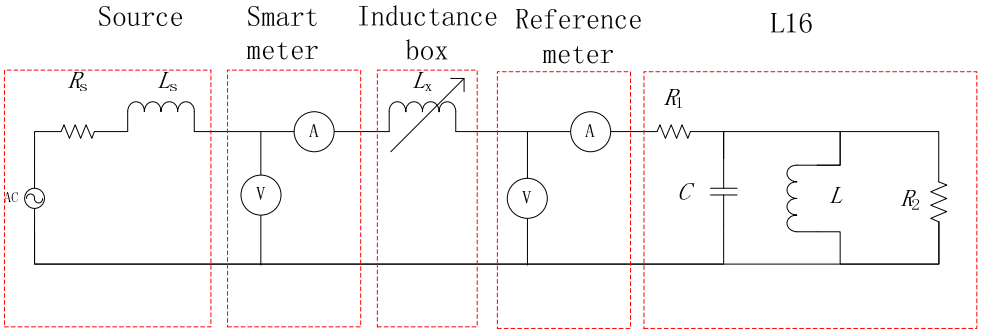

Fig 6-22 Equivalent circuit of measurement with L16 using inductance box

Apparently, resonance occurs at different frequency point with source impedance variation when this power supply serves the capacitive load – L5, L13 and L16. Using the electric models for L1 and L16 built in chapter 5, it is possible to draw an equivalent measurement circuit for each sort of loads and they are shown in Fig 6-21 and Fig 6-22 respectively. It is noticed that the capacitor *C* in Fig 6-22 should be the component that forms the resonant circuit with the source impedance. Then because of the inconstant transfer impedance (increasing with frequency) of BCI probe, the noise injected into the coupling electric circuit is also disequilibrium in the frequency range – higher injection level in high frequency. Thus it may result in a situation that the injected noise at high frequency is higher than the one at low frequency where even if the resonance occurs as shown in Fig 6-19.

	L1		L16	
L (μH)	Power (No injection) (W)	Power (With injection) (W)	Power (No injection) (W)	Power (With injection) (W)
0	6.6	6.6	5.7	5.6
10	6.6	6.7	5.7	5.6
50	6.7	6.6	5.7	5.6
100	6.6	6.6	5.6	5.7
200	6.6	6.7	5.6	5.7
300	6.6	6.6	5.7	5.7
400	6.6	6.6	5.7	5.7

Table 6-1 Smart meter readings of L1 and L16 using inductance box

Resonance causes high harmonic current at specific frequency and some of their amplitudes are even comparable to the fundamentals. This may influence some accurate electric measurement instruments. Fortunately, the equipment under test (EUT) - the VOLTCRAFT VSM-101 smart meter - seems to work quite well. Table 6-1 shows the readings of this smart meter when using it to measure the power of L1 and L16. What should be noticed is that the readings are not stable which have 0.2 W variations in both positive and negative direction.

The principle of this category of the smart meter to calculate the consuming power is based on the definition of the average power during a short sampling time which can be mathematically represented by

$$P = \frac{1}{\mathrm{T}}\int_0^{\mathrm{T}} v(t)i(t)dt \qquad (6\text{-}1)$$

where *v*(*t*) and *i*(*t*) are the real-time value of voltage and current respectively and T is a short sampling period.

The power for reference meter, besides, sampling method in time domain is also calculated in frequency domain by using

$$P = \sum_{k=1}^{N} V_k I_k \cos(\theta_{vk} - \theta_{Ik}) \quad (6\text{-}2)$$

where V_k and I_k are the amplitude of k^{th} harmonics of voltage and current respectively, then θ_{vk} and θ_{ik} are the phases of k^{th} harmonics of voltage and current respectively.

Both Equation (6-1) and Equation (6-2) are able to lead to the constant result of consuming power.

Table 6-2 and Fig 6-23 to 6-24 show the result from Equation (6-1) or Equation (6-2) based on the data collected by the reference meter. There are about 2.3 W differences between the smart meter readings and the results from the reference meter. However, this is caused by the power consuming of the voltage divider used to protect the digitizer and the current shunt used for measurement.

Even though as Fig 6-24 shows the power is influenced slightly in the reference measurement, with 0.2 W error tolerance it is not able to find out whether the smart meter is influenced or not. Fig 6-25 and Fig 6-26 illustrate the power consuming of L5 and L13 respectively. Both L5 and L13 show that the disturbance has limit influence on their power consuming. Since the imposed noise does not reach the level as standard observed suggests, it could be the reason why there is no significant phenomenon.

	L1		L16	
L (μH)	Power (No injection) (W)	Power (With injection) (W)	Power (No injection) (W)	Power (With injection) (W)
0	4.257	4.253	3.333	3.456
10	4.260	4.256	3.328	3.438
50	4.258	4.255	3.331	3.424
100	4.260	4.257	3.328	3.428
200	4.254	4.254	3.328	3.428
300	4.251	4.254	3.330	3.431
400	4.255	4.255	3.328	3.437

Table 6-2 Power of L1 and L16 via digitizer using inductance box

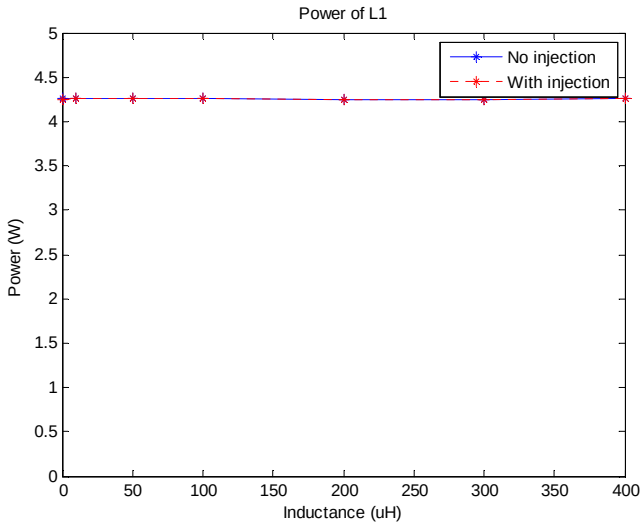

Fig 6-23 Power of L1 using inductance box

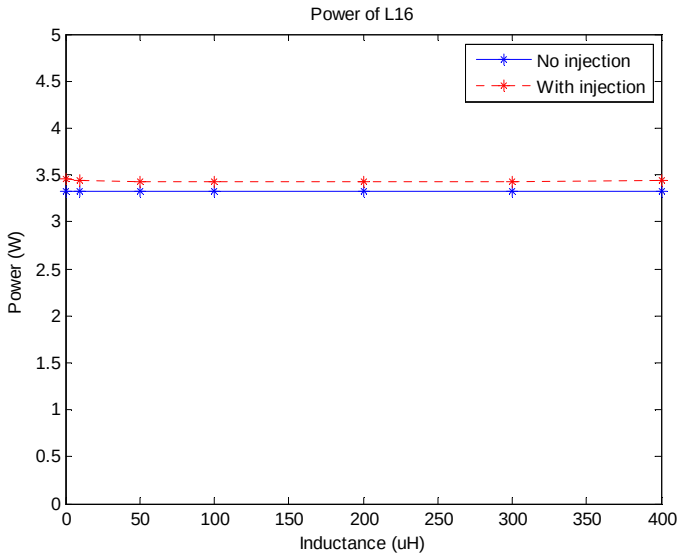

Fig 6-24 Power of L16 using inductance box

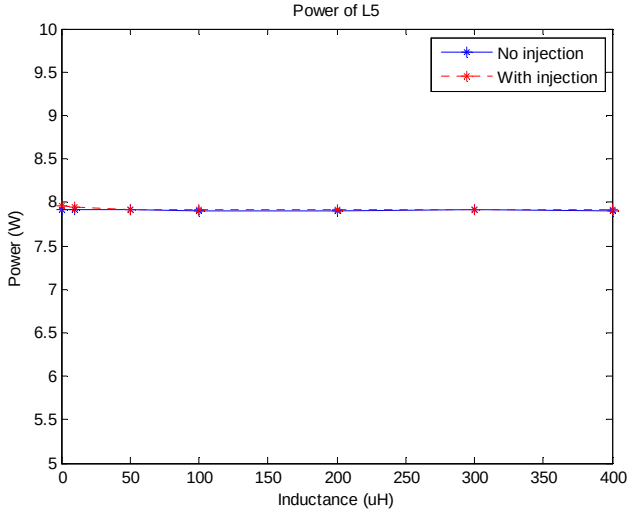

Fig 6-25 Power of L5 using inductance box

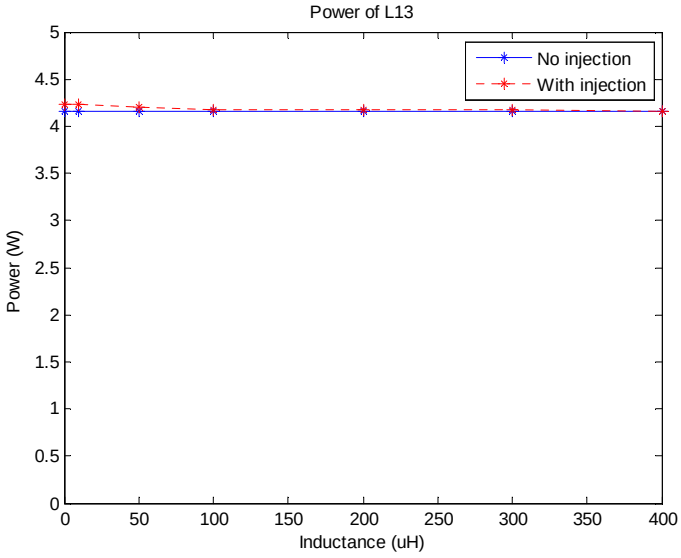

Fig 6-26 Power of L13 using inductance box

Since some of the current harmonics are comparable to the fundamental when there is injection, the root mean square (RMS) current can be heavily influenced.

RMS current according to its definition can be obtained by

$$I_{\mathrm{rms}} = \sqrt{\frac{1}{\mathrm{T}}\int_0^{\mathrm{T}} i^2(t)dt} \tag{6-3}$$

or

$$I_{\mathrm{rms}} = \sqrt{\sum_{\mathrm{k}=1}^{\mathrm{N}} I_{\mathrm{pk}}^2} \tag{6-4}$$

where $i(t)$ is the real-time current value and I_{pk} is the amplitude of k^{th} current harmonics.

By applying Equation (6-3) and Equation (6-4), both of L1's and L16's RMS current are achieved. Table 6-2 shows the RMS current values of both loads with source impedance varying and they are also displayed graphically in Fig 6-27 and Fig 6-28.

	L1		L16	
L (μH)	I_{rms}(No injection) (A)	I_{rms} (With injection) (A)	I_{rms}(No injection) (A)	I_{rms} (With injection) (A)
0	0.04185	0.04181	0.03327	0.1396
10	0.04178	0.04159	0.03324	0.1284
50	0.04145	0.04135	0.03315	0.1198
100	0.04159	0.04149	0.03321	0.1224
200	0.04131	0.04120	0.03316	0.1240
300	0.04105	0.04103	0.03310	0.1266
400	0.04082	0.04079	0.03305	0.1284

Table 6-3 RMS current of L1 and L16

As what the figures illustrate, injected noise makes a big difference for this capacitive load L16 on its RMS current. This could lead to a very dangerous situation that the load or other instruments in this circuit may be overheated and destroyed by this high current. In addition, for some explicit devices with sensitive chips, their performances may be affected by the possible strong electromagnetic field resulting from high RMS current. Fig 6-29 and Fig 6-30 illustrate the RMS current performances for L5 and L13.

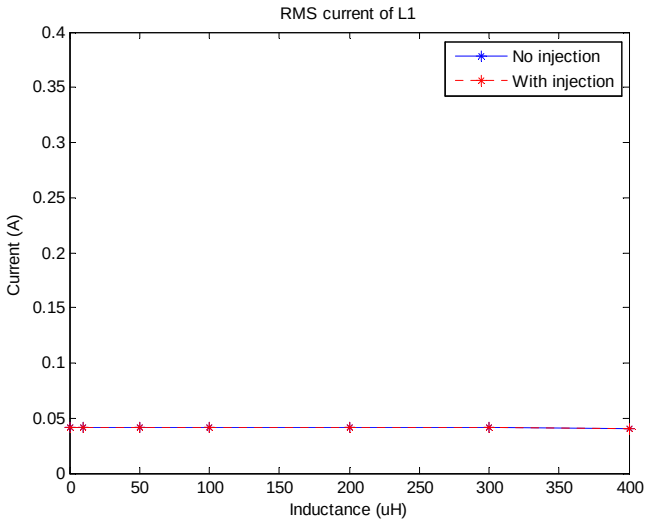

Fig 6-27 RMS current of L1 using inductance box

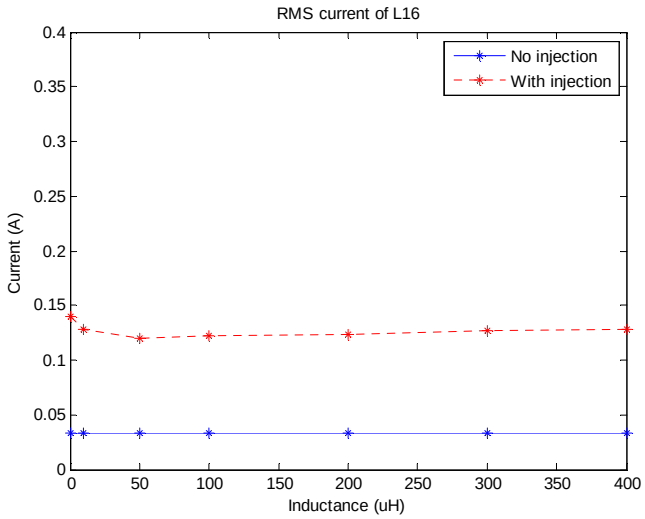

Fig 6-28 RMS current of L16 using inductance box

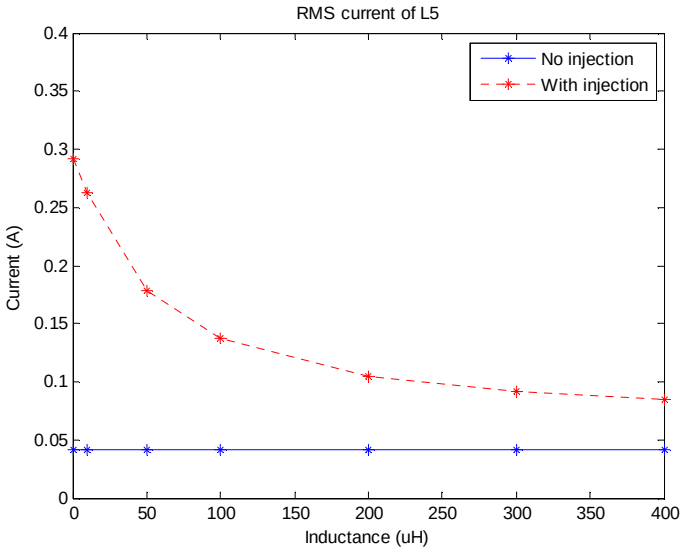

Fig 6-29 RMS current of L5 using inductance box

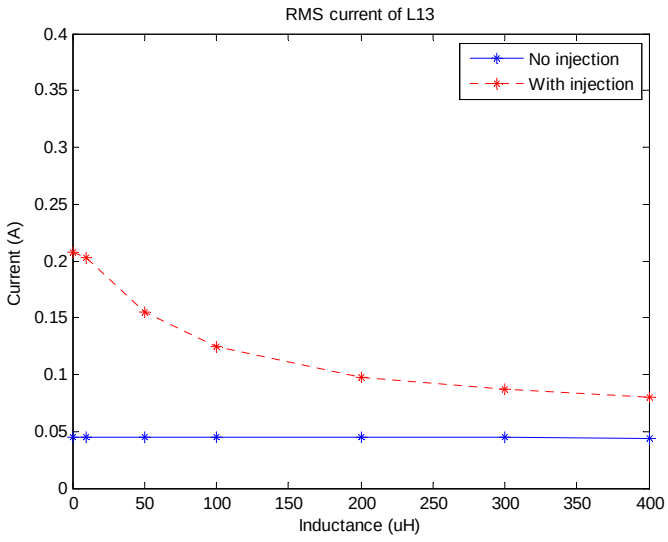

Fig 6-30 RMS current of L13 using inductance box

6.2 Measurements with variable-capacitance box

Similar as in section 6.1, a variable-capacitance box is connected in parallel with the power supply as shown in Fig 6-31. In this case, the values of 0F, 10nF, 50nF, 100nF, 200nF, 300nF and 400nF are applied to the capacitance box and the measurement is implemented under the same conditions as before.

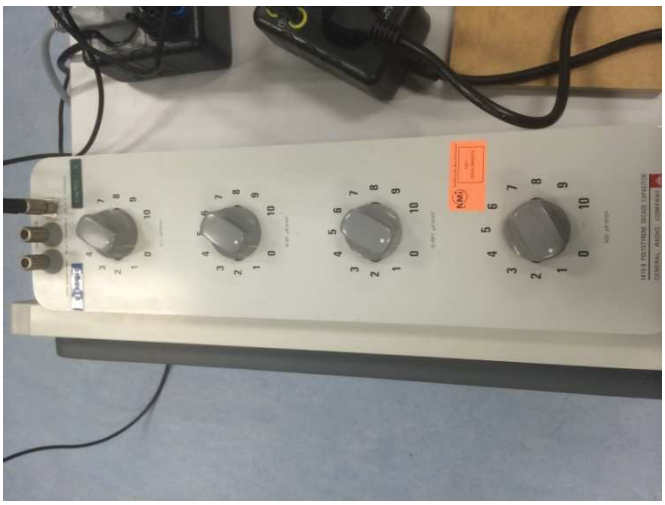

Fig 6-31 The variable-capacitance box

In this case, the measurement equivalent circuits for L1 and L16 will be a little different and they are illustrated in Fig 6-32 and Fig 6-33 respectively.

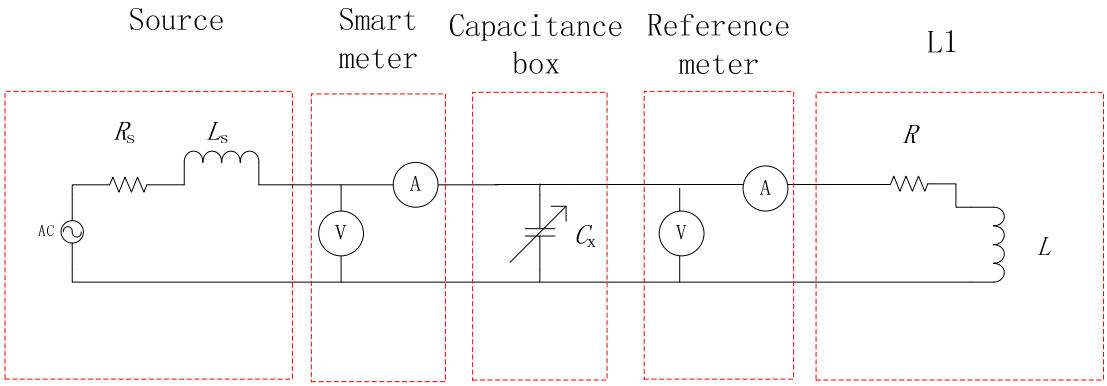

Fig 6-32 Equivalent circuit of measurement with L1 using capacitance box

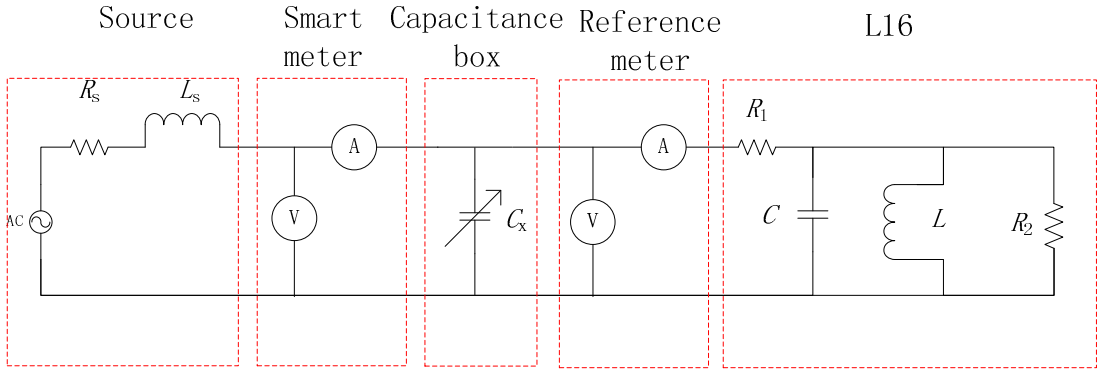

Fig 6-33 Equivalent circuit of measurement with L16 (L5 or L13) using capacitance box

As it can be concluded from section 6.1, the inductor at source side and the capacitor at load

side are able to form a series resonant circuit and it will allow high resonance current to pass through the circuit. The circuit in Fig 6-32 seems to have the same function of resonance. But the resonance current will not reach the load, yet it will pass through the capacitance box. Since our measurement device – the digitizer is set at the load side. It will not detect this resonance current. Of course, this resonance current will not influence the load. However, this will not hold true when it comes to the capacitive loads in Fig 6-33, because the capacitor inside the load will still allow a part of resonance current to pass by. From Fig 6-34 to Fig 6-49 they display the current and voltage performance when the measurement was applied to different loads.

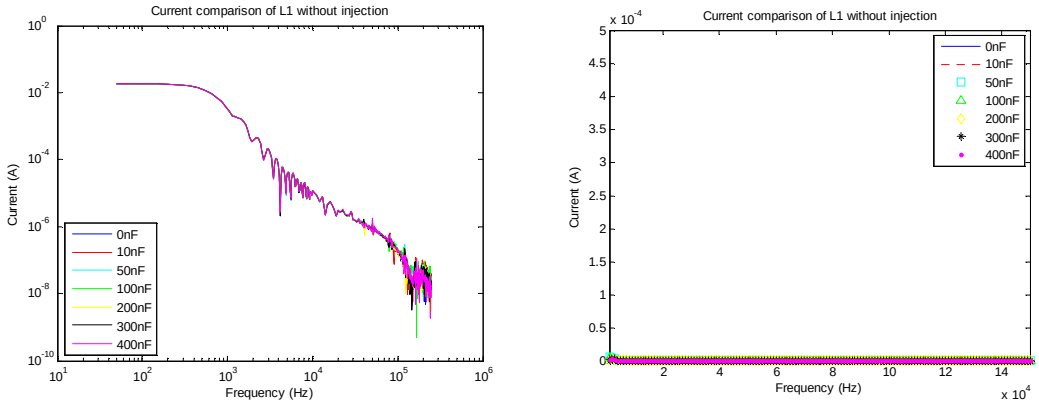

Fig 6-34 Current comparison of L1 without injection using capacitance box

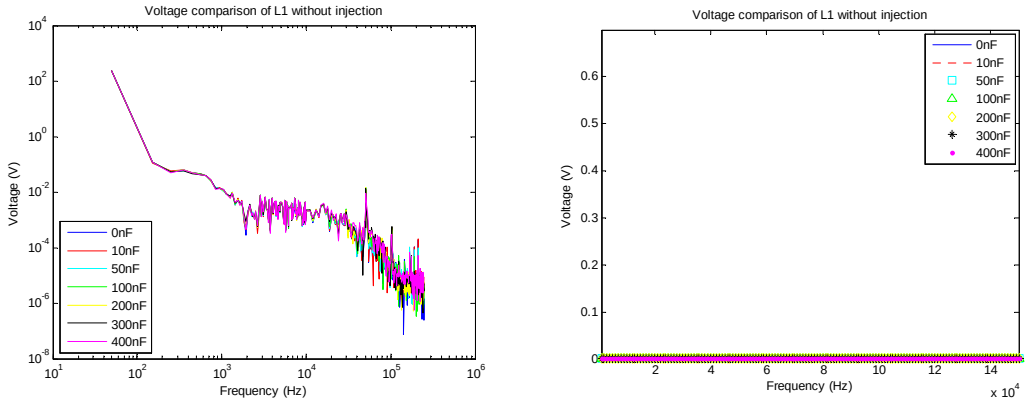

Fig 6-35 Voltage comparison of L1 without injection using capacitance box

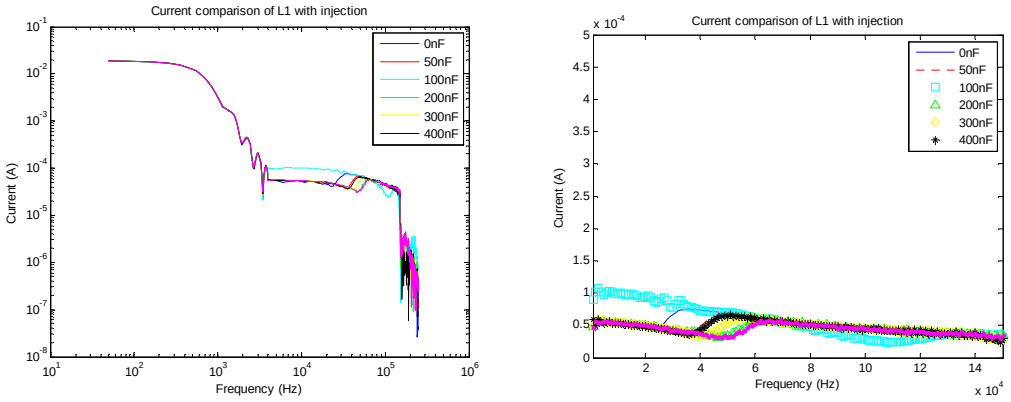

Fig 6-36 Current comparison of L1 with injection using capacitance box

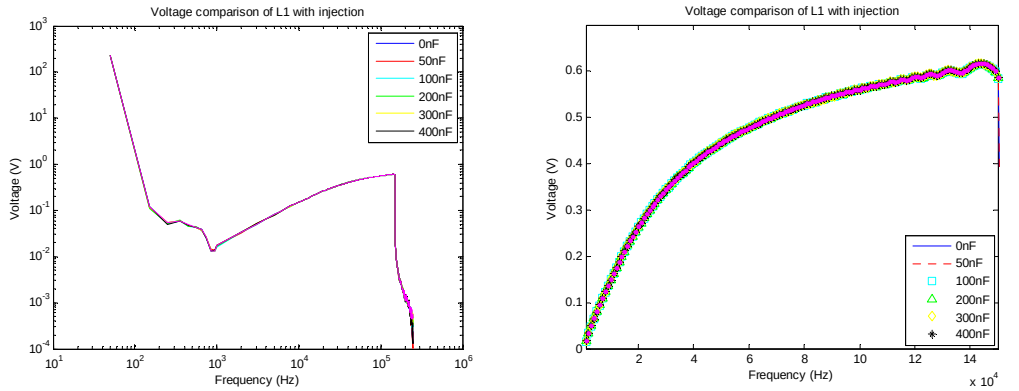

Fig 6-37 Voltage comparison of L1 with injection using capacitance box

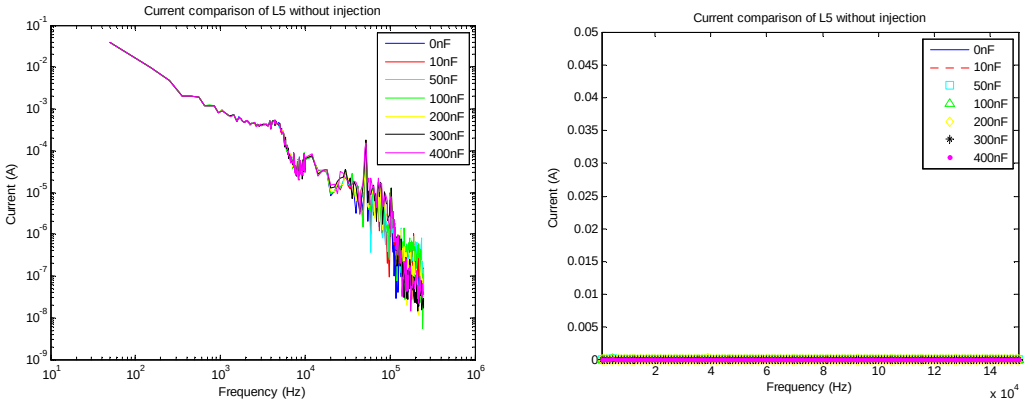

Fig 6-38 Current comparison of L5 without injection using capacitance box

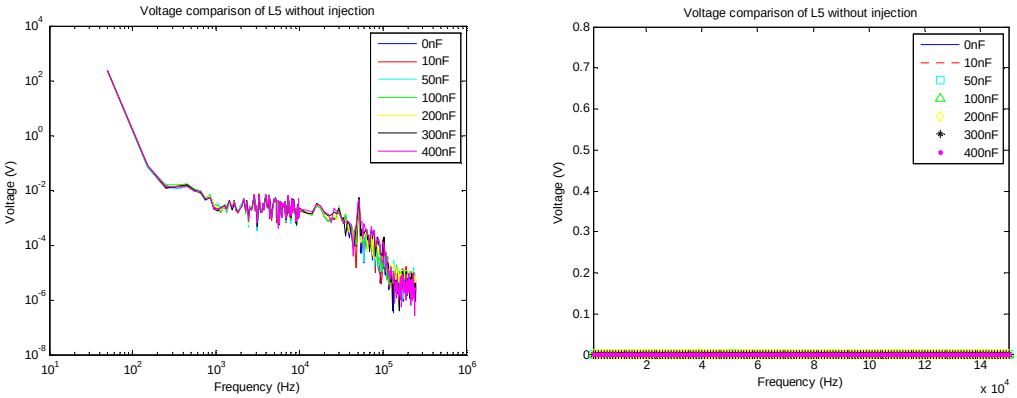

Fig 6-39 Voltage comparison of L5 without injection using capacitance box

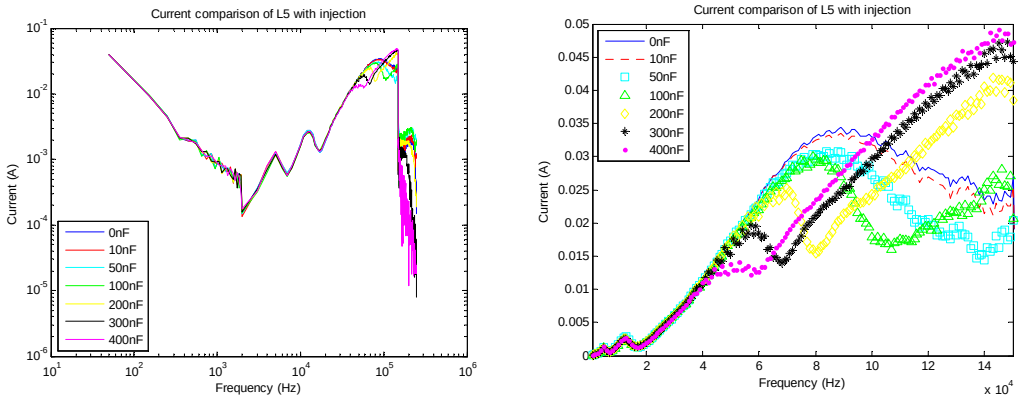

Fig 6-40 Current comparison of L5 with injection using capacitance box

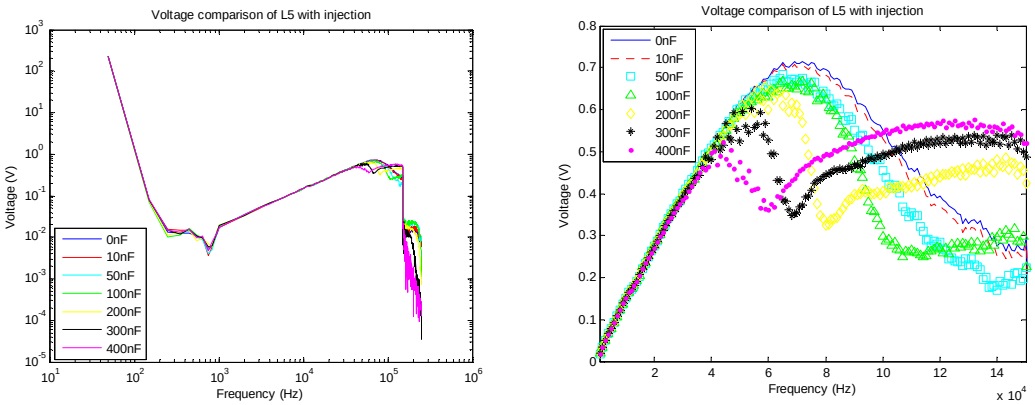

Fig 6-41 Voltage comparison of L5 with injection using capacitance box

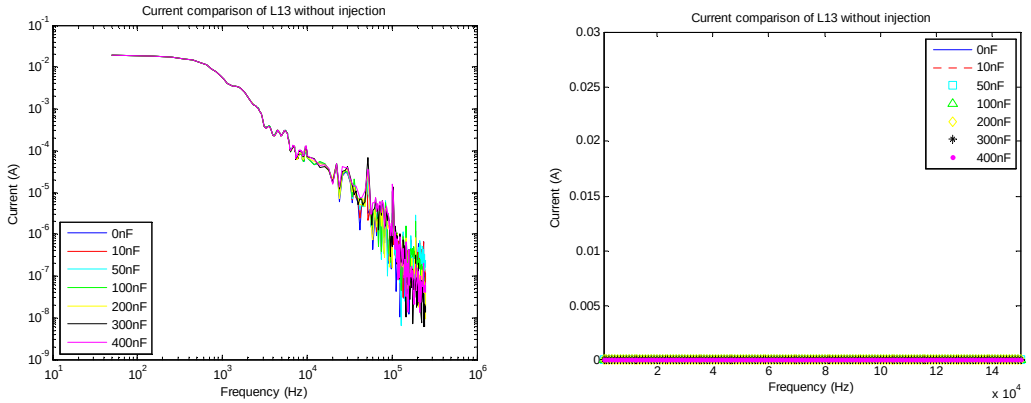

Fig 6-42 Current comparison of L13 without injection using capacitance box

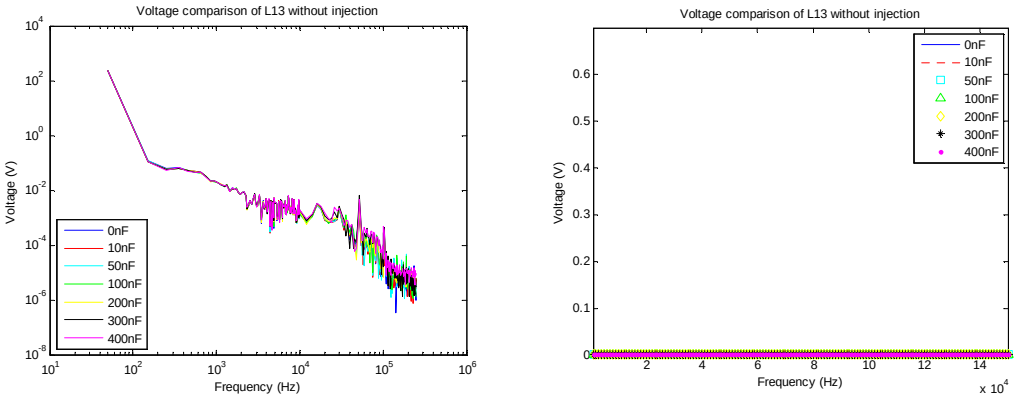

Fig 6-43 Voltage comparison of L13 without injection using capacitance box

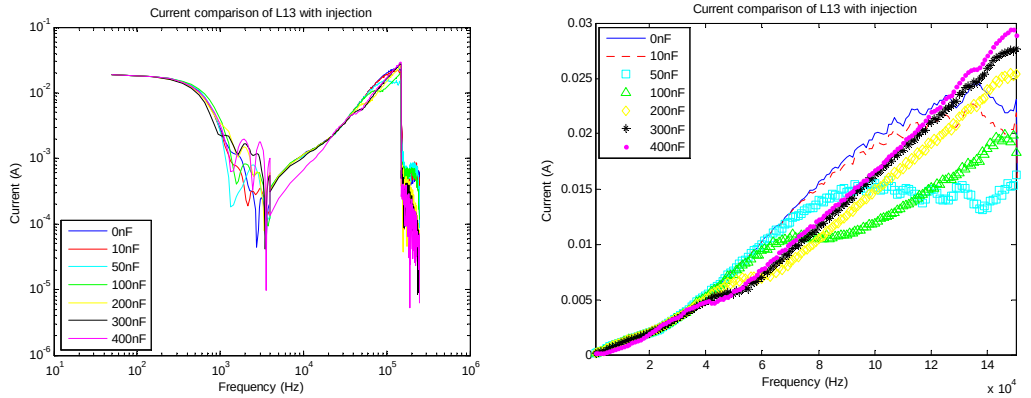

Fig 6-44 Current comparison of L13 with injection using capacitance box

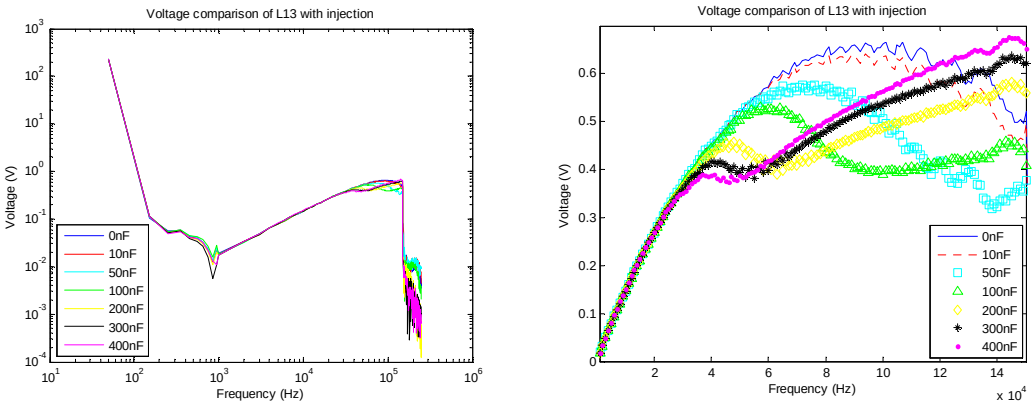

Fig 6-45 Voltage comparison of L13 with injection using capacitance box

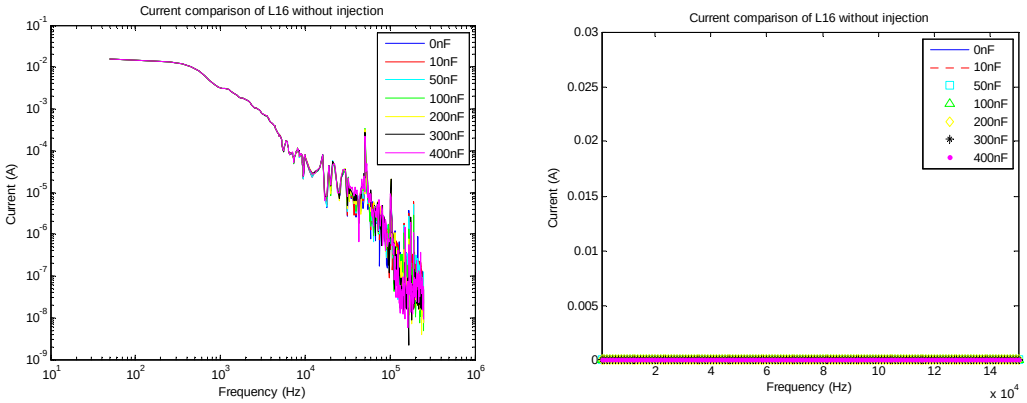

Fig 6-46 Current comparison of L16 without injection using capacitance box

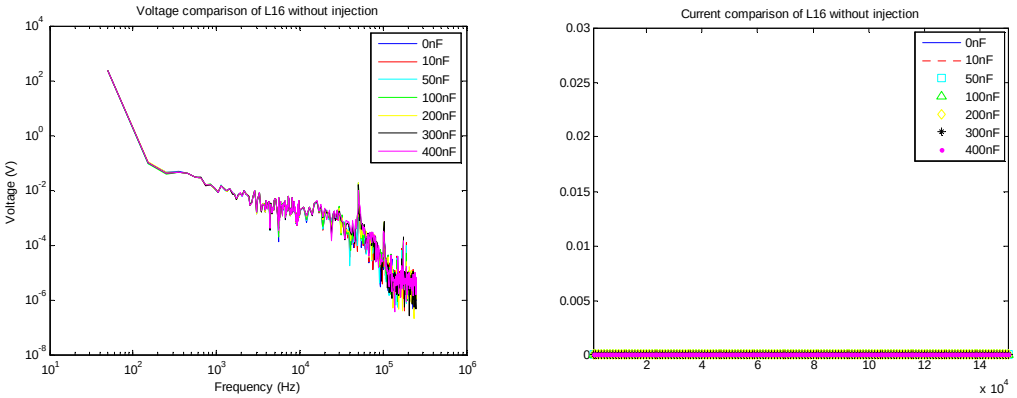

Fig 6-47 Voltage comparison of L16 without injection using capacitance box

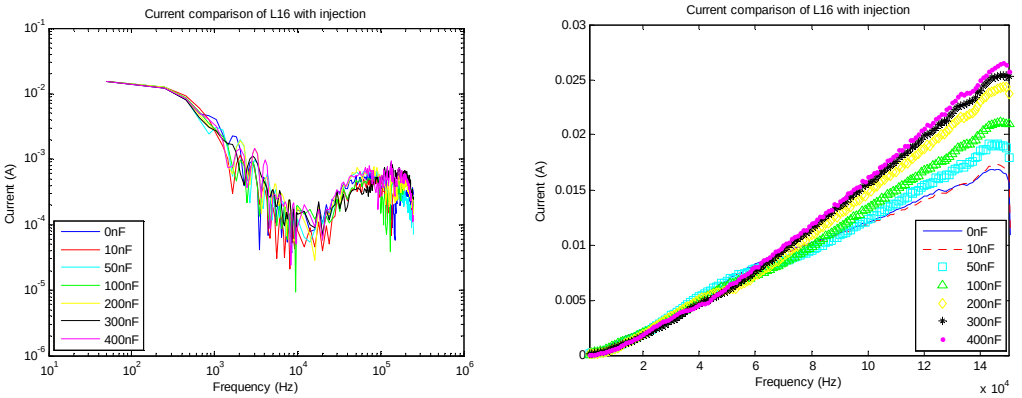

Fig 6-48 Current comparison of L16 with injection using capacitance box

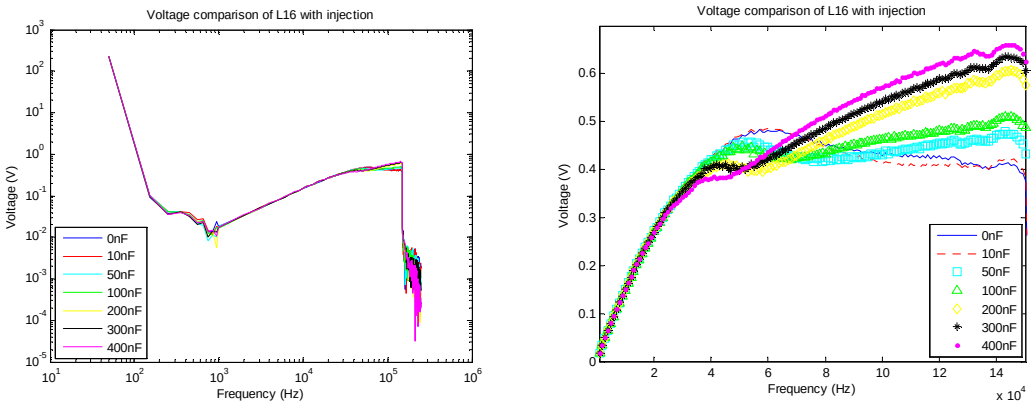

Fig 6-49 Voltage comparison of L16 with injection using capacitance box

The 1 kHz – 150 kHz noise still makes a big difference for capacitive loads. Therefore, similarly, by applying Equation (6-1) to Equation (6-4), it is able to find the influence on the power and RMS current measured by the reference meter when disturbance is injected.

	L1		L16	
C (nF)	Power (No injection) (W)	Power (With injection) (W)	Power (No injection) (W)	Power (With injection) (W)
0	6.6	6.6	5.6	5.6
10	6.6	6.6	5.6	5.6
50	6.7	6.7	5.7	5.7
100	6.7	6.6	5.7	5.6
200	6.6	6.7	5.6	5.6
300	6.7	6.6	5.6	5.7
400	6.6	6.6	5.6	5.7

Table 6-4 Smart meter readings of L1 and L16 using capacitance box

Table 6-4 lists the readings from the smart meter and obviously there is no significant influence on its readings. Then Fig 6-50 and Fig 6-51 respectively illustrate the power consuming for L1 and L16 measured by reference meter.

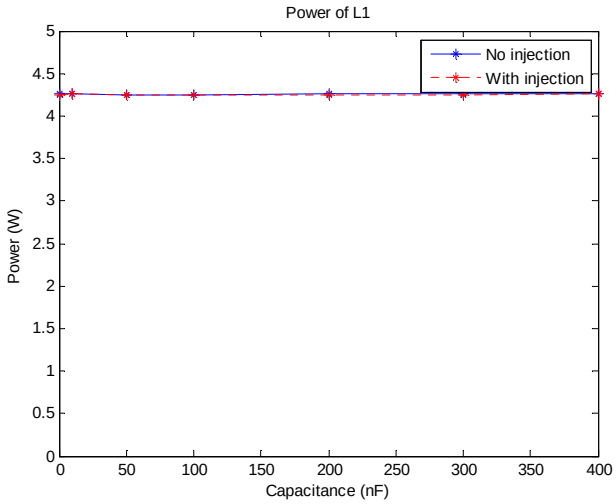

Fig 6-50 Power of L1 using capacitance box

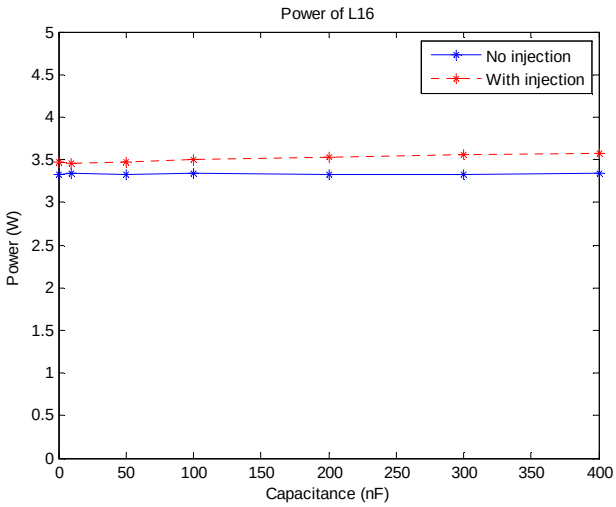

Fig 6-51 Power of L16 using capacitance box

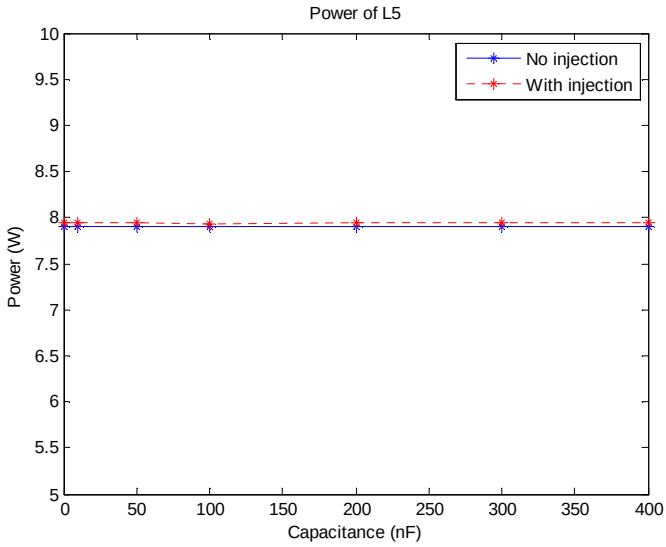

Fig 6-52 Power of L5 using capacitance box

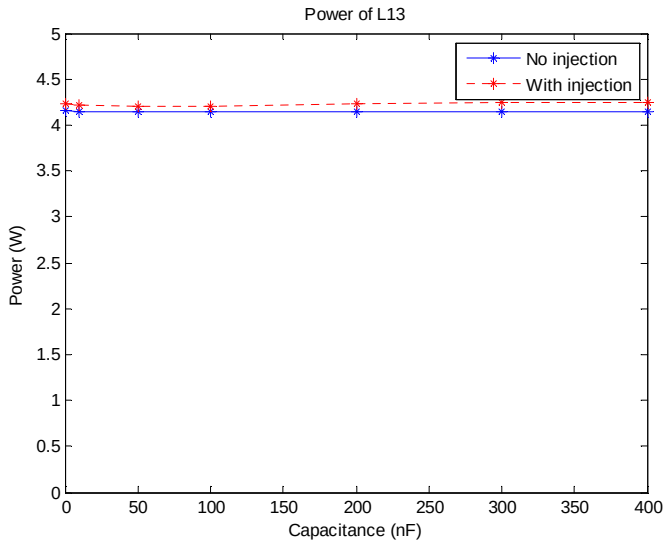

Fig 6-53 Power of L13 using capacitance box

Similarly, the nearly 2.3 Watt power difference is caused by the consuming of the voltage divider and current shunt. In addition, the 0.1 Watt's difference on L16 in Fig 6-51 is not enough to distinguish the smart meter's accuracy which works with 0.2 Watt's variation. Then the power for the other loads (L5 and L13) obtained by the reference meter are shown in Fig 6-52 and Fig 6-53 respectively.

As shown in Fig 6-34 to Fig 6-49, significant current harmonics are induced by the injecting noise and some of their amplitudes are even higher than the fundamental component. Thus, it is reasonable to conclude that their RMS currents will be of obvious difference compared with the ones without injections.

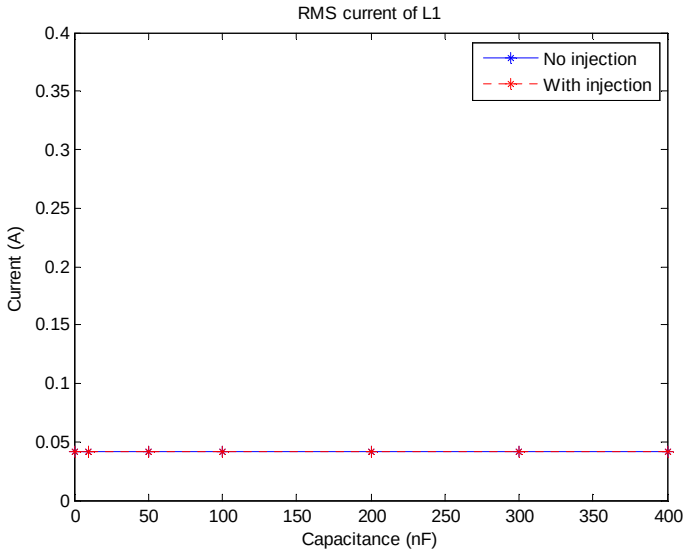

Fig 6-54 RMS current of L1 using capacitance box

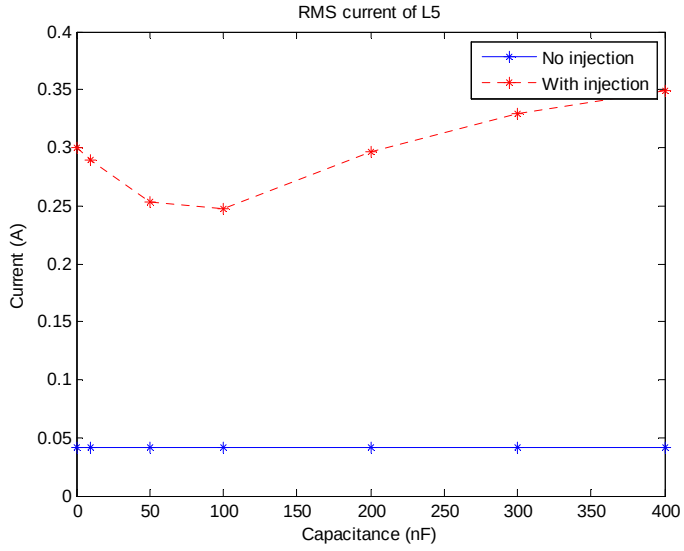

Fig 6-55 RMS current of L5 using capacitance box

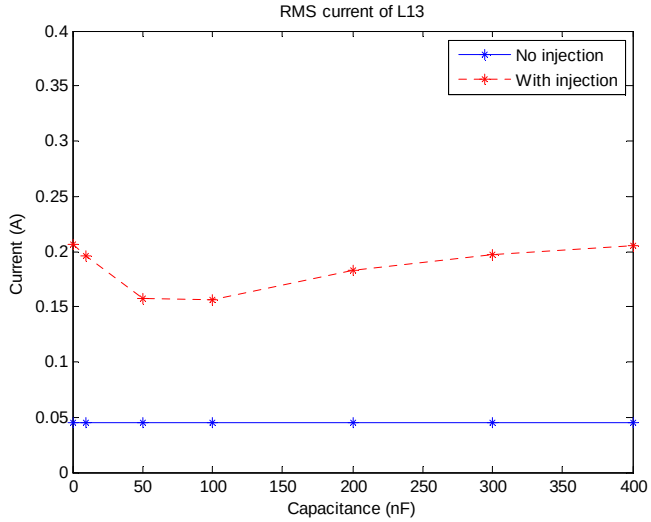

Fig 6-56 RMS current of L13 using capacitance box

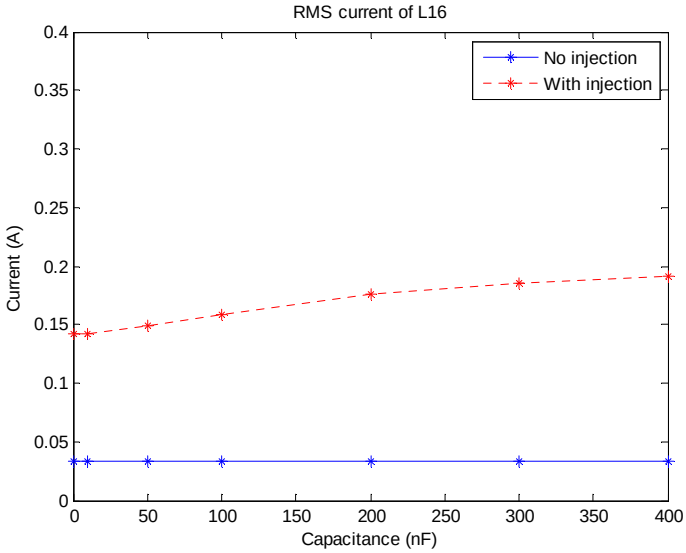

Fig 6-57 RMS current of L16 using capacitance box

6.3 Summary and possible explanations

What can be concluded from these two experiments is that, when a load is inductive like L1, it has a great tolerance for different categories of sources. This means that when it is used for immunity test, the selection of power supply is relatively insignificant. However, for a load like L16 whose electrical property will vary at certain frequency, the immunity test will lead to different results depending on the source it chooses. Therefore, it is necessary to measure the source and load impedance first before using them for further tests.

The reasons why there is no clear influence on the smart meter being observed can be various. The first possible reason could be that the measuring technology this smart meter based on is insensitive with noise. According to [42], there were only 8% smart meters that showed serious problem in its test and all of them were based on Rogowski coils. Nevertheless, the smart meter used in this experiment is based on shunt the category of which was also unaffected as

well in [42]. Secondly the sample rate this smart meter applied might be as good as the one used in the reference meter but it cannot be sure other smart meters have the same accuracy. In addition, as what has been demonstrated before, the injection was not able to match the requirements as IEC 61000-4-19 suggests. This is because on one hand the used loads and the inductance or capacitance box are not capable of such high current as the standard requires, on the other hand the signal generator also cannot provide such injection.

7 Conclusions and recommendations

7.1 Conclusions

Transfer impedance as one of great importance parameter for current probes is able to be conformed via VNA at high frequencies and via spectrum analyzer at low frequencies. For the purpose of application, current probes can be divided into two types, the current monitor probe and the BCI probe. Due to the different turns ratio of those two kinds of probes, the influence resulting from the secondary side on the measurement of transfer impedance is of significant difference. The input impedance on the primary side (wire through the probe) plays an important role when measuring the transfer impedance of a BCI probe while it is insignificant when measuring target is a monitor probe.

The two-probe method to measure source or load impedance is not suitable when it works at the frequency range 2 kHz – 150 kHz because of the lack of phase information. Instead, the three-probe method proposed in this thesis is able to put the phase information into impedance calculation leading to the accurate result. Furthermore, the simple instruments such as current probe, signal generator and digitizer are all normal and accessible experimental equipments for electricity labs and there is no complex mathematical or electrical knowledge behind. Therefore, it is no problem to duplicate this method for further research and measurement. In addition, this method is able to realize the in-situ measurement which means that the measurement can be finished without interrupting the EUT's operation and it does not need to a special lab to accomplish them. With the necessary equipments as mentioned above, the measurement is possible to be simply implemented where the EUT is.

Whatever sorts of sources or loads are, the three-probe method is able to accomplish the in-situ measurement successfully. Due to some of the measurement targets may get saturated when injected by both power source and noise source together, the in-situ measurement may result in a great difference compared with the power-off measurement. However, it is the actual status when the target is under immunity test or under normal work with disturbances.

Resonance will occur when the noise or harmonics meets the resonant frequency which depends on the property of the source and load. As far as we know, most of the source is inductive so that it will become much more sensitive when the load has capacitive property. When noise is injected into such circuit, the current and voltage of the load will be significantly influenced. For such load, it needs to be careful to choose the power supply when it is used for immunity test. Using the same load to test in different labs could result in distinct results. Until now, such resonance has no obvious effect on the smart meter VOLTCRAFT VSM-101.

7.2 Recommendations

Based on the achievements so far, the following aspects are worth to investigate as a subsequent research for this work.

Firstly, use three-probe method to measure the impedance at high frequencies to verify that whether this approach is capable of it. Since some electric equivalent models may change when the environment becomes from low frequencies to high frequencies, the mathematical deduction may need to improve.

Secondly, change the injection signal from multiple harmonics to single harmonics and adjust the injection amplitude to avoid saturation. Then program one routing that is able to inject this single harmonics one by one automatically and program another one to sweep and collect the data used for FFT analysis. At last, compare the result with the one in this thesis.

Thirdly, strong signal as the standard suggests could be used to find out the difference between the reading of smart meter and the result of the reference meter.

In addition, due to the inconstant transfer impedance of current probes at low frequency, the “flat” injection signal will be reshaped after it is injected into the coupling circuit by injecting probe. The reshaped signal makes it difficult to achieve some useful information from the measurement result, for example it is not able to accurately locate the resonance frequency from the current or voltage measurement due to the disequilibrium injection. Therefore, injection calibration according to the injecting current probe transfer impedance is also worth to investigate.

At last, the smart meter based on Rogowski coils can be selected as the EUT and repeat this experiment all over again.

Reference

[1] Robert Smolenski, “Conducted Electromagnetic Interference (EMI) in Smart Grids”, published by Springer, London 2012.

[2] CENELEC SC 205A, “Study Report on Electromagnetic Interference between Electrical Equipment/Systems in the Frequency Range below 150 kHz”, SC205A/SEC0260/R, April 2010.

[3] E. O. Anders Larsson, Math H. J. Bollen, Mats G. Wahlberg, C. Martin Lundmark and Sarah K. Ronnberg, “Mearurements of High-Frequency (2-150 kHz) Distortion in Low-Voltage Networks”, IEEE Transactions on Power Delivery, vol.25, No.3, July 2010.

[4] CENELEC SC 205A, “Study Report on Electromagnetic Interference between Electrical Equipment/Systems in the Frequency Range below 150 kHz ED.2”, SC205A/SEC0339/R, April 2013.

[5] Budi Sudiarto, Aji Nur Widyanto and Holger Hirsch, “Voltage and Current Distortion Correlation Characteristics of Compact Fluorescent Lamp in Frequency Range of 2-150 kHz”, IEEE Quality in Research, published on 2013 International Conference.

[6] Frank Gronwald, Ralf Conrads, Reinhard Janssen and Thomas Weber, “Efficient Immunity Testing of Smart Meter Devices in the Frequency Range 2-150 kHz”, in 22nd International Conference on Electricity Distribution, June 2013.

[7] Marco Liserre, Frede Blaabjerg and Steffan Hansen, “Design and Control of an LCL-Filter-Based Three-Phase Active Rectifier”, IEEE Transactions on Industry Applications, vol.41, No.5, Sept 2005.

[8] IEC 61000-4-19, Electromagnetic compatibility (EMC) - Part 4-19: Testing and measurement techniques - Test for immunity to conducted, differential mode disturbances and signalling in the frequency range 2 kHz to 150 kHz at a.c. power ports, 2014.

[9] Bernd W. Jaekel, “Current Situation in the Frequency Range from 2 to 150 kHz with regard to Electromagnetic Compatibility”, 22nd International Conference on Electromagnetic, Sept 2012.

[10] E. O. A Larsson and M. H. J. Bollen, “Emission and Immunity of Equipment in the Frequency Range 2 to 150 kHz”, IEEE Bucharest Power Tech Conference, 2009.

[11] S. Ronnberg, M. Wahlberg, M. Bollen, A. Larsson and M. Lundmark, “Measurements of Interaction between Equipment in the Frequency Range 9 to 95 kHz”, 20th International Conference on Electricity Distribution, June 2009.

[12] M. Bollen, W. Wahlberg and S. Ronnberg, “Interaction between Narrowband Power-line Communication and End-User Equipments”, IEEE Transactions on Power Delivery, vol. 26, No.3, July 2011.

[13] J. Kirchhof and G. Klein, “Deficits and Uncertainties in Photovoltaic Inverter Test Procedures”, 24th European Photovoltaic Solar Energy Conferrence and Exhibition, Sept 2009.

[14] SWEDAC Report MI-10-062 “Noise” and Standards for Electricity Meters, EN 50470, 2010

[15] M. Hattori, “Malfunctions Due to Electromagnetic Disturbances from Power Electronics Equipment”, 1998 National Convention of the IEE Japan.

[16] CIS/S/341/RQ, “Result of Questionnaire CISPR/S/337/Q on Electromagnetic Compatibility in the Range 9 kHz to 30 MHz”, 2011.
[17] CISPR/1226/RQ, “Result of Questionnaire CISPR/1216A/Q on Electromagnetic Compatibility in the Range 9 kHz to 30 MHz”, 2012.
[18] TC210/SEC0597B/INF, “National Committee Responses to Questionnaire TC210/SEC0591/Q on EMC of Non-ratio Services”, 2009.
[19] A. Larsson, M. Bollen and M. Lundmark, “Measurement and Analysis of High-Frequency Conducted Disturbances”, 19th International Conference on Electricity Distribution, 2007.
[20] Kye Yak See and Junhong Deng, “Measurement of Noise Source Impedance of SMPS Using a Two Probes Approach”, IEEE Transactions on Power Electronics, May 2004 .
[21] Vuttipon Tarateeraseth, Bo Hu, Kye Yak See and Flavio G. Canavero, “Accurate Extraction of Noise Source Impedance of an SMPS Under Operating Conditions”, IEEE transaction on Power Electronics, Jan 2010.
[22] Douglas Smith, “High Frequency Measurements and Noise in Electronic Circuits”, published by Van Nostrand Reinhold, New York 1993.
[23] “Probe Fundamentals”, published by Tektronix, 2009.
[24] Douglas Smith, “Current Probes, More Useful Than You Think”, IEEE International Symposium on Electromagnetic Compatibility, 1998.
[25] “Model 94430 Series Current Probes Manual”, published by ETS-LINDGREN L.P., REV D – PN 399246, April 2013.
[26] Kenneth Wyatt, “The HF Current Probe: Theory and Application”, EMC Directory & design guide 2012.
[27] ”F75 Current Probe Manual”, published by Fischer Custom Communications, Inc., 2004.
[28] “Current Probe Calibration”, published by Fischer Custom Communications, Inc.
[29] Sekiguchi, H. and Funaki, T., “Proposal for Measurement Method of Transfer Impedance of Current Probe”, IEEE Transactions on Electromagnetic Compatibility, 2014.
[30] “7600 Precision LCR Meter Model B Instruction Manual”, published by QuadTech Inc., 1997.
[31] “Agilent E4980A Precision LCR Meter User’s Guide Ninth Edition”, published by Agilent Technologies, 2012.
[32] Ian B. Darney, “Circuit Modeling for Electromagnetic Compatibility”, published by SciTech, 2013.
[33] Sergey Miropolsky, Stephan Frei and Jörg Frensch, “Modeling of Bulk Current Injection (BCI) Setups for Virtual Automotive IC Tests”, 9th International Symposium on EMC joint with 20th International Wroclaw Symposium on EMC, 2010.
[34] S. Akue Boulingui and A. Cisse Ndoye, “A model of the Bulk Current Injection Probe”, 2010.
[35] Flavia Grassi, “Accurate modeling of ferrite-core effects in probes for Bulk Current Injection”, IEEE International Conference on Microwaves, Communications, Antennas and Electronics Systems, 2009. COMCAS 2009.
[36] Flavia Grassi, Filippo Marliani and Sergio A. Pignari , “Circuit Modeling of Injection Probes for Bulk Current Injection”, IEEE Transactions on Electromagnetic Compatibility, 2007.

[37] Flavia Grassi, Filippo Marliani and Sergio A. Pignari , “Improved lumped-pi circuit model for bulk current injection probes”, IEEE Transactions on Electromagnetic Compatibility, 2005.

[38] Flavia Grassi, Filippo Marliani and Sergio A. Pignari , “SPICE Modeling of BCI Probes Accounting for the Frequency-Dependent Behavior of the Ferrite Core”.

[39] “CIP 9136A Current Injection Probe 10 kHz – 400 MHz Manual”, published by TESEQ, 2012.

[40] “Bulk Current Injection Probe Test Procedure”, published by A.H. Systems inc, 2005.

[41] James McLean and Robert Sutton, “Dependence of the time- and frequency-domain response of BCI injection probes on the common- mode characteristic impedance of the cable bundle”, IEEE International Symposium on Electromagnetic Compatibility (EMC), 2010.

[42] Henri Schouten, “Low frequency range 2-150 kHz, practical experiences and test possibilities”, Technique report, Milestones in Metrology 4th Edition, Venice 2012.